CHAPTER 20.2 SEISMIC DESIGN OF STEEL BRIDGES

TABLE OF CONTENTS

20.2.1 INTRODUCTION

Seismic bridge design has been improving and advancing based on research findings and lessons learned from past earthquakes, such as the 1989 Loma Prieta and the 1994 Northridge, USA, the 1995 Hyogo-ken Nanbu (Kobe) in Japan, the 1999 Jiji (Chi-Chi) in Taiwan, and the 2008 Wenchuan in China. The California Department of Transportation (Caltrans) shifted to a displacement-based design approach emphasizing capacity design after the 1994 Northridge earthquake and published *Seismic Design Criteria* (*SDC*), Version 1.1, which focused mainly on typical concrete girder bridges in 1999 (Caltrans, 1999) and Caltrans *Guide Specifications for Seismic Design of Steel Bridge* (*Guide*), the first edition in 2001 (Caltrans, 2001).

In the 18 years since the first edition of the *Guide* was published, Caltrans adopted the *AASHTO LRFD Bridge Design Specifications* beginning in 2006 and has published several versions of the *SDC*, the latest being *SDC* Version 2.0 in 2019 (Caltrans, 2019a). The American Association of Highway and Transportation Officials (AASHTO) published the first edition of *AASHTO Guide Specifications for LRFD Seismic Bridge Design* in 2009 and the second edition in 2011 (AASHTO, 2011). The American Institute of Steel Construction (AISC) updated its *Seismic Provisions for Structural Steel Buildings* in 2016 (AISC, 2016). Significant research progress has been made on the seismic design of steel bridges, including shear links, buckling-restrained braces, ductile end cross frames, and integral bent cap connections. With the aid of all this information, Caltrans thoroughly revised and updated the *Guide* to the second edition and renamed as the *Caltrans Seismic Design Specifications for Steel Bridges* (*SDSSB*) in 2016 (Caltrans, 2016a). The most significant changes of the second edition are related to shear links, buckling-restrained braces, ductile end cross frames, and integral bent cap connections. The *SDSSB* was developed as a consensus document to achieve uniformity in the seismic design of steel bridges in California.

This Chapter first addresses earthquake damage to steel bridges, seismic bridge design philosophies, and concepts for steel girder bridges in general, then discusses seismic design basis, seismic analysis and modeling, general seismic design considerations, seismic retrofit practice with several major steel bridge retrofit projects, and finally presents two seismic design examples for steel girder bridges.

20.2.2 EARTHQUAKE DAMAGE TO STEEL BRIDGES

Recent earthquakes, particularly the 1989 Loma Prieta and the 1994 Northridge earthquakes in California, the 1995 Hyogo-Ken Nanbu earthquake in Japan, the 1999 Jiji earthquake in Taiwan, and the 1999 Kocaeli earthquake in Turkey, have caused the collapse of, or severe damage to, a considerable number of major bridges. Past earthquakes have shown that steel bridges have many desirable performance characteristics that are not seen in concrete bridges. Damage induced in steel bridges can take many forms depending on the ground motion, site conditions, overall configuration, and specific details of bridges (Astaneh-Al, 1994; Bruneau, 1998; Yashinsky et al., 2014). Most of the damage to steel bridges has taken one of the following forms:

- Unseating of the superstructure at in-span hinges or simple supports due to inadequate seat lengths or restraint (Figure 20.2.2-1).

- Concrete column brittle failure due to deficiencies in shear design and inadequate ductility (Figure 20.2.2-2).

- Steel column brittle failure due to inadequate ductility (Figures 20.2.2-3 and 20.2.2-4).

- Anchorage assembly failure due to poor reinforcement details in the concrete (Figure 20.2.2-5).

- End cross frame inelastic buckling (Figure 20.2.2-6).

(a) San Francisco-Oakland Bay Bridge East Span 1989 Loma Prieta Earthquake

(b) Highway Viaduct, 1995 Nanbu Earthquake Japan

Figure 20.2.2-1 Unseating of Superstructure

Figure 20.2.2-2 Concrete Column Brittle Failure, 1995 Hyogo-Ken Nanbu Earthquake, Japan

Figure 20.2.2-3 Iwaya Viaduct Steel Pier Failure, 1995 Hyogo-Ken Nanbu Earthquake, Japan (Goto, 2014)

**Figure 20.2.2-4 Tateishi Viaduct Steel Pier Failure.
1995 Hyogo-Ken Nanbu Earthquake, Japan (Goto, 2014)**

**Figure 20.2.2-5 Anchorage Assembly Failure – Santa Ana River Bridge,
1994 Northridge Earthquake (Astaneh-Al, A. et al., 1994)**

Figure 20.2.2-6 End cross frame inelastic buckling
Old Road Bridge, 1994 Northridge Earthquake (Astaneh-Al, A. et al., 1994)

20.2.3 PERFORMANCE-BASED SEISMIC DESIGN CRITERIA

In the newly published *SDC* (Caltrans, 2019a), Bridges are categorized as "Important", "Recovery", or "Ordinary". Depending on their structural features, Recovery and Ordinary bridges are further classified as "Standard" or "Nonstandard". For Ordinary Standard bridges, the displacement-based one-level safety-evaluation design ("no-collapse" design) is required in the Caltrans *SDC* and *SDSSB.* Nonstandard bridge features include irregular geometry and framing (multi-level, variable width, bifurcating, or highly horizontally curved superstructures, different structure types, outriggers, unbalanced mass and/or stiffness, high skew) and unusual geologic conditions (soft soil, moderate to high liquefaction potential and proximity to an earthquake fault). In this case, project-specific criteria need to be developed and approved to address their nonstandard features.

Caltrans has designated "Life-Line" routes throughout the State of California that are critical and must be kept open to allow the movement of emergency vehicles and equipment required in the aftermath of major earthquakes. Bridges on these "Life-Line" routes are designated as "Important Bridges". Bridges on vital links for rebuilding damaged areas and providing access to the public shortly after an earthquake are designated "Recovery Bridges". Both Important and Recovery bridges require project-specific criteria for two-level design. Recovery bridges are designed for enhanced performance above Ordinary bridges but less than the performance of Important bridges. The first level of the Safety Evaluation Earthquake (SEE) design is to achieve the performance ("no collapse") of a bridge under severe earthquakes that have only a small probability of occurring during the useful life of the bridge. The second level of the Functionality Evaluation Earthquake (FEE) design is to ensure the performance (service)

of a bridge during earthquake events that have a relatively small magnitude but may occur several times during the life of the bridge. These project-specific criteria include guidelines for the development of site-specific ground motion estimates, capacity design to preclude brittle failure modes, rational procedures for connection design, and the definition of limit states for various performance objectives.

20.2.4 EARTHQUAKE RESISTING SYSTEMS AND STRUCTURAL COMPONENT CLASSIFICATIONS

An earthquake resisting system *(ERS)* is a structural system designed to withstand earthquakes. *ERS* provides a reliable and uninterrupted load path for transmitting seismically induced forces into the ground and sufficient means of energy dissipation and/or restraint to control seismically induced displacements reliably.

For steel girder bridges, the inertial forces generated by the deck must be transferred to the substructure through girder flanges, webs, cross frames, lateral bracings, end diaphragms, shear keys, and bearings. Slab-on-steel girder bridges are generally designed to ensure that inelastic deformation occurs in the ductile substructure elements. As alternatives, inelastic deformations may be permitted in end cross frames or seismic isolation bearings to prevent damage in other parts of the structure (Zahrai and Bruneau, 1998, 1999a and 1999b; Carden et al., 2006a and 2006b; Bahrami et al., 2010; Uang et al., 2014; Monzon et al., 2014). Figure 20.2.4-1 shows ERS in the transverse direction in a steel girder bridge.

For steel substructures, such as steel multi-column bents or towers, *ERS* includes ductile steel Moment Frames (MF), Concentrically Braced Frames (CBF), and Eccentrically Braced Frames (EBF). For an MF as shown in Figure 20.2.4-2, the primary inelastic deformation is expected to occur in the columns. For a CBF as shown in Figure 20.2.4-3, diagonal members are designed to yield when the members are in tension and to buckle inelastically when they are in compression. For EBF as shown in Figures 20.2.4-4 and 20.2.4-5, a short beam segment designated as a *"link"* is designed and detailed in a ductile manner. For components expected to behave inelastically, elastic buckling (local compression, global flexural, and lateral torsion buckling) and fracture failure modes shall be avoided. All connections and joints shall be designed to remain essentially elastic.
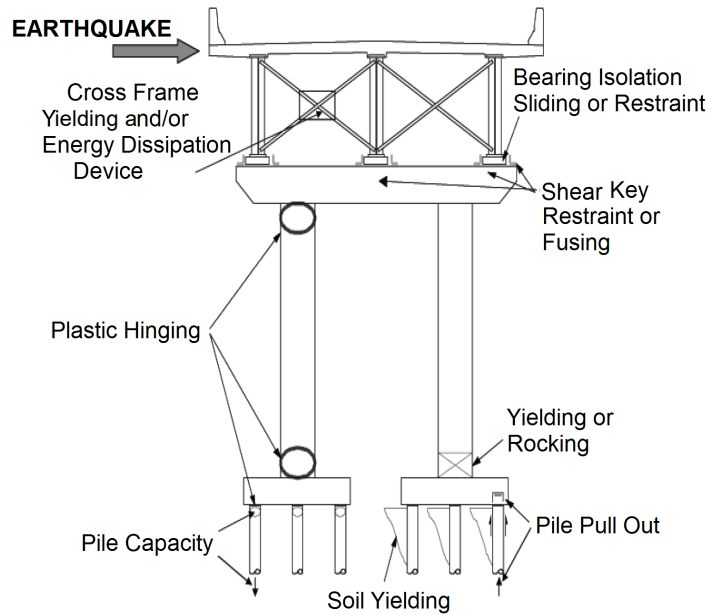
Figure 20.2.4-1 Earthquake Resisting Systems in Transverse Direction in Steel Girder Bridge

Figure 20.2.4-2 Moment Frame – Bayshore Viaduct in San Francisco

**Figure 20.2.4-3 Concentrically Braced Frame –I-5 Ramp in
Sacramento Valley Station**

**Figure 20.2.4-4 Eccentrically Braced Frames - Self-Anchor Suspension
Bridge Tower – San Francisco Oakland Bay Bridge East Span**

Figure 20.2.4-5 Eccentrically Braced Frames – Temporary Tower for San Francisco Oakland Bay Bridge East Span Construction

Structural components in ERS of a steel bridge are classified into two categories: Ductile and Capacity-protected. Ductile or seismic-critical components are those expected to experience significant damage, but not to fail, under the demands generated by the design earthquake. Ductile components are pre-identified and well-detailed to behave inelastically for several cycles without significant degradation of strength or stiffness. Capacity-protected components are those expected to experience minimum damage and to behave essentially elastic under the design earthquake. *SDSSB* Table 2.1-1 summarizes the structural component classification for Ordinary steel bridges

## 20.2.5   SEISMIC DESIGN BASIS

20.2.5.1   Displacements

The displacements in a global and local ductile system shall satisfy the following requirement:

$$\Delta_D \leq \Delta_C \qquad\qquad (SDSSB\ 2.6.1\text{-}1)$$

where Δ_D is the displacement demand determined by equivalent static analysis or elastic dynamic analysis with consideration of effective section properties under the design

earthquake (in.) and Δ_C is the displacement capacity determined by using a static pushover analysis in which both material and geometric nonlinearities are considered (in.).

The deformation (displacement or rotation) capacity of a steel component or a frame is defined as the deformation corresponding to the expected damage level limit as specified in the *SDSSB* Table 2.5-1, not to exceed the deformation when the lateral resistance degrades to a minimum of 80 percent of the peak resistance. The *SDSSB* Table 2.5-1 provides quantitative strain and ductility limits corresponding to the three damage levels, minimal, repairable, and significant as compared to minimal, moderate, and major in the *SDC* (Caltrans, 2019a). Figure 20.2.5-1 shows typical load-deformation curves. The displacement and rotation measurements are commonly used for a structural system and an individual member, respectively. In Figure 20.2.5-1, Δ_y is yield displacement which is the lateral displacement of a component or a frame at the onset of forming the first plastic hinge (in.); θ_y is yield rotation which is the rotation at the onset of yielding in the extreme tension fiber; Δ_u is ultimate lateral displacement capacity, the lateral displacement of a component or a system corresponding to its expected damage level limit as specified in the *SDSSB* Table 2.5-1, not to exceed that displacement when the lateral resistance degrades towards a minimum of 80 percent of the peak force resistance (in.); θ_u is ultimate rotation capacity, rotation corresponding to its expected damage level at which the extreme fiber reaches its strain limit as specified in Table 2.5-1, not to exceed that rotation when the moment resistance degrades towards a minimum of 80 percent of the peak moment resistance; M_y is yield moment at the onset of yielding of an extreme fiber (kip-in.). M_u is peak moment or ultimate moment (kip-in.); V_y is lateral force corresponding to the onset of forming the first plastic hinge (kip); V_u is peak lateral load or ultimate lateral load capacity (kip).

(a) Moment-Rotation Curve (b) Lateral Load-Displacement Curve
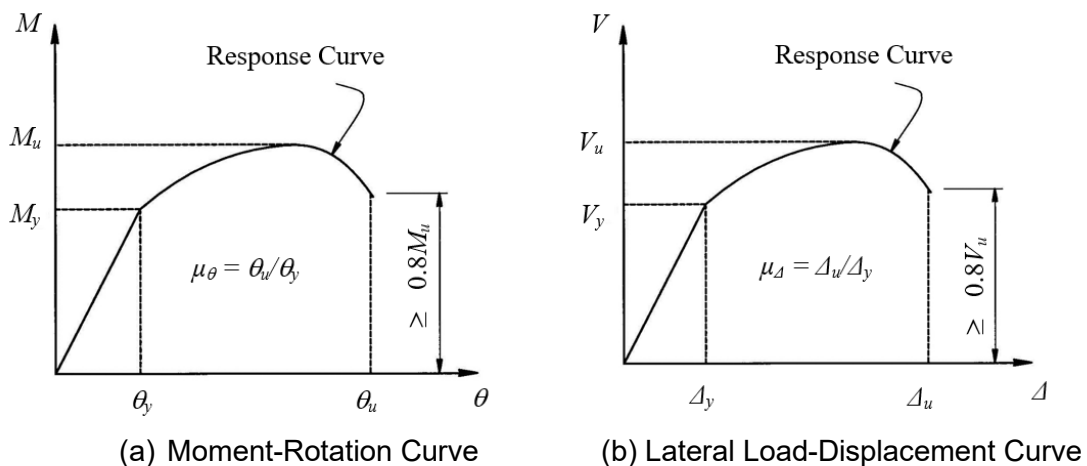
Figure 20.2.5-1 Typical Load-Deformation Curves

20.2.5.2 Forces

The *SDSSB* requires that the forces in a capacity-protected component shall satisfy:

$$F_D \leq F_C \qquad\qquad (SDSSB\ 2.6.2\text{-}1)$$

where F_D is the force demand (axial/shear force and moment as appropriate) on a capacity-protected component determined by the joint equilibrium of overstrength forces of adjacent ductile components. F_C is the design strength or factored resistance (axial/shear force and moment as appropriate) of a capacity-protected component.

20.2.5.3 Overstrength

The Overstrength force for a ductile component is used to design the capacity-protected component to ensure that fusing occurs in the ductile component and the capacity-protected components remain essentially elastic. It is taken as its idealized plastic strength multiplied by an overstrength factor, Ω, which accounts for expected material strength variations between a ductile component and adjacent members, and the actual strength of a ductile component greater than its idealized plastic strength. The overstrength factor, Ω shall be determined by the project-specific criteria. Based on research recommendations, the following overstrength factors, Ω, may be used:

For shear in I-shaped links	Ω = 1.75
For shear in box-shaped links	Ω = 1.50
For buckling-restrained braces	Ω = 1.00
For all other cases	Ω = 1.20

Test results (McDaniel, et al., 2002; Dusicka, et al., 2002 and 2010) for shear links used in the new San Francisco-Oakland Bay Bridge tower show that the overstrength factor of 1.25 for I-shaped links as specified in the *AISC Seismic Provisions* (AISC, 2016) is significantly lower than measured overstrength factors, 1.83 to 1.94. An overstrength factor of 2.0 is recommended for the capacity design of adjoining members of links (McDaniel et al., 2002). An overstrength factor of 1.75 for box-shaped links is based on experimental research by Berman and Bruneau (2008). Since the idealized plastic shear strength is taken as the expected nominal shear strength multiplied by a factor of 1.17 to consider strain hardening as specified in Article 5.3.4.2 of the *SDSSB*, overstrength factors, Ω = 1.75, and Ω = 1.50 should be used for I-shaped and box-shaped links, respectively.

Since the strength of buckling-restrained braces (*BRB*) is established basis on testing and strain hardening is considered by the strain hardening adjustment factors (Lanning et al., 2013), ω_C and ω_T, as specified in Article 5.4.3.2 of the *SDSSB*, an overstrength factor, Ω = 1.0 is used.

An overstrength factor, Ω = 1.2 is recommended for all other cases, similar to that used for concrete structures in Article 4.4.2.1 of the *SDC*.

20.2.6   SEISMIC ANALYSIS AND MODELING

20.2.6.1   Seismic Analysis Methods

The *SDSSB* Article 3.1.1 specifies that Equivalent Static Analysis (ESA) (Article 4.2.1 of the *SDC*) or Elastic Dynamic Analysis (EDA) (Article 4.2.2 of the *SDC*) aredetermineetermined displacement demands for a steel bridge, and Inelastic Static Analysis (ISA) (Article 5.2.2 of the *SDC*), i.e., pushover analysis is used to determine displacement capacities of a steel bridge. The *SDSSB* Article 5.1.3 specifies that moment-curvature analysis can be used to determine idealized plastic moment capacity.

20.2.6.2   Moment-Curvature Analysis

The moment-curvature analysis is used to evaluate the behavior of a cross-section. In a moment-curvature analysis for a ductile structural steel component, the following assumptions are usually made:

- Plane sections before bending remain plane after bending

- Shear and torsional deformation are negligible

- Stress-strain relationships for steel are known

The steel cross-section is divided into layers or elements with the proper stress-strain relationship (Figure 20.2.6-1). The state of stresses and strains are traced explicitly for all elements during the analysis. A set of typical moment-curvature curves for a steel I-section is shown in Figure 20.2.6-2.
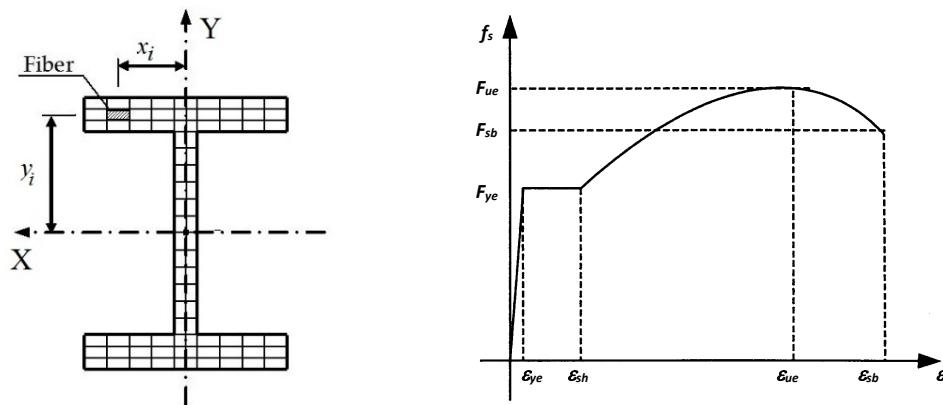

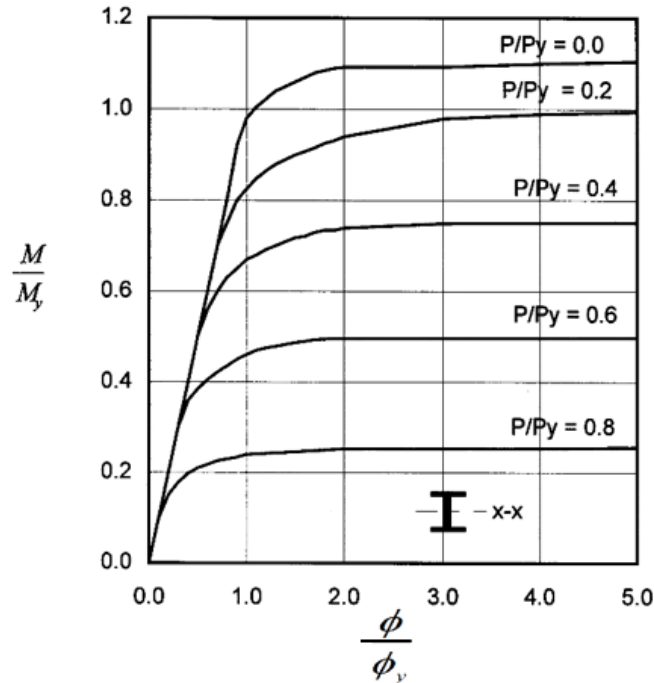**Figure 20.2.6-1 Steel Cross-Section and Stress-Strain Curve**

Figure 20.2.6-2 Typical Moment-Curvature Curves for Steel I-Section

20.2.6.3   Pushover Analysis

20.2.6.3.1 Basic Principles

Inelastic Static Analysis, commonly referred to as the "pushover analysis", is used to determine the displacement capacity of a steel bridge substructure. In a pushover analysis, a stand-alone portion from a bridge structure (such as a bent frame single or multi-columns) is isolated and statically analyzed considering whatever nonlinear behavior is deemed necessary (most common is material and geometric nonlinear behavior). The analysis can utilize one of the three modeling methods discussed below, but plastic hinge or distributed plasticity model are widely used. The analytical frame model is first subjected to the applied tributary gravity load and then is pushed laterally in several load (or displacement) increments until a collapse mechanism, or a given failure criterion is reached.

Pushover analysis can be categorized into three types: (1) elastic-plastic hinge, (2) refined plastic hinge, and (3) distributed plasticity. The simplest method, elastic-plastic hinge analysis, may be used to obtain an upper bound solution. The most accurate method, distributed plasticity analysis, can be used to obtain a better solution. Refined plastic hinge analysis is an alternative that can reasonably achieve both computational efficiency and accuracy.

In an elastic-plastic hinge (lumped plasticity) analysis, material inelasticity is considered

using concentrated "zero-length" plastic hinges, which maintain plastic moment capacities and rotate freely. When the section reaches its plastic moment capacity, a plastic hinge is formed, and element stiffness is adjusted. For regions in a framed member away from the plastic hinge, elastic behavior is assumed. It does not, however, accurately represent the distributed plasticity and the P-δ effect. This analysis provides an upper bound solution.

In the refined plastic hinge analysis, a two-surface yield model considers the reduction of plastic moment capacity at the plastic hinge due to the presence of axial force, and an effective tangent modulus accounts for the stiffness degradation due to distributed plasticity along a frame member. This analysis is similar to the elastic-plastic hinge analysis in efficiency and simplicity but also accounts for distributed plasticity.

In the distributed plasticity analysis, the spread of inelasticity through the cross-sections and along the length of the members is modeled explicitly. This analysis is also referred to as plastic zone analysis, spread-of-plasticity analysis, or elastoplastic analysis by various researchers. In this analysis, a member needs to be subdivided into several elements along its length to model the inelastic behavior more accurately. Two main approaches have been successfully used to model the plastification of members in a second-order distributed plasticity analysis:

- The cross-sectional behavior is described as an input for the analysis using moment-thrust-curvature (M-P-ϕ) and moment-thrust-axial strain (M-P-ε) relations, which may be obtained separately from a moment-curvature analysis or approximated by closed-form expressions.

- Cross-sections are subdivided into elementary areas, and the state of stresses and strains are traced explicitly using the proper stress-strain relations for all elements during the analysis.

20.2.6.3.2 Example – Bayshore Viaduct Steel Multi-Column Bent

20.2.6.3.2.1 Problem Statement

The as-built details of a steel bridge bent frame of the Bayshore Viaduct in San Francisco consisting of a bent cap plate girder and two welded built-up columns supported on a stiff pile group foundation as shown in Fig. 20.2.6-3. Steel is ASTM Grade A36. For simplicity and illustration purposes, grillage connections of steel columns to concrete pile caps are assumed as fixed, and the soil-foundation-structure interaction is ignored. Estimate the lateral displacement capacity of the steel multi-column bridge bent by using the pushover analysis.
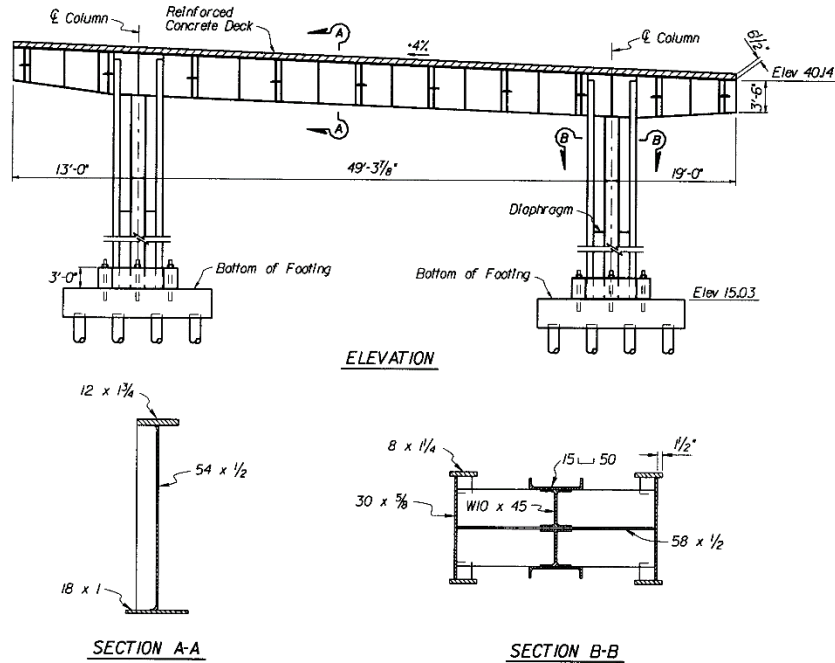
Figure 20.2.6-3 As-Built Plan of Steel Bent

20.2.6.3.2.2 Analysis Modeling

The bent frame members are divided into several beam elements, as shown in Fig. 20.2.6-4. The properties of beam elements are defined by two sets of relationships for moment-curvature, axial force-strain, and torsion-twist for the cap beam and columns, respectively. The available ultimate curvature is assumed as 20 times the yield curvature. The total tributary superstructure dead load of 880 kips is discretely applied at longitudinal girder bearing locations. A lateral displacement is applied incrementally at the top of the bent column until a collapse mechanism of the bent frame is formed.

Figure 20.2.6-4 Steel Bent Analytical Model

20.2.6.3.2.3 Displacement Capacity

The displacement capacity evaluation is performed by push-over analysis using the ADINA (Automatic Dynamic Incremental Nonlinear Analysis) (ADINA, 1997). The resulting lateral load vs. displacement response at the top of columns is shown in Fig. 20.2.6-5. The sudden drops in the response curve are due to several beam elements reaching their ava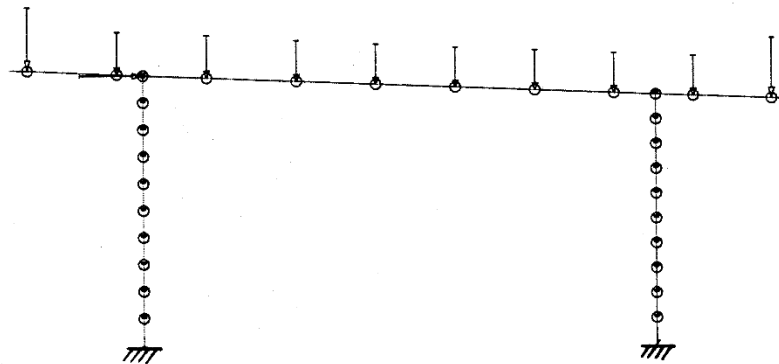ilable ultimate curvatures. The yield displacement Δy = 0.98 in. (Point A) and the available ultimate displacement capacity (corresponding to a 20% reduction from the peak lateral load) $\Delta \mu$ = 2.48 in. (Point C) are obtained.
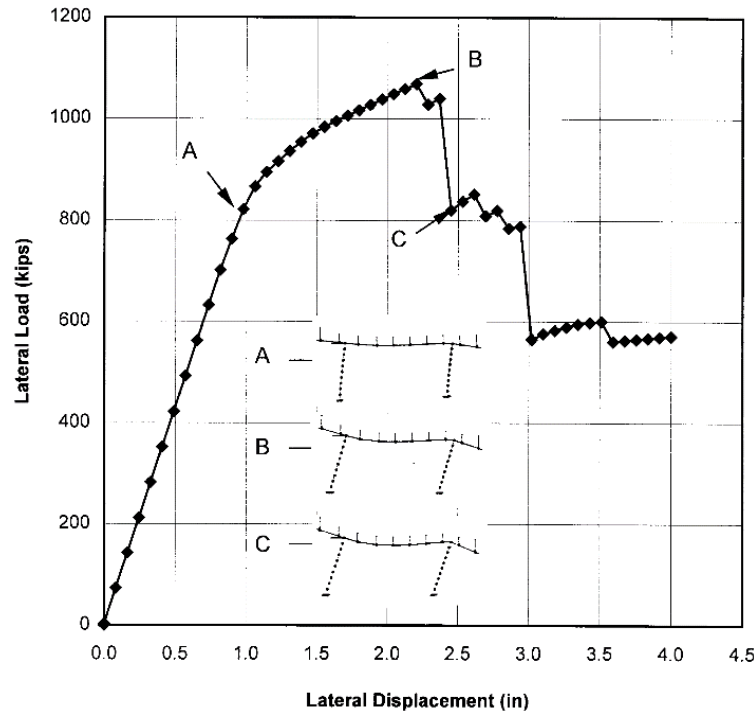
Figure 20.2.6-5 Lateral Load vs. Displacement Curve

20.2.6.4   Structural Modeling

The *Guidelines for Nonlinear Analysis for Bridge Structures in California* (Aviram et al., 2008) presents a collection of general recommendations for the modeling and analysis of highway bridges and overpasses subjected to earthquake ground motions required for the design or evaluation of the capacity and ductility of critical bridge components and systems.

The *SDSSB* Article 3.2 provides general modeling principles for steel bridge members. The *SDC* Article 6.3 presents the modeling guidelines for abutments. In general, the dynamic behavior of a steel bridge structure can be predicted by the finite element method. The elements can be frames (beams), shells, solid elements, or other types of

elements idealizing the real structures. Two types of finite element models, simplified and detailed, are typically used for the dynamic analysis of a steel bridge structure. A simplified model uses two-dimensional or three-dimensional frame elements, in so-called "stick" models to represent superstructures and columns. A detailed model uses solid elements for the superstructure deck, shell elements for steel girders, and frame elements for columns.

For straight steel girder bridges, the simplified modeling procedure provides a good dynamic result (Itani and Sedarat, 2000). A model using five elements per span is sufficient for a good representation of the first three vibration modes of a span (ATC, 1996).

Structural steel shall be modeled to represent actual testing behavior. The stress-strain relationships for structural steel provided in Appendix A of the *SDSSB* may be used in the analysis.

Both P-Δ and P-δ effects are required to be considered in the determination of displacement demands and capacities. Initial imperfections, as specified in Article 3.2.4 of the *SDSSB*, are required to determine the displacement capacity. Effective section properties, as specified in Article 3.2.5 of the *SDSSB*, are needed in *ESA* and *EDA* analyses. For latticed members, effective section properties (Duan et al., 2000) provided in Appendix B of the *SDSSB* should be used in lieu of a refined analysis.

20.2.7   SEISMIC DESIGN CONSIDERATIONS

20.2.7.1 Minimum Seat Width Requirements

The minimum seat width requirement is to prevent unseating of steel superstructures at hinges, piers/bents, and abutments. The seat width must be available to accommodate the anticipated thermal movement and the relative longitudinal earthquake displacements. Caltrans *SDC* specifies the required support lengths at hinges, bents, and abutments.

20.2.7.2 Bearing Assemblies

Caltrans practice is to not use steel rocker bearings for new bridges in California due to their poor seismic performance. Depending upon the expected seismic forces and displacement, particularly on skewed structures, continuous girders are suggested with an appropriate bearing system, such as elastomeric**,** polytetrafluoroethylene (PTFE) spherical bearings, or isolation bearings. To transfer forces and displacements from the superstructure to the substructure, these bearings should be used in combination with transverse and/or longitudinal restraining systems, such as concrete shear blocks, extra strong pipes, or steel bumpers attached to the steel superstructure used to engage concrete blocks on the bent caps.

20.2.7.3 Ductile End Cross Frames

End cross frames or diaphragms, as shown in Figure 20.2.4-1, are the main components to transfer the lateral seismic loads from the deck down to the bearing locations. Although steel girder bridges are usually designed to ensure that inelastic deformation occurs in the ductile substructure elements, structures on rigid walls, or otherwise, can allow inelastic deformations to occur in end cross frames to prevent damage in other parts of the structure. *SDSSB* Chapter 6 provides detailed requirements for slab-on-steel girder bridges.

20.2.7.4 Connection and Splices

SDSSB Chapter 7 provides requirements for connections and splices. Splices in the inelastic regions of ductile components are not permitted. The design strength of splices and connections for ductile members is required to be greater than the overstrength capacities of members being connected and spliced. The design strength of splices and connections for capacity-protected members is required to be greater than the design strengths of members being spliced and connected. Yielding in the gross section is the preferred failure mode to prevent fracture in the net section and block shear rupture failure. The nominal strength of the gusset plates is based on the effective width by Whitmore's method.

20.2.7.5 Welds

Welds located in the expected inelastic region of ductile components are preferably complete penetration welds. Partial penetration groove welds are not recommended in these regions. If fillet welds are the only practical solution for some inelastic regions such as shear links, Quality control (QC), and Quality assurance (QA) inspection procedures for Fracture Critical Members specified in AASHTO/AWS D1.5 Bridge Welding Code (AWS, 2020) are recommended. These details require the designer to document information in the plans and specifications so that the contractor may understand what loading is anticipated at these connections, and then the proper welding, testing, and perhaps repair methods can be used.

20.2.7.6 Limiting Slenderness Ratios

To ensure that reliable inelastic deformations can be achieved in ductile components, the width-to-thickness ratios of elements are required not to exceed the limiting values specified in *SDSSB* Tables 4.2-1 to 4.2-3. The limiting width-to-thickness ratio of elements for ductile components, λ_{ps}, corresponds to λ_{hd} for highly ductile members in the *AISC Seismic Provisions* (AISC, 2010a) and is deemed adequate for considerable ductility demands without local buckling under the Design Seismic Hazards *(DSH)*. Limiting width-to-thickness ratios for links for eccentrically braced frames specified in the *SDSSB* Table 4.2-2 are recommended by Bruneau (2013). The limiting width-to-thickness ratio of elements for capacity-protected components, λ_r, corresponds to limits for

noncompact/slender elements given in the *AISC Specifications* (AISC, 2010b).

To avoid early deterioration of beam-column flexural strength and ensure ductility due to global buckling, the limiting slenderness ratios KL_b/r for columns and braces, and L_b/r_y for flexural members, are recommended to be checked in accordance with the *SDSSB* Table 4.3-1.

20.2.7.7 Concrete End Diaphragms and Integral Abutments

A concrete end diaphragm is preferred over steel end cross frames at seat-type abutments. These diaphragms distribute the longitudinal earthquake loads over the area of the backwall to improve mobilization of the soil behind the abutments, thus reducing the seismic demands on the columns. Even if the soil-abutment interaction is not accounted for, soil-abutment interaction during smaller earthquakes will reduce bridge movement and damage.

The concrete end diaphragm shall be continuous with the deck and extended as close as possible to the bottom flange of the girder. The end diaphragm should be designed to resist permanent loads, live loads, transverse and longitudinal wind, and lateral seismic loads. The concrete diaphragm to steel girder connection should include continuous reinforcement that is placed both behind the girder and through drilled holes in the girder web near the front face of the diaphragm to resist flexural stresses. Headed anchors shall be welded to the girder web to resist longitudinal shear and punching stresses. The connection of the diaphragm to the steel girder should be able to resist the longitudinal seismic soil pressures without the girder punching through it.

An integral diaphragm abutment connected with a concrete or steel superstructure can provide sustained soil mobilization when the abutment engages the backfill longitudinally and transversely. This type of interaction can increase the bridge's energy damping capacity, thus reducing seismic loads to the columns. The longitudinal resistance is limited to the smaller of either the passive capacity of the approach fill, structural capacities, or foundation capacities. The transverse resistance is governed by the foundation capacity. Seismic details of integral abutments for concrete superstructures have been well developed. Seismic integral abutment details for steel superstructures and applicability for longer span bridges, however, have not been developed and further research is needed. It should be pointed out that the bridge length might also affect the effectiveness of details. For longer span bridges, the integral abutment may not contribute much to the structural response, while shorter span bridges are generally more sensitive to the abutment response.

20.2.7.8 Integral Connection Systems

Integral connections between steel girder superstructures and concrete substructures make the entire structure act as one system to enhance the seismic performance of the bridge and may result in more economical foundations. The Integral connection systems are effective for short-span bridges. They become less effective as the effect of the frame action reduces with increasing span length. The use of this system can also eliminate the

need to raise the elevation of the bridge and improve aesthetics. The provisions specified in *SDSSB* Article 6.5 are based on research of integral concrete bent cap connection conducted by Patty et al. (2001). Integral steel box bent cap design requirements can be found in Wassef et al. (2004).

20.2.7.9 Shear Connectors

Shear connectors are required on the top flanges of girders, end cross frames, and diaphragms to transfer seismic demands from the concrete deck to substructure supports. For the transverse seismic load, the effective shear connectors should be taken as those located on the top of end cross frames or diaphragms, and flanges of girders within the longitudinal girder direction no further than $9t_w$ on each side of the outer projecting elements of the bearing stiffener group. For the longitudinal seismic load, the effective shear connectors should be taken as all those located on the girder flange within the tributary span length of the support. Force demands are specified in *SDSSB* Article 6.7.

20.2.8 SEISMIC RETROFIT PRACTICE

20.2.8.1 General

Since the 1971 San Fernando earthquake in Los Angeles, Caltrans has been engaged in a continuous bridge seismic safety retrofit program. The state's bridge earthquake retrofit program involves approximately 2,200 structures and costs more than $12 billion in construction. All 9 long span, steel, toll bridges have been seismically retrofitted. For important bridges, project-specific seismic design criteria need to be developed.

This section presents typical retrofit strategies for steel girder superstructures, steel bents, and seismic retrofit design examples for steel girder bridges, truss bridges, movable bridges, and suspension bridges.

20.2.8.2 Steel Girder Superstructures

There are two basic retrofit strategies for steel girder bridges. The first strategy is to allow the bearing system to deform and slide as a fuse and thus protect the substructure from being subjected to any potential larger seismic forces and, at the same time, prevent the unseating of the superstructure spans. This strategy may be preferred if the fusing force is low enough that the substructure can survive with little or no retrofit. The second strategy is to make sure that the bearings, without failure, transfer the full seismic force to the substructure. Retrofitting the substructure may be required. In both strategies, a superstructure retrofit is needed, although the extent is typically more significant with the fixed bearing scheme.

20.2.8.2.1 Simply Supported Girders

There are several methods of preventing the collapse of simply supported steel girders in the longitudinal direction. Since the 1970s, an early common approach was to use cable restrainers, as shown in Figures 20.2.8-1 and 20.2.8-2.
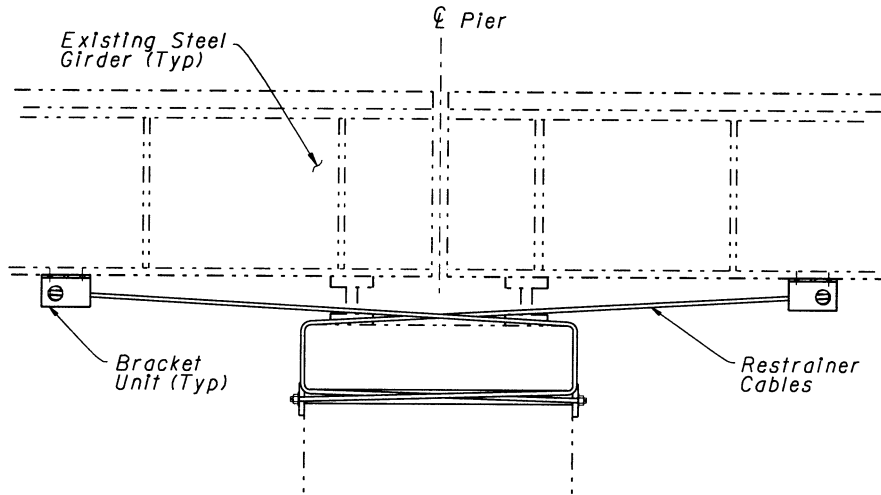
Figure 20.2.8-1 Bent Cap Cable Restrainers
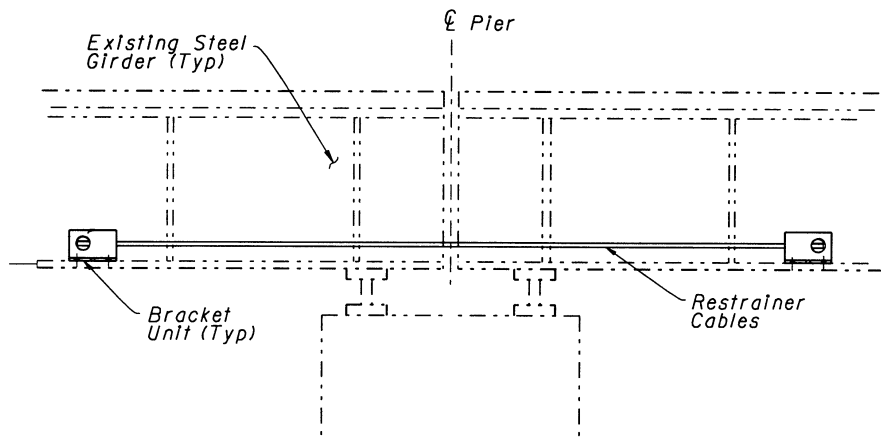
Figure 20.2.8-2 Girder to Girder Restrainer

When the expected longitudinal displacement is larger than the available seat width, a seat extender (Figure 20.2.8-3) or catcher (Figure 20.2.8-4) can be used together with or without cable restrainers. Catchers are designed to limit the superstructure drop to less than 6 inches which is a typical height in traditional rocker/keeper bearing systems; of course, the drop can be made much less. The catcher may also provide additional seat width. Seat extenders attached to abutments and drop caps typically consist of additional concrete scabbed onto the existing face, as shown in Figures 20.2.8-3, and are designed

as a corbel. One special consideration for catchers is to make sure to leave enough room to access the bearing for inspection and replacement. Clear details and notes to explain the intent are required, as the restraint of temperature movement can cause service failures in other parts of the bridge.
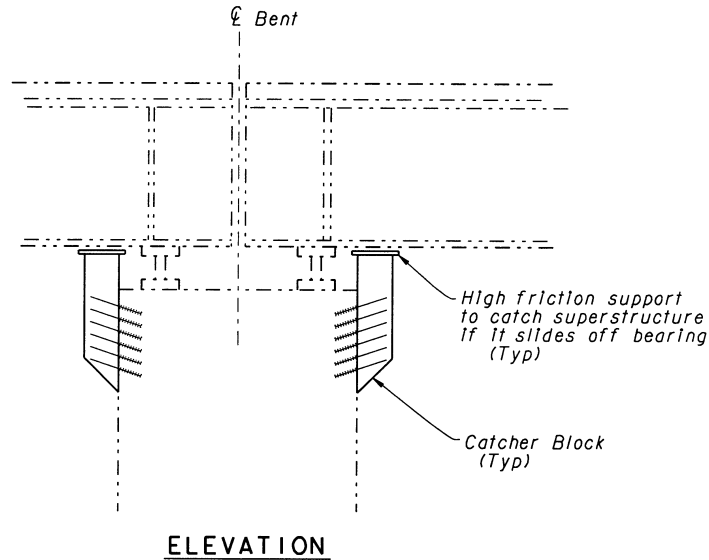
Figure 20.2.8-3 Seat Extenders for Steel Girder Bridge

Figure 20.2.8-4 Catchers for Steel Girder Bridge

Another retrofit solution is to provide continuity for simply supported girders over a support by bolting webs together with splice plates (Figure 20.2.8-5). The splice plate must be designed to support eccentric dead load shears assuming the span becomes unseated. The splice plate is bolted to the girder webs and has slotted or oversized holes to allow

for temperature movement. This retrofit solution usually works for most low skewed girders in a straight alignment but not for irregular structures. Again, clear details and notes to describe the intent are required, as the restraint of temperature movement can cause service failures in other parts of the bridge.
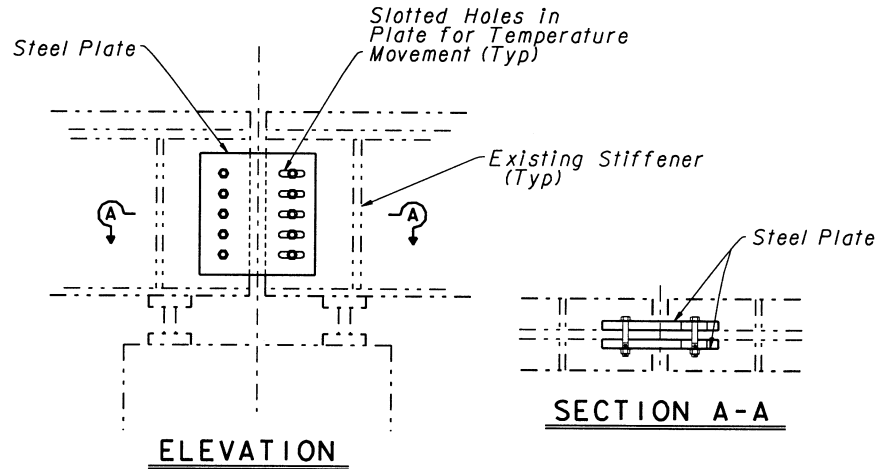

Figure 20.2.8-5 Continuous Splice Plates

20.2.8.2.2   Continuous Girders with In-Span Hinges

For older continuous steel girders, hinges are typically placed near the point of zero dead load moment. These hinges can be either seat type, as shown in Figure 20.2.8-6(a), or hanger type, as shown in Figure 20.2.8-6(b). The hanger-type hinges are designed for strengths that are typically larger than forces that can be imparted onto the hanger bar from an extreme event; thus, retrofitting the hanger bar is unnecessary. Hanger-type hinges typically have more seismic resistance than seat-type hinges but may still be subjected to seismic damage. It can usually be assumed that any seat-type hinge used with steel girders will need additional transverse, longitudinal, and vertical restraints in even moderately severe seismic areas. Considerations should be given to replacing them or adding supplemental transverse and vertical restraints. Cross bracings or diaphragms on both sides of the hinge pin may have to be improved to limit wobble and racking. In-span hinge details are rarely used in the design of modern steel girder bridges.

(a)   (b)
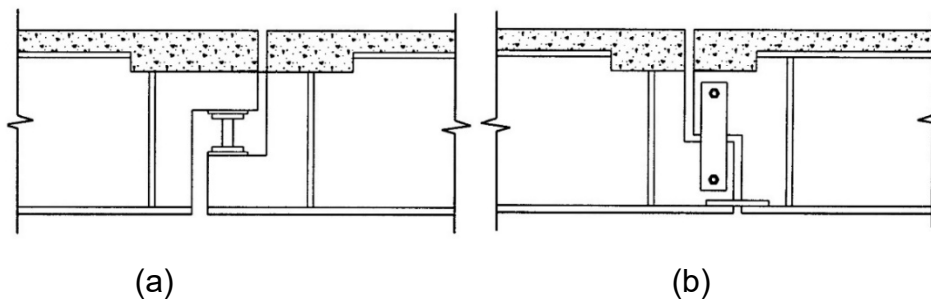
Figure 20.2.8-6 In-Span Hinges

20.2.8.3   Steel Substructures

Steel substructures (bents) for older girder bridges usually include two types: trestle bents, typically found in bridges spanning canyons, and built-up open-section columns often found on elevated viaducts.

Trestle steel bents are commonly supported on pedestals resting on a rock or relatively dense foundations. In general, the truss members in these bents have very large slenderness ratios that lead to very early elastic buckling under low-magnitude earthquake loading. Retrofitting of this type of bent consists primarily of balancing between member strengthening and enhancing the tensile capacity of the foundation by keeping connection capacities larger than member capacities. In many situations, foundation retrofit is not needed where the bent height is not large, and a stable rocking behavior of the bent can be achieved. Strengthening of the members can be obtained by increasing the cross-sectional area of the truss members or reducing the unsupported length of the members. Figure 20.2.8-7 shows the retrofit of the Castro Canyon Bridge in Monterey County, California. The bent retrofit consists of member strengthening and the addition of a reinforced concrete block around the bent to pedestal connection. In this bridge, the pedestals were deeply embedded in the soil, which added to the uplift capacity of the foundation. For very tall trestle bents, foundation tie-downs, in addition to member strengthening, might be needed to sustain large overturning moments.

Built-up open section columns are typically I-shaped sections including angles and plates bolted or riveted together. These members may fail due to yielding, local and global flexural buckling, or lateral torsional buckling. For members containing a single I-shaped section, lateral torsional buckling typically governs. Retrofit of built-up columns consists of enclosing the section by bolting channel sections to the flanges. Figure 20.2.8-8 shows this type of retrofit. Installation of these channels is made possible by providing access through new elliptical hand holes. These holes are later covered by tack welded or screwed cover plates or may be left open. For larger members with an open section, as shown in Figure 20.2.8-8, retrofit consists of closing the existing cross section into a multi-cellular box section.
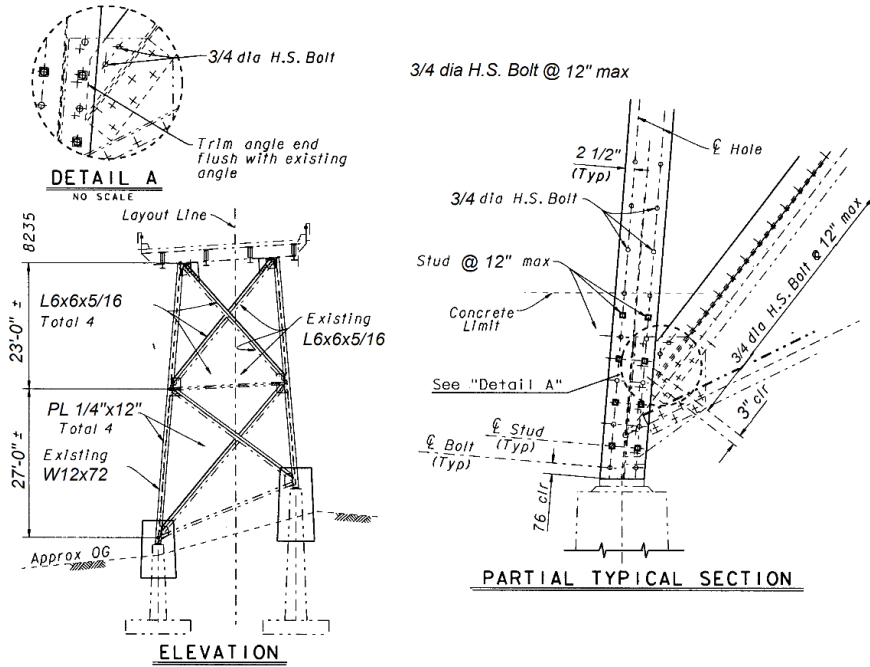
Figure 20.2.8-7 Trestle Bent Retrofit
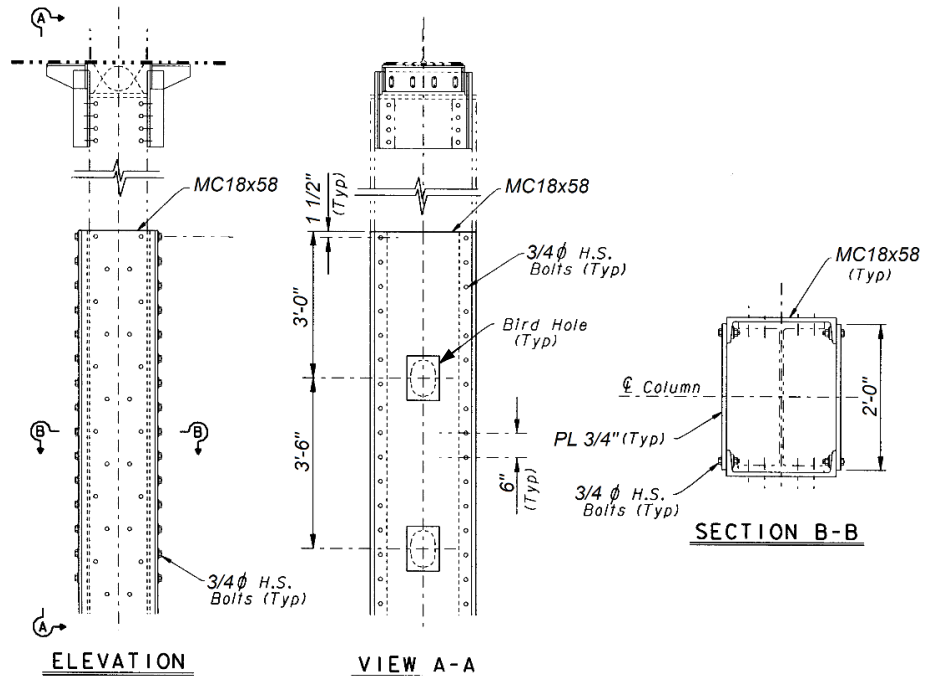

Figure 20.2.8-8 I-Shape Column Retrofit

20.2.8.4   San Francisco Bayshore Viaduct

20.2.8.4.1   Bridge Description

The San Francisco Bayshore Viaduct is the elevated structure supporting I-80 over ten city blocks between the 4th and 15th streets in the city of San Francisco. It serves as the western approach for the San Francisco-Oakland Bay Bridge linking points south along Highway 101. The structure was built in 1955.

The superstructure width varies from 26 ft to 76.77 ft and consists of a series of simply supported girder spans with a total length of 7,502 ft. Most of the spans are steel plate girders composite with reinforced concrete decks supported on steel rocker bearings mounted on steel bent cap webs supported on single or multi-column steel bents (Figure 20.2.8-9), multi-column concrete bents (Figure 20.2.8-10) or pier wall bents. At 5th, 6th, and 7th Streets, the superstructure is a simply supported reinforced concrete box girder span on multi-column concrete bents. Span lengths range from 14.11 ft to 118.11 ft. Column heights range from 12 ft to 40 ft. Columns are supported on pile foundations or spread footings. The cable restrainers connecting steel girders and the bent caps and lateral shear keys at the abutments were added in 1973.

Figure 20.2.8-9 San Francisco Bayshore Viaduct – Steel Column Bents

Figure 20.2.8-10 San Francisco Bayshore Viaduct – Concrete Column Bents

20.2.8.4.2   Seismic Retrofit Performance Criteria

The seismic retrofit design of the San Francisco Bayshore Viaduct was based on the no collapse philosophy. After a major earthquake, the structure is expected to be closed until inspected and approved by Caltrans for emergency and/or vehicular traffic.

The objectives of the seismic retrofit are:

- To prevent the superstructure girders from unseating from bent caps.

- To provide ductile mechanisms to transfer seismic forces in both longitudinal and transverse directions effectively.

- To limit the local buckling of steel columns, especially single column bents.

- To ensure the column plastic moment can be developed at the top of the footing.

20.2.8.4.3   Seismic Retrofit Analysis

The structure is 8 miles away from the San Andreas Fault with an anticipated M_w = 8.0 magnitude earthquake. The maximum horizontal bedrock acceleration at the structure site is expected to be 0.5g. The depth of bedrock is greater than 150 ft. Liquefaction potential is likely in the fine sand layers.

Three sets of Acceleration Response Spectra (ARS) curves as shown in Figures 20.2.8-11 to 20.2.8-13 were developed for the project.
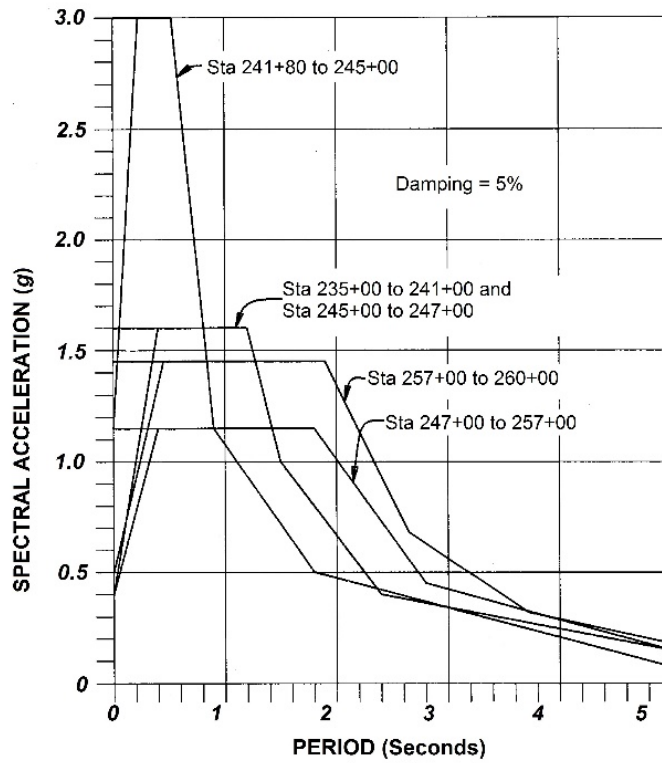
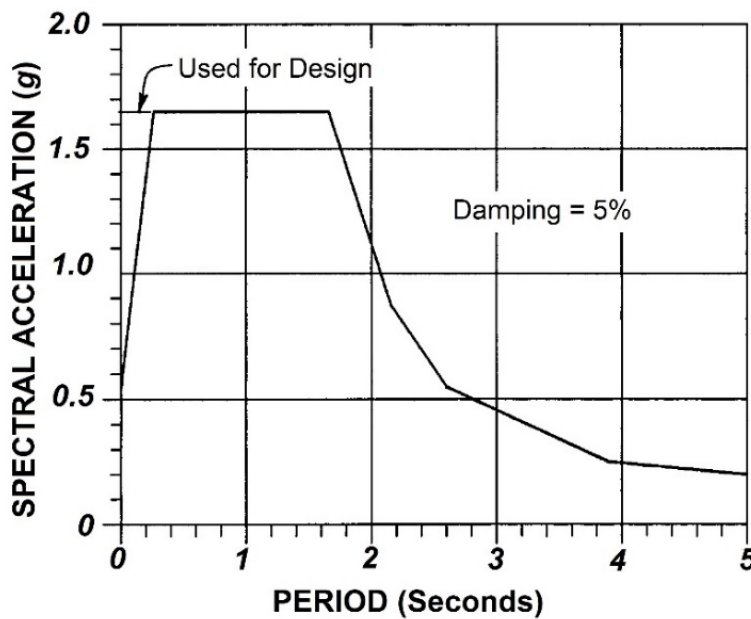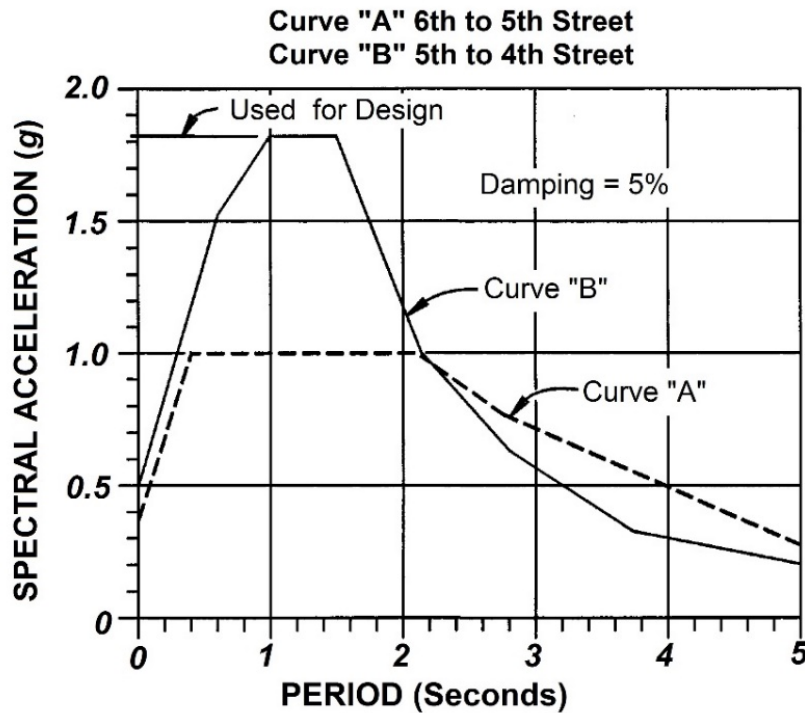**Figure 20.2.8-11 ARS Curves for Bayshore Viaduct from 16th to Bryant Streets**

Figure 20.2.8-12 ARS Curves for Bayshore Viaduct From Bryant to 6th Street

Curve "A" 6th to 5th Street
Curve "B" 5th to 4th Street

Figure 20.2.8-13 ARS Curves for Bayshore Viaduct From 6th to 4th Streets

The elastic dynamic response spectrum analysis was performed for the existing structure using STRUDL with several computer models (Akkari and Hoffman, 1993).

In the as-built structure model, the simply supported superstructure spans were modeled with a pin at one side of the bent cap and a roller at the other side of the cap with a cable element across the cap, and the bases of columns were assumed fixed. In the retrofitted structure model, the bottoms of columns that are not retrofitted were assumed to form plastic hinges and were modeled with a pinned connection at the bottoms of the columns. A dynamic-equivalent static analysis utilizing small portions of the structure was used to check the results obtained from STRUDL.

The static pushover analysis was performed using equivalent static load factors based on ARS curves as discussed above. Loads are applied to the bent cap from the center of gravity of the superstructure. Displacement demands in the transverse direction were calculated assuming a fixed-free standing cantilever for single column bents and fixed-fixed frame condition for two-column bents. Displacement demands in the longitudinal direction were based on a fixed-fixed condition due to bearing retrofits, energy absorption when slotted holes in bearing catchers close, and load reduction due to the out-of-phase motion.

Displacement capacity of steel column bents, Δ_c, was taken as the sum of yield displacement due to flexural bending, plastic displacement due to plastic hinge rotation, as shown in Figures 20.2.8-14 and 20.2.8-15, and displacement due to anchor rod ductility (not shown in those figures).

$$\Delta_c = \Delta_y + \Delta_{pl}$$

Δ_y = Yield Displacement

Δ_{pl} = Plastic Displacement
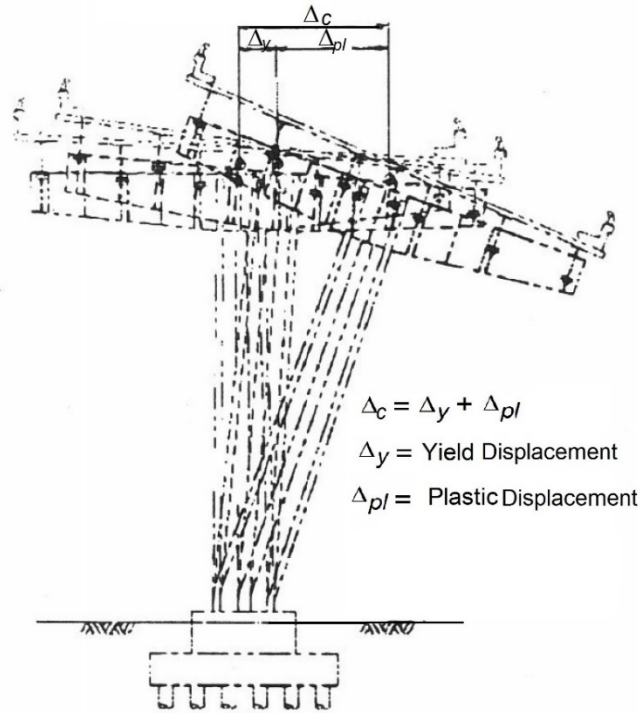
Figure 20.2.8-14 Displacement of Single Steel Column Bent

$$\Delta_c = \Delta_y + \Delta_{pl}$$

Δ_y = Yield Displacement

Δ_{pl} = Plastic Displacement
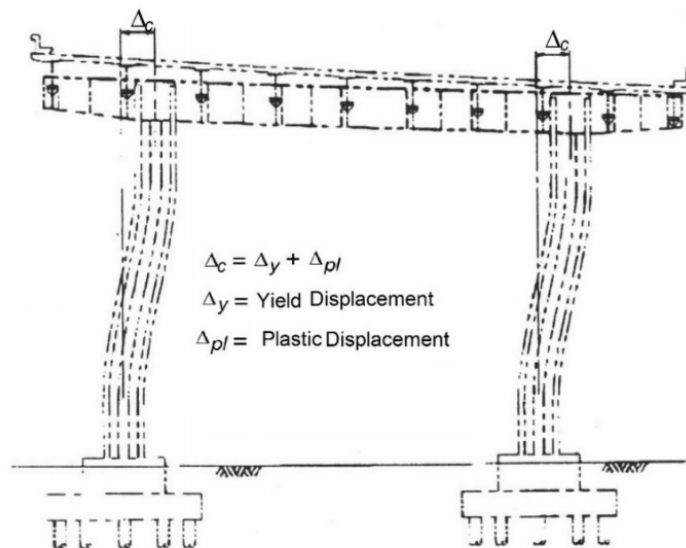
Figure 20.2.8-15 Displacement of Double Steel Column Bent (Un-retrofitted)

20.2.8.4.4   Retrofit Strategies

San Francisco Bayshore Viaduct was seismically retrofitted in 2001. The seismic retrofit strategy of steel built-up columns was proof-tested by Holombo et al. (1995). A total of

three 5/8th scale steel bridge columns were tested to evaluate the performance at high levels of ductility. The first and second tests were typical "as-built" columns, while the second modeled a retrofitted box-shaped column. The as-built column specimen achieved a displacement ductility of 4. The retrofitted specimen achieved a displacement ductility of 6.

The superstructure retrofit included:

- Adding girder seat extensions or catcher beams at all steel caps (Figure 20.2.8-16).

- Providing restraining rods.

The substructure retrofit included:

- Providing knee braces at all steel bents. (Figure 20.2.8-17).

- For multi-column concrete bents: retrofitting bent cap, columns, and footings at Bents across 5th, 6th, and 7th Streets to act as super bents; retrofitting columns and footings at approximately every fourth bent between those streets; and adding diagonal steel cross bracing at every bent (Figure 20.2.8-18).

- For pier wall bents: retrofitting the footing only by increasing the footing depth with the addition of a top mat of steel and adding new piles.

- For single and multi-column steel bents: retrofitting columns by adding cover plates, grillages, and footings at most locations (Figure 20.2.8-19); adding external columns at the other few locations where clearance is a problem; and adding cross bracings at some multi-column bents.
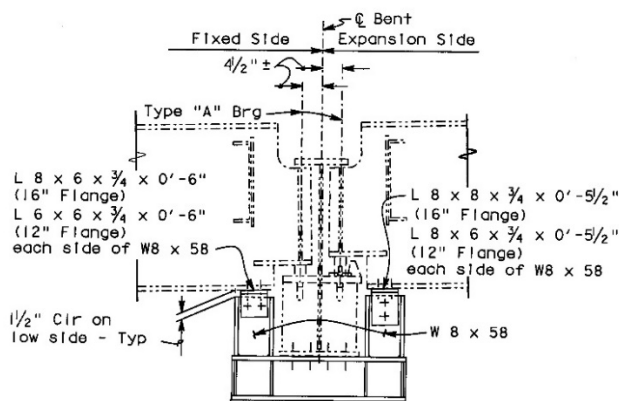
Figure 20.2.8-16 Bayshore Viaduct Superstructure Girder Seat Extension
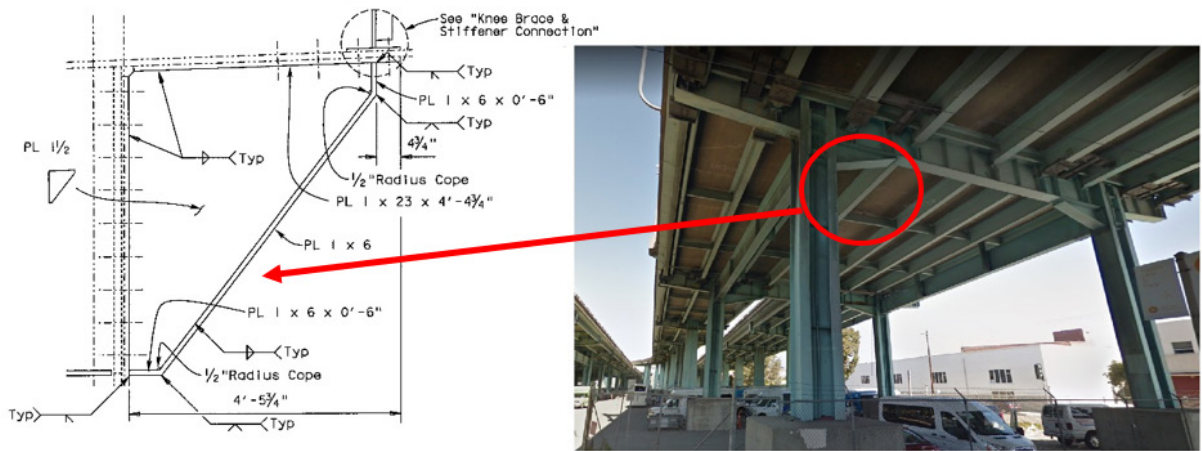
Figure 20.2.8-17 Bayshore Viaduct Bent Cap Knee Brace

Figure 20.2.8-18 Concrete Bent Retrofit - Diagonal Cross Bracings
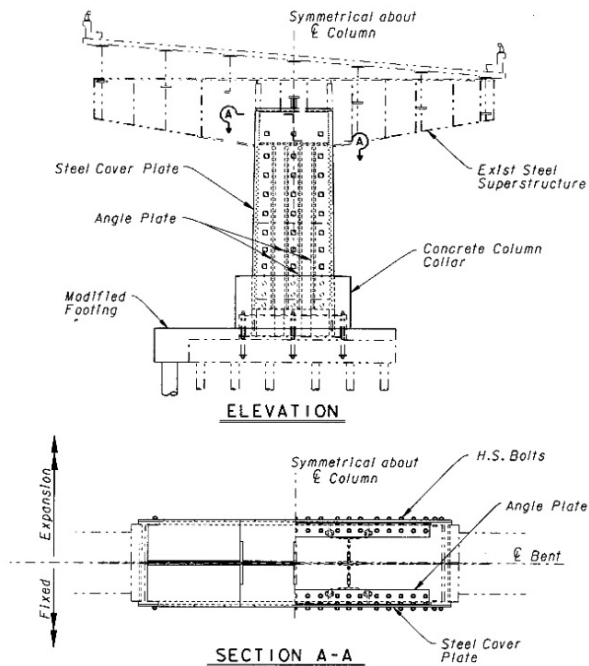
Figure 20.2.8-19 Steel Column, Grillage, and Footing Retrofit

20.2.8.5   Antioch Bridge

20.2.8.5.1   Bridge Description

The Antioch Bridge (Figure 20.2.8-20) is on State Route 160 in the city of Antioch and was completed in 1978. The bridge is 9,432.75 ft long and comprised of two main structures: the main channel crossing and a slab structure. The main structure is 8,650 ft long with 40 spans arching over the San Joaquin River, with the midsection rising as high as 147 ft to allow for ship passage. The bridge is 43.5 ft wide and carries one lane of traffic in each direction, as shown in Figure 20.2.8-21. The superstructure consists of two weathering steel plate girders that are continuous over the piers. The steel girders are in excellent condition, having formed the expected uniform protective outer coating with no degradation in structural capacity.

Figure 20.2.8-20 Overview of Antioch Bridge
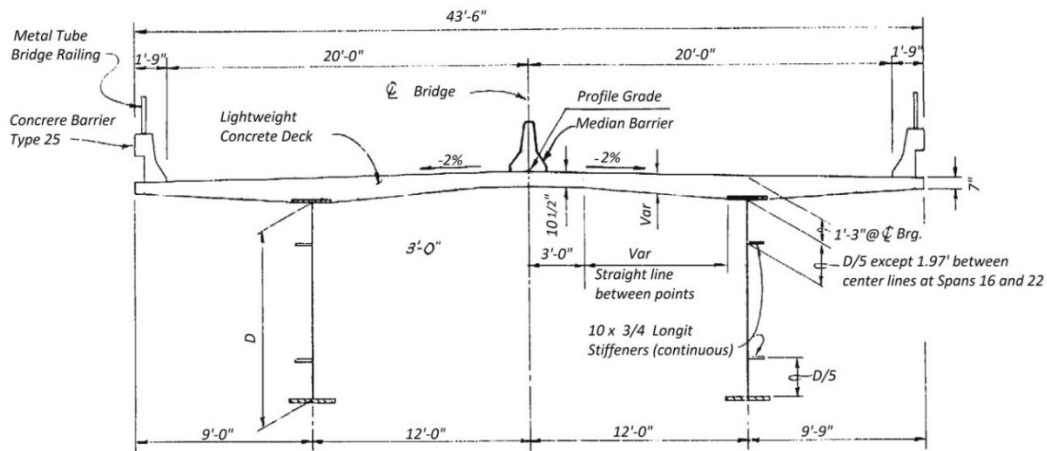
Figure 20.2.8-21 Typical Cross Section of Main Channel Crossing

20.2.8.5.2   Seismic Retrofit Performance Criteria

The bridge's average daily traffic is 15,000, a relatively small number compared to other toll bridges in Northern California. However, because it crosses the San Joaquin River, which is an important navigational channel, Antioch Bridge is classified as an "Important Bridge", and project-specific seismic design criteria (Caltrans, 2011) were based on the SEE, specified as the 1000-year return period design earthquake. Retrofit performance is "no collapse" with permissible damages in parts of the pier pile groups and the deck expansion joints.

20.2.8.5.3   Seismic Retrofit Analysis

Three sets of ARS curves were developed for the retrofit design, as shown in Fig. 20.2.8-22. In addition to ARS design curves, seven sets of pier-specific kinematic time histories

were developed for seven earthquake time histories; with each pier having three-component kinematic motions for the design earthquake.
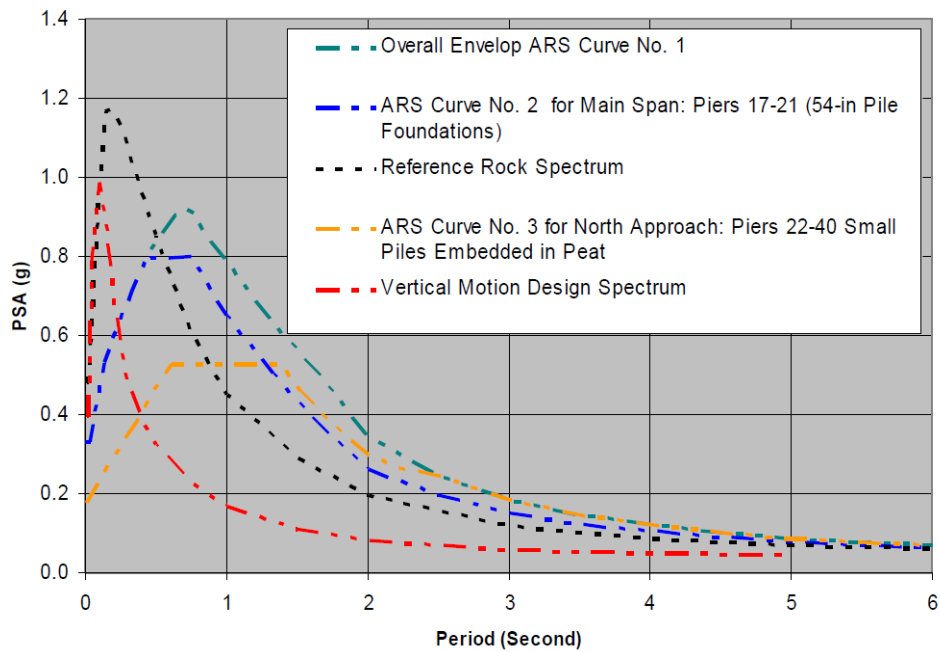
Figure 20.2.8-22 Site-Specific Design ARS Curves

The as-built bridge was initially analyzed with a global dynamic analysis based on ARS curves with an equivalent 6x6 matrix stiffness for the pile group at each pier. The SAP2000 global model (Figure 20.2.8-23) was developed with effective stiffness for all the structural members and as-built boundary conditions to assess the vulnerabilities and also to formulate the retrofit strategy. Later, the as-built bridge and the retrofitted bridge were analyzed with a global dynamic analysis using Nonlinear Time History Analysis (NTHA). Individual piers with the piles and their respective soil springs attached to them were modeled separately to perform pushover analysis and determine each pier's displacement capacity. These displacement capacities were compared to the displacement demands obtained from the NTHA of the retrofitted global model to verify whether the retrofit scheme worked.
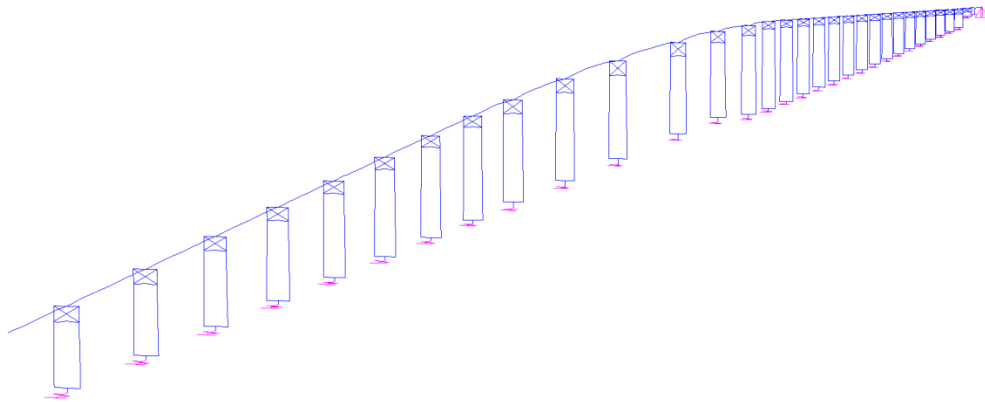
Figure 20.2.8-23 SAP2000 Global Model

The analysis of the existing bridge exposed the following deficiencies during the SEE.

- Shear failure in the existing columns and the bent caps.

- Premature failure of existing rebar couplers at the base of the columns due to known test failures of the same brand types used in other projects.

- Stability of the bridge was undermined by damage in the pile groups.

- Pin hanger hinges failure due to possible misalignment of the girders.

Although the existing superstructure carries only two traffic lanes and is relatively light, isolating the superstructure proved to be an effective solution. Single-surface friction pendulum isolation bearings were selected for the design due to the restricted vertical clearances. Two sizes were used to accommodate different magnitudes in loading conditions. The larger bearings are 7.2 ft in diameter, 9.2 in. thick, and have 23 in. of maximum displacement capacity. The smaller ones are 5.8 ft in diameter, 7.2 in. thick, and have 20 in. of maximum displacement capacity.

20.2.8.5.4   Retrofit Strategies

The seismic retrofit of the Antioch Bridge based on isolating the superstructure is a simple but effective solution. Implementing this scheme by adding steel cross braces to the concrete pier frames was necessary to stiffen up the tall and flexible piers to make the isolation of the superstructure effective. Shop fabricated segments of the steel braces were field assembled with bolted connections, and the bracings were easily integrated into the existing concrete frame by connecting the two different elements through a cast-in-place concrete pedestal. Due to steel's lightweight, the additional weight of the bracing could be accommodated within the capacity of the existing foundation. Not requiring a foundation retrofit meant significant savings in the construction cost and also minimized the disturbance to the sensitive environment.

The seismic retrofit design started in 2008 and project construction, as shown in Figure 20.2.8-24, was completed in April 2013. Final main channel crossing retrofit measures included (Kim, 2012; Caltrans, 2011):

- Replacing existing bearings at all 39 piers and abutments with seismic isolation bearings (Figure 20.2.8-25).

- Installing cross frame bracings from Pier 12 to Pier 31 (Figure 20.2.8-26).

- Adding shear keys at intermediate hinges (near Pier 7, 14, 25, and 32).

- Installing longitudinal restraining brackets at Piers 5, 11, 19, 20, 28, and 36 to prevent the superstructure frames from sliding down under seismic loads.
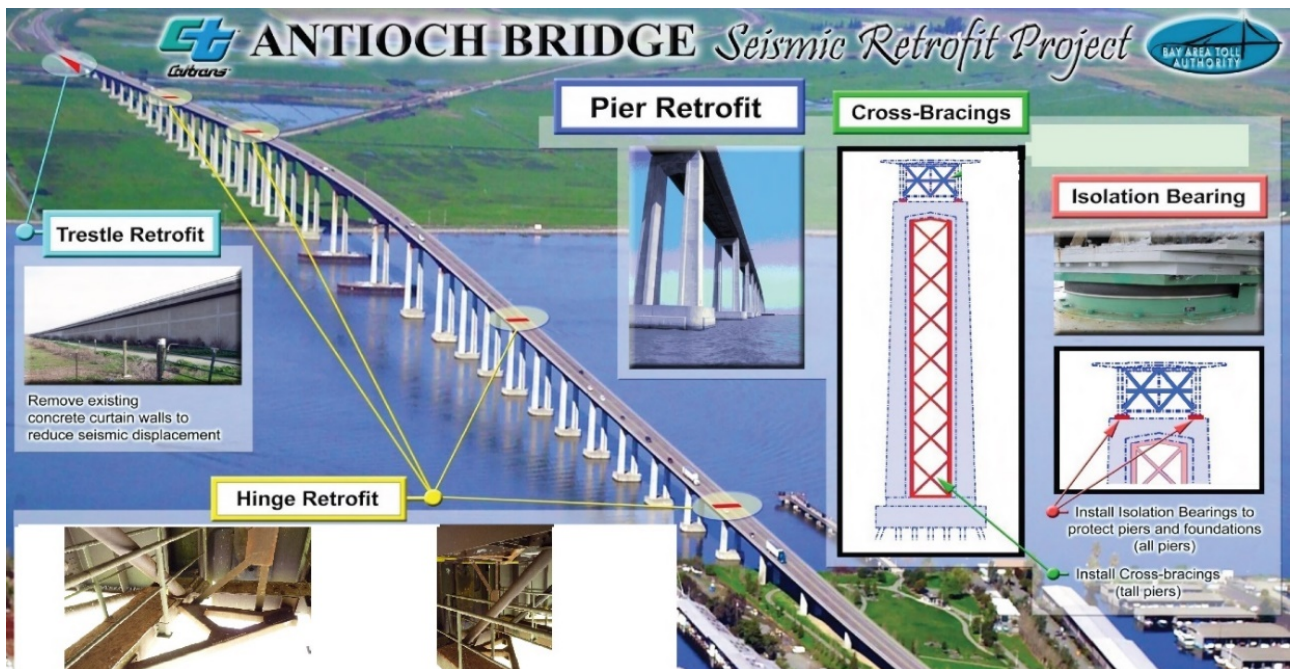

Figure 20.2.8-24 Antioch Bridge Seismic Retrofit Project

Figure 20.2.8-25 Typical Seismic Isolation Bearings Installed

Figure 20.2.8-26 Pier Cross Frame Bracings under Construction

20.2.8.6   Dumbarton Bridge Main Span

20.2.8.6.1   Bridge Description

The Dumbarton Bridge is on State Route 84 connecting the cities of Newark and East Palo Alto and is the southernmost crossing of the San Francisco Bay. It was completed in 1982. The bridge is 8,600 ft long and carries three lanes of traffic in each direction with a separate bike/pedestrian lane. The bridge is comprised of five main structures: the main channel crossing, east and west approach structures, and east and west trestle structures, as shown in Figure 20.2.8-27.

The main channel crossing extends from Pier 16 to Pier 31 and is 3,150 ft in length. The spans vary in length from 175 ft to a maximum of 340 ft. for the main span (Span 23). The superstructure consists of four frames of continuous twin steel box sections with a composite concrete deck. The superstructure is 10 ft 7½ in. deep and tapers down to 8 ft 1½ in. at the end spans. The deck is 85 ft wide. At each pier, the steel boxes have cross frames to resist lateral seismic movement and are supported on a reinforced concrete pier cap that connects two columns. Four extra strong steel pipes connect each steel box to the pier cap. Two In-span hinges are located in Spans 21 and 25, which allow thermal movement and locks under seismic movement with thrust buffers.

Figure 20.2.8-27 Dumbarton Bridge

The substructure at each pier consists of two hollow concrete columns battered in a V-shape in the transverse direction, as shown in Figure 20.2.8-28. The longitudinal bars in the columns have staggered couplers at the base, which are about 8 ft from the bottom, with a rated capacity of 80 ksi minimum. The columns for Piers 17 through 26 are supported on a single pile cap (at mean sea level) supported on 54 in. diameter concrete-filled prestressed hollow concrete piles. These piles have a varying free standing height

in water with pile tip elevation of -40 to -60 ft. These piles are rigidly connected to the pile cap through dowels. The columns at Pier 16 and Pier 27 to Pier 31 are supported on concrete pile caps, rigidly connected through dowels to 20 in. diameter, 0.344 in. thick steel pipe piles filled with concrete. At the bottom of the pile cap, a tremie seal of 4 ft below the mud line was poured from Pier 27 to Pier 31 and 10.5 ft at Pier 16.

The east and west approach structures are 2,850 ft and 2,600 ft in length, respectively, and consist of four frames. The superstructure is 85 ft wide, 8.25 ft deep, and consists of five precast, prestressed delta shaped girders with a composite concrete deck. The substructure at each pier consists of two hollow concrete columns battered in a V-shape in the transverse direction similar to the main channel crossing.

Both east and west trestle structures are 600 ft long with 20 spans, each 30 ft long. The deck is a 17 in. thick reinforced concrete slab with three expansion joints in each structure. The deck is supported on a concrete bent cap with 7- 20 in. concrete piles at each bent.
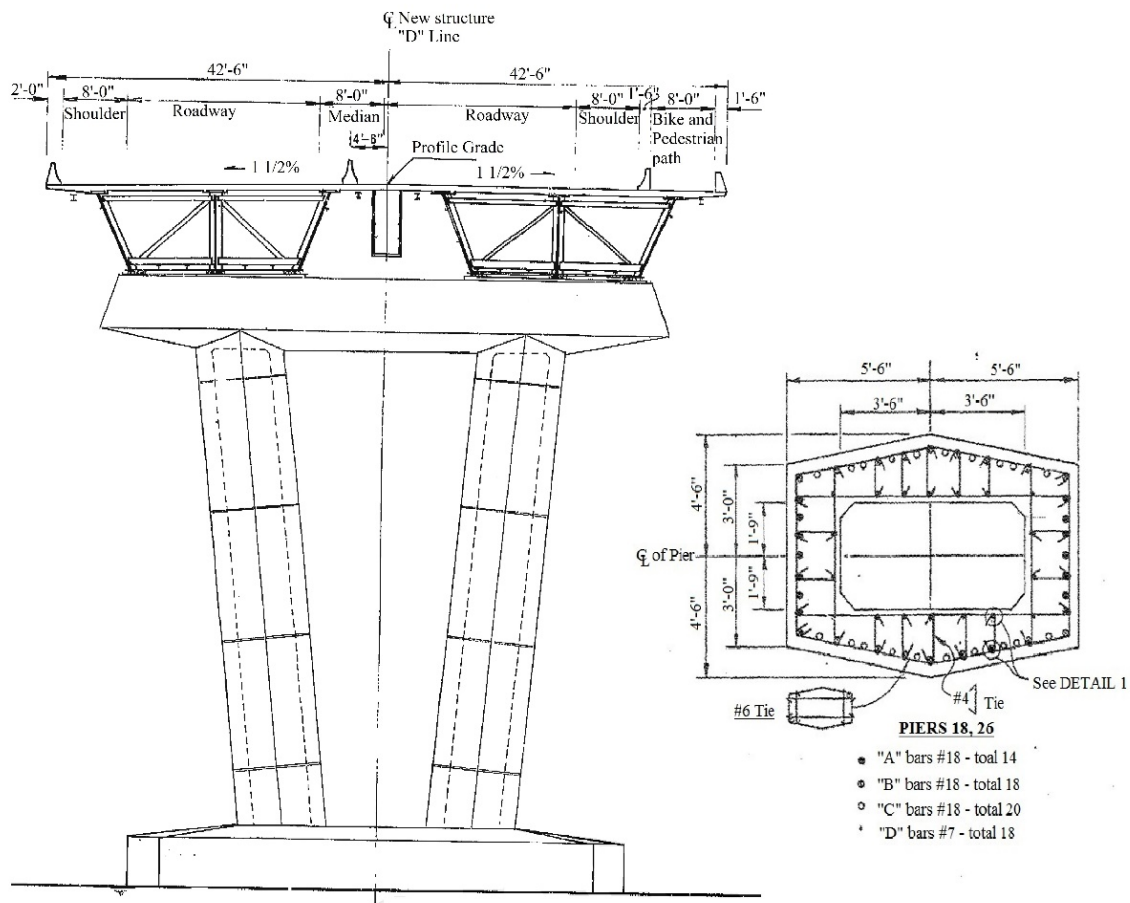

**Figure 20.2.8-28 Typical Section of Main Channel Crossing**

20.2.8.6.2   Seismic Retrofit Performance Criteria

Dumbarton Bridge is classified as an "Important Bridge". The seismic performance criteria for the Dumbarton Bridge were twofold: the SEE and the FEE. The SEE performance is specified as the 1000-year return period design earthquake with acceptable damage at predetermined locations. FEE performance is specified for acceptable damage by opening the bridge to full traffic within 6 months after a design earthquake event. The repairs to acceptable damage could be done under traffic with lane closures.

20.2.8.6.3 Seismic Retrofit Analysis

Two sets of ARS curves, as shown in Figure 20.2.8-29, were developed. ARS Curve 1 covers Piers 1 through 16 and Piers 27 through 44, representing 20-in. diameter pipe piles with a buried pile-cap. ARS Curve 2 covers Piers 17 through 26, representing 54-in. diameter concrete piles with a long cantilever pile extending the above mud-line.

In addition to ARS design curves, seven sets of pier-specific kinematic time histories were developed, with each pier having three-component kinematic motions for the given earthquake.
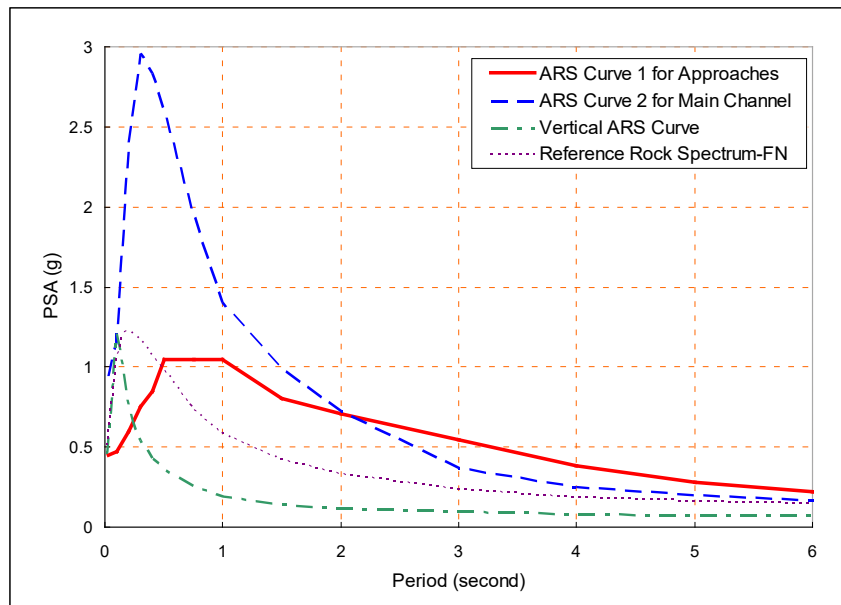
Figure 20.2.8-29 Site-Specific Design ARS Curves

ARS and NTHA of the entire structure (global models) were performed to capture the overall dynamic response of the bridge using SAP2000. The global model included east and west approaches and the main channel crossing as shown in Figure 20.2.8-30. The ARS global model was based on effective stiffness for all the structural members with as-built boundary conditions. ARS analysis was performed using site-specific ARS curves for both tension and compression models.
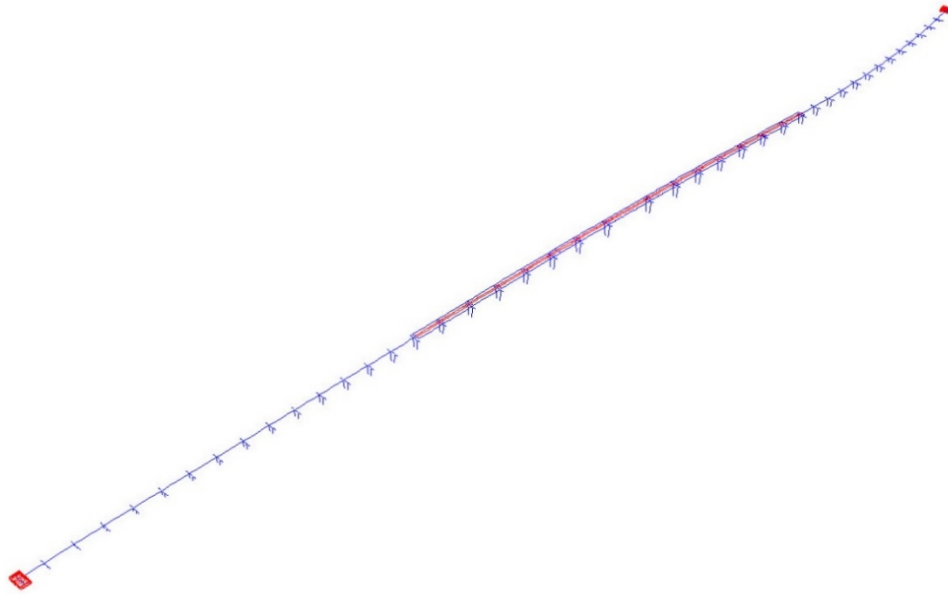
Figure 20.2.8-30 SAP2000 Global Model

The global model for NTHA was based on the as-built condition for approaches and retrofitted condition for the main channel crossing with friction pendulum isolation bearings modeled as nonlinear elements from the SAP library. Demands for an average of seven sets of time histories were computed. The soil-foundation-structure interaction (SFSI) was captured with a 6x6 linear spring and mass matrix at the top of piles at each pier.

Local models or Stand-Alone models of Piers 17 and 23 within the main channel crossing were developed to conduct SFSI analysis in the two principal directions - transverse and longitudinal. SFSI was modeled using depth varying non-linear *p-y, t-z,* and *q-z* curves representing nominal and overstrength foundation conditions. Moment-curvature relationships were developed to model plastic hinges for hollow columns, prestressed hollow concrete piles filled with concrete, pier caps to diaphragm connections, and pedestal supporting columns. Pipe pile hinges were modeled with *P-M-M* (axial load-biaxial moments) fiber hinge with a plastic hinge length of 1.5 times the pile diameter. These models were used to perform non-linear static pushover analysis to predict the sequence of failure of each component of the pier. Both ARS and NTHA displacement demands for pile caps, superstructures, and columns (shafts) were obtained from global models in transverse and longitudinal directions. These displacement demands were used in the pushover analysis of local models to check the response of all the members of the pier. Figure 20.2.8-31 shows the local model for Pier 23, one of the tallest piers, supporting the longest main span.
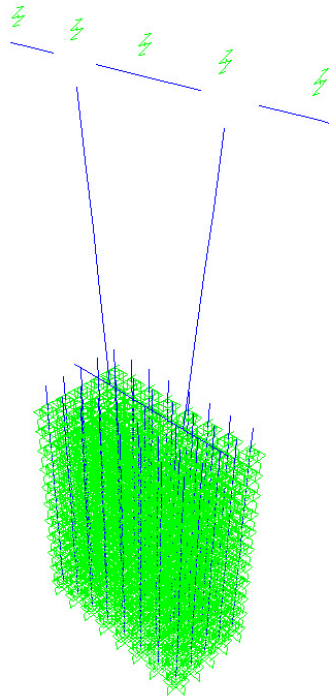
Figure 20.2.8-31 Typical Local Model - Pier 23

Results of pushover analyses, of selected piers, of the main channel crossing showed deficiencies in foundations. Hinges formed in the prestressed concrete piles at the pile cap connection and below ground. Plastic hinges in the columns also formed. Results of a finite element analysis on the steel box superstructure showed elastic buckling of the thin webs and yielding of the vertical stiffeners when subjected to displacement demands from the ARS global model demands. Results obtained from global models, local models, and steel box superstructure models showed the following deficiencies:

- Plastic hinging of the 54 in. diameter concrete filled prestressed hollow concrete pile

- Elastic buckling of the thin web panels at sections close to the pier support

- Buckling of the compression and subsequent failure of tension braces in steel box cross frames at the pier.

- Plastic hinging of columns at the bottom where columns have couplers at the base.

20.2.8.6.4   Retrofit Strategies

Experimental tests of 1/3 scale models of Pier 23 and Pier 37 were performed to verify the flexural capacity of Dumbarton Bridge hollow columns, and joint shear capacity of column-pier cap joint and column-pedestal joint (Phillippi et al., 2010). These tests

showed the reliable ductile behavior of hollow columns with a ductility of five. In both of these tests, the bent cap-column and the column to pedestal joints remained essentially elastic.

The seismic retrofit design started in early 2007, and construction was completed on February 21, 2013. The main channel crossing retrofit included (Masroor et al., 2013):

- Installing 96 low height friction pendulum isolation bearings (Figure 20.2.8-32).

- Strengthening existing steel box cross frames at the piers to raise the steel box girders five inches to install isolation bearings.

- Constructing new cross frames at Pier 16 and Pier 31 (Figure 20.2.8-33).

- Strengthening the pile caps by providing a top mat of reinforcement.

- Strengthening and widening existing pier caps by adding concrete bolsters on the sides to increase torsion capacity and to accommodate isolation bearings.

- Retrofitting existing in-span hinges between frames by adding hinge assembly units to restrain longitudinal seismic movements beyond thermal (Figure 20.2.8-34).

- Installing seismic isolation joints at Pier 16 and Pier 31 by removing a portion of the existing steel box and the existing isolation joint (Figure 20.2.8-35).

Figure 20.2.8-32 Typical Isolator Bearing Installed

Figure 20.2.8-33 Typical Strengthened Cross Frame at Piers
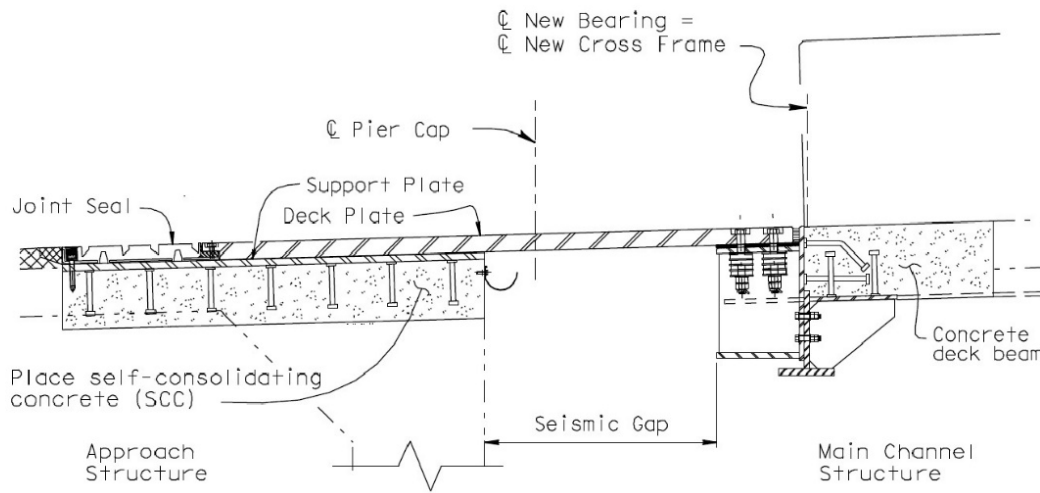
Figure 20.2.8-34 Seismic Joint Detail
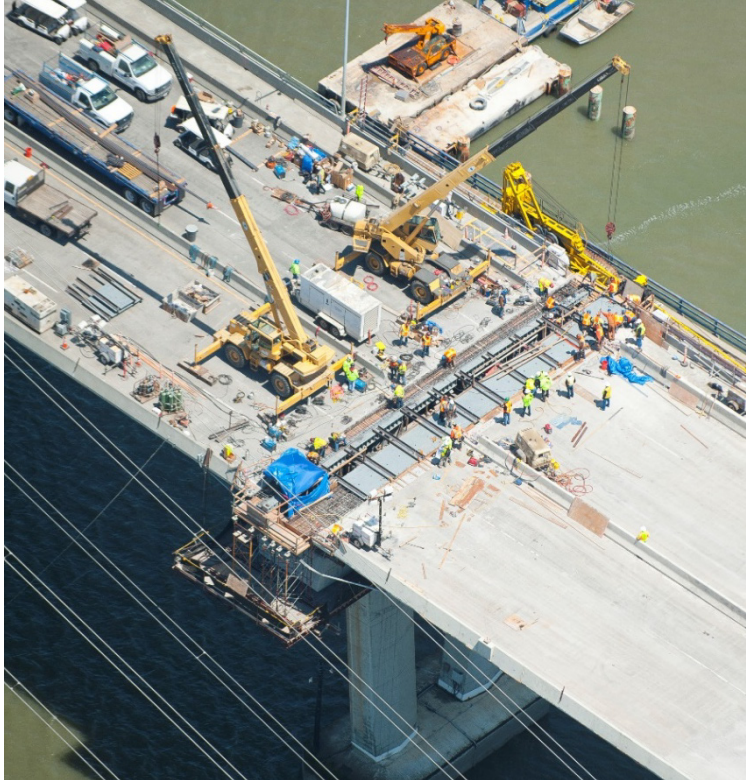
Figure 20.2.8-35 Seismic Isolation Joint at Pier under Construction

20.2.8.7   Sacramento River Paintersville Bridge

20.2.8.7.1   Bridge Description

The Sacramento River Paintersville Bridge is located near the Town of Courtland, California, over the Sacramento River on State Route 160. It is one of the oldest movable bridges crossing the Sacramento River. This bridge (Figure 20.2.8-36), with a total length of 588 ft and a width of 21 ft, includes three parts: Pratt steel through truss approach spans of each 120 ft, the double leaf Strauss bascule main spans of 226.3 ft, and the tower truss spans of each 57 ft. All four piers have the same dimensions, including three parts: a pier cap at the top, a pier wall in the middle, and two 10 ft diameter columns at the bottom. The piers are supported by timber piles embedded into loose sandy and soft clay soil. The sliding/rocking bearings are used to support the truss on the seat type abutments, and the fixed bearings (anchor bolts) are connected to the piers. All truss members are built-up members with angles, channels, and plates. The bridge (Figure 20.2.8-37) was built in 1923. The original wooden deck was replaced with a steel grid deck in 1953 and rehabilitated in 2000.
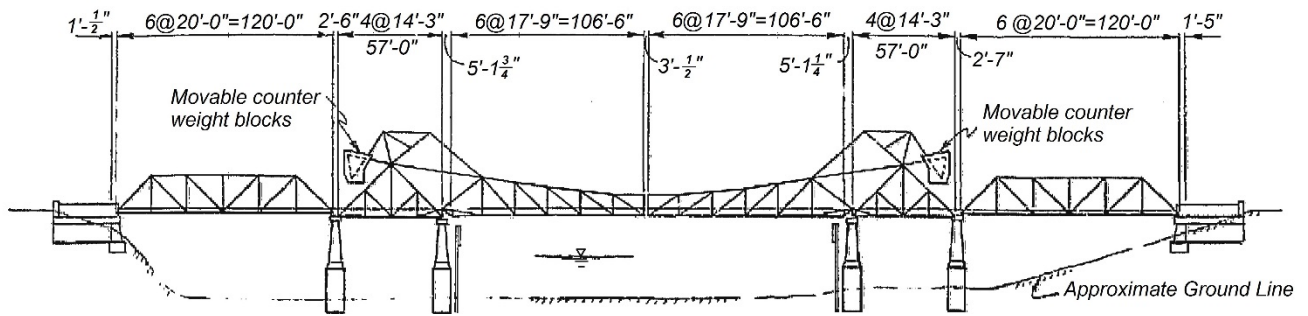
Figure 20.2.8-36 Elevation of Sacramento River Paintersville Bridge

Figure 20.2.8-37 Overview of Sacramento River Paintersville Bridge

20.2.8.7.2   Seismic Retrofit Performance Criteria

The seismic retrofit design of Paintersville Bridge was based on no collapse criteria. The structure is expected to suffer repairable damage without closure following a major earthquake. Force Demand/Capacity (*D/C*) ratios were checked for the seismic retrofit acceptance measurement (Caltrans, 2015).

20.2.8.7.3   Seismic Retrofit Analysis

The bridge site is underlain by Holocene alluvium deposits, including gravel, sand, and silt with organic matter from the present-day stream and river system, and surrounded by

Holocene basin deposits. Based on the geologic information, a V_{s30} of 886 ft/sec. was assumed to apply to the foundation materials. According to Caltrans ARS Online Tool, the nearest controlling active fault is the Great Valley 06 (Midland) alt2 (Fault ID No. 116), with a maximum magnitude of M_W = 6.58 and the closest rupture distance of 4.6 miles. The ARS is controlled by USGS 5% probability of exceedance in 50 years (975-year return period) spectrum accelerations. The ARS curve with a peak ground acceleration of 0.32g, as shown in Figure 20.2.8-38, was developed for the project.
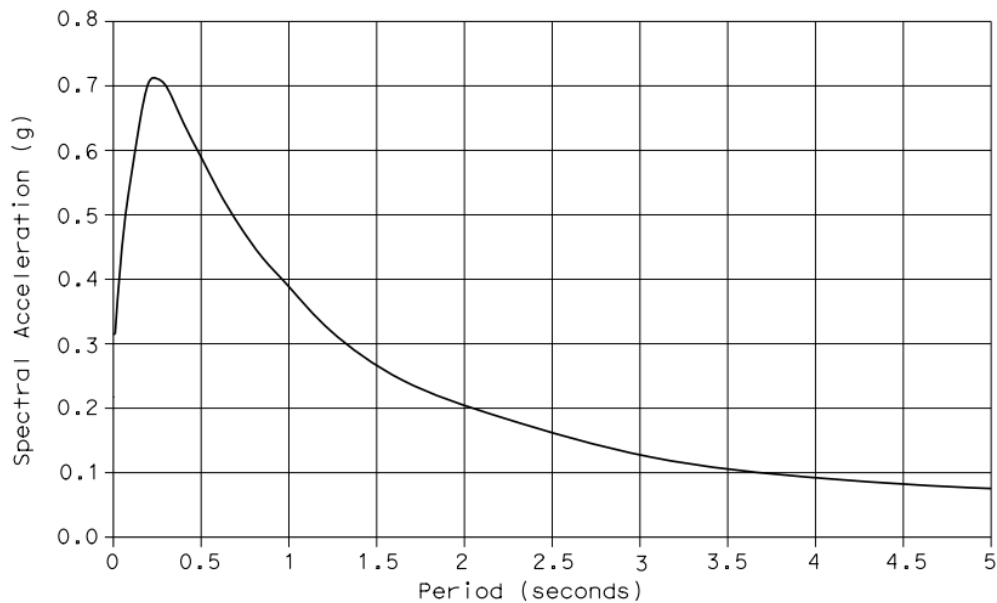
Figure 20.2.8-38 ARS Curves for Paintersville Bridge

Bridge member force demands were evaluated by CSIBridge (CSI. 2019). A 3-D frame model was developed and linear elastic analyses, including static and dynamic, were performed. Effective section properties for latticed members (Duan et al., 2000), were used in the analysis. A standard response spectrum analysis with the CQC3 combination rule was used to calculate member dynamic responses, including axial forces and bi-axial moments. Figure 20.2.8-39 shows a detailed 3-D bridge model.
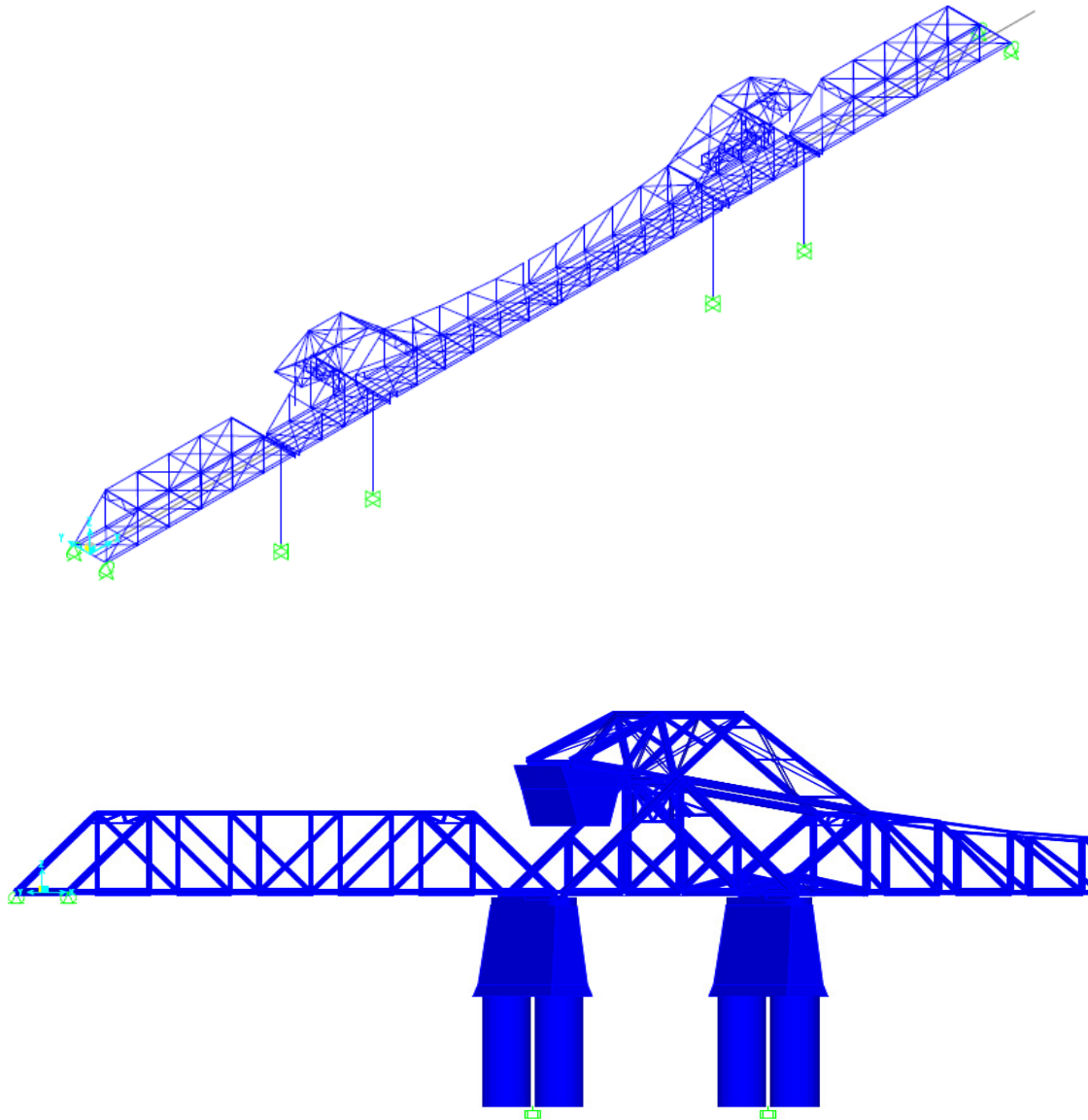
Figure 20.2.8-39 Paintersville Bridge Global Model

In the CSIBridge model, the soil-pile system was modeled by two different methods: one was by a 6 x 6 stiffness matrix at the bottom of each column, and another was by soil *p-y* springs attached to timber piles, as shown in Figure 20.2.8-40. Since the bridge substructure has a strong pier wall/column with weak timber piles, the pile lateral capacity and vertical capacity are major concerns for the bridge's overall stability under seismic events.
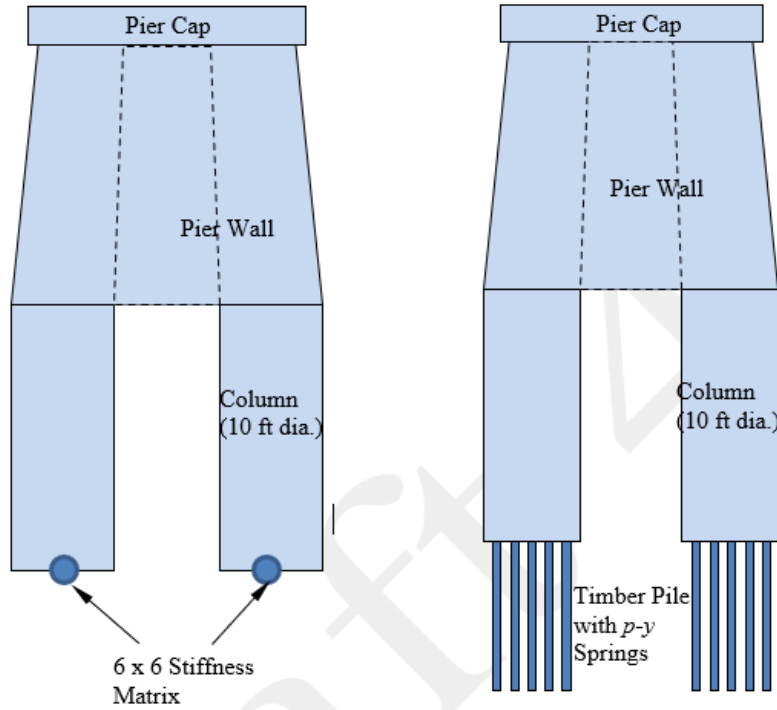
Figure 20.2.8-40 Soil-Pier-Pile Model

Abutment slope stability analyses were performed considering different soil layers including liquefiable soil layers. Figure 20.2.8-41 shows the slope sliding analysis with the abutment embedded into the slope. Abutment *D/C* evaluation was based on the Factor of Safety of abutment slope stability.
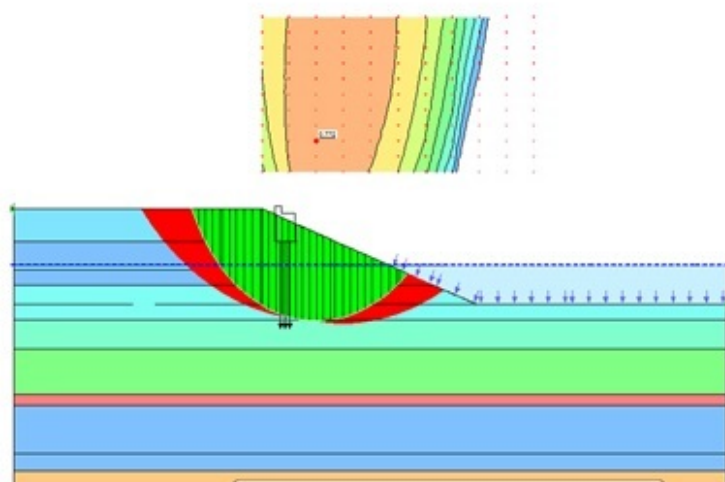
Figure 20.2.8-41 Abutment Slope Stability Model

20.2.8.7.4 Retrofit Strategies

The retrofit scheme for the bridge is shown in Figure 20.2.8-42. Retrofit construction was completed in 2021.
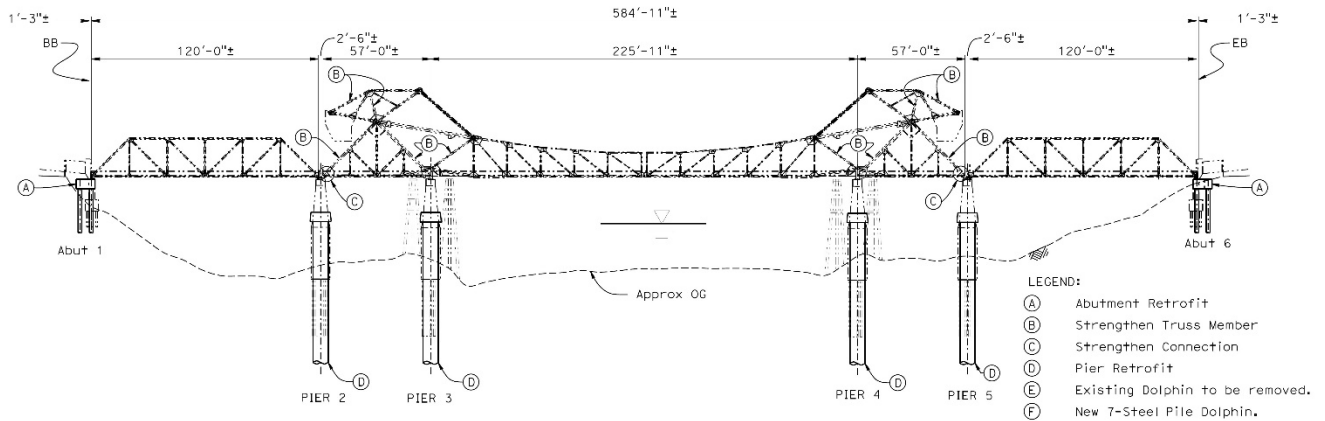
Figure 20.2.8-42 Paintersville Bridge Retrofit Scheme

The main retrofit included:

- Installing 24 in. diameter CISS concrete piles at each abutment to provide necessary slope stability (Figure 20.2.8-43).

- Installing two 96 in. diameter CISS concrete piles and piles caps at each pier (Figure 20.2.8-44).

- Strengthening of the stiffening truss members by the replacement of the lacing with perforated plates and/or additional plates (Figure 20.2.8-45).

- Strengthening truss connections at Piers 2 and 5 (Figure 20.2.8-46).
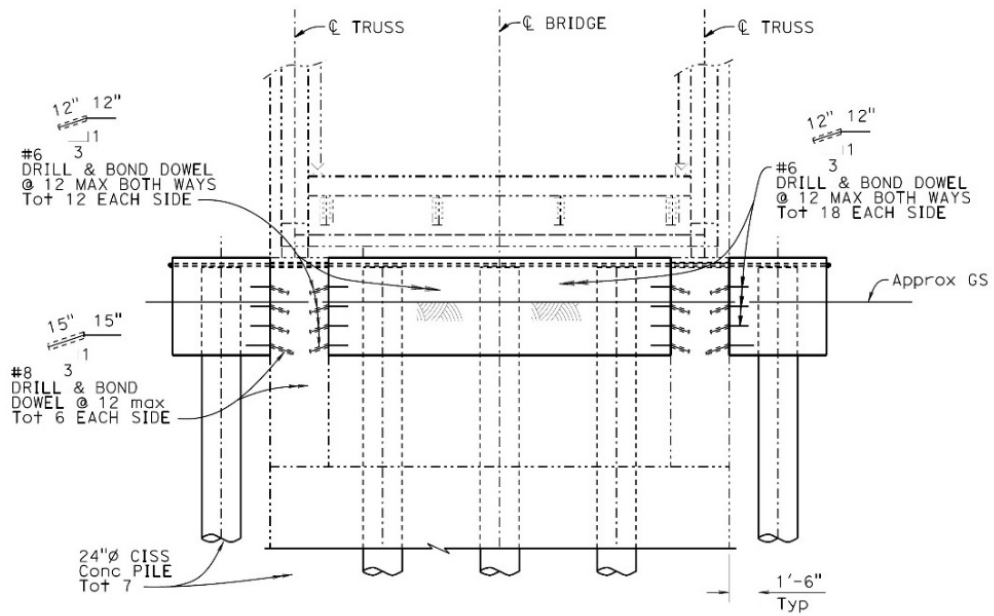
Figure 20.2.8-43 Abutment Retrofit
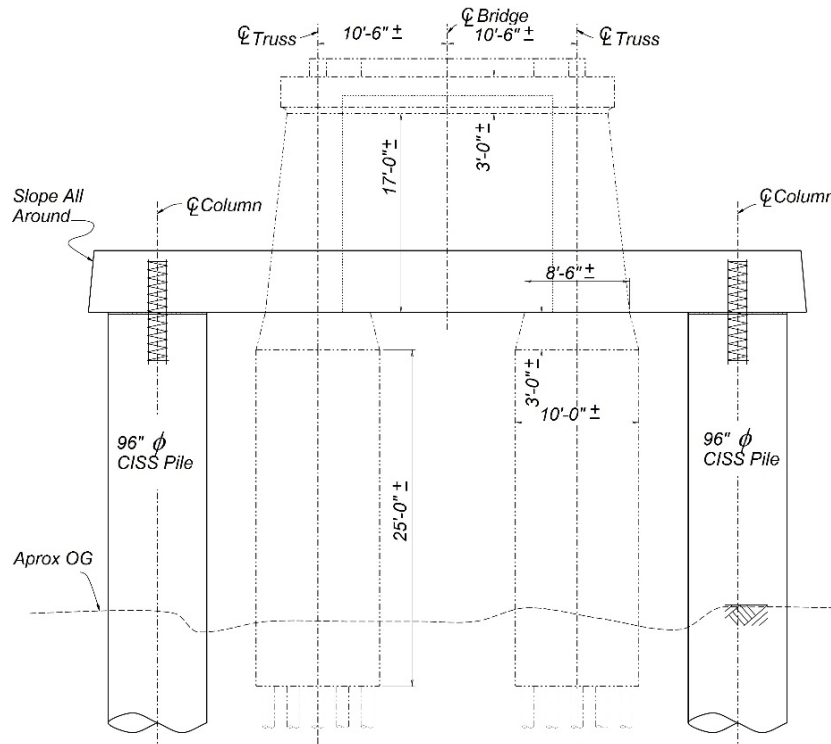
Figure 20.2.8-44 Pier Retrofit

Chapter 20.2 – Seismic Design of Steel Bridges

L/8, Typ

L/4

L/4

L = 18'-6"± (LIMITS OF NEW COVER PLATES)

Max OF 6 LACING BARS TO BE REMOVED FOR INSTILLATION
OF NEW COVER PLATES
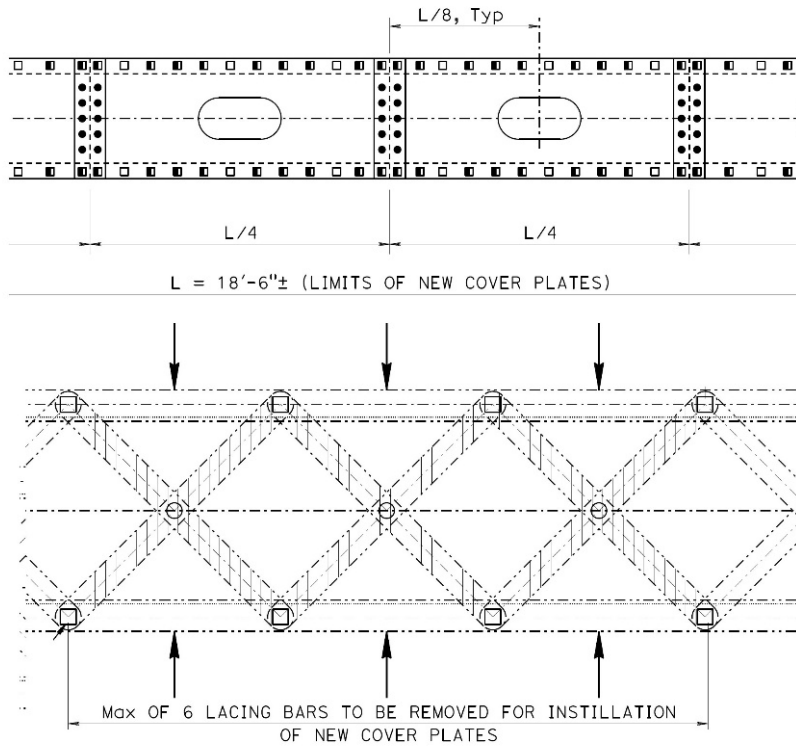
Figure 20.2.8-45 Truss Member Retrofit

2'-6"

⅜" PL Tot 2
PLACE EACHSIDE
OF MEMBER

EXISTING ⅜"± PLATE
EACHSIDE OF MEMBER

₵ BEARING

TOP OF Exist PIER

Exist 1¼" Dia
ANCHOR BOLTS

Exist 1¾" Dia
ANCHOR BOLTS

½" STIFFENER ₽

ANGLE 6X6X¾"

DRILL AND BOND
1½"ø ANCHOR
BOLTS INTO
2½"ø HOLE, Typ
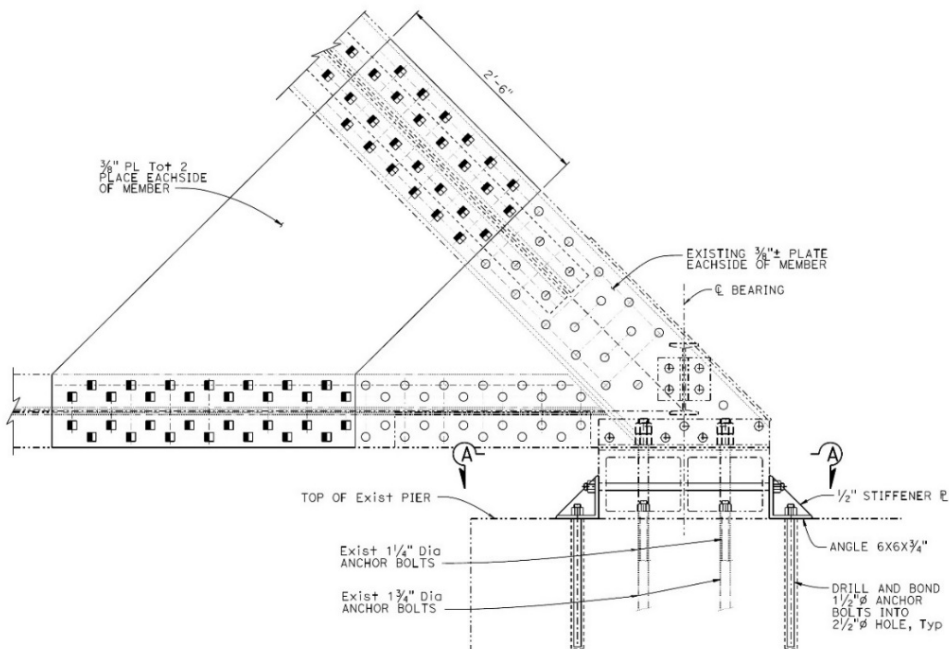
Figure 20.2.8-46 Truss Connection at Pier Retrofit

Chapter 20.2 – Seismic Design of Steel Bridges

20.2-55

20.2.8.8   Richmond-San Rafael Bridge Main Span

20.2.8.8.1   Bridge Description

The Richmond-San Rafael Bridge (Figure 20.2.8-47) is the northernmost east-west crossing of the San Francisco Bay, connecting the cities of Richmond and San Rafael. The bridge carries two lanes of I-580 traffic on its 36 ft roadways in each direction. The 4.5 miles long bridge opened to traffic on August 31, 1956 and consists of three distinct structures: the parallel single deck concrete trestles, the east and west plate girder approach structures, and the main double-deck steel truss spans.

Figure 20.2.8-47 Overview of Richmond-San Rafael Bridge

The low lying eastbound and westbound concrete trestles, with a combined length of over 6,500 ft, connect the west abutment at point San Quentin to the west end of the west plate girder approach structure. The trestle structure is comprised of a series of 50 ft long spans, including precast prestressed lightweight concrete I-girders and cast-in-place lightweight concrete deck slabs, supported on concrete bent caps with four or five 24 in. diameter concrete cylinder piles.

The east and west approach structures, which transition from single deck to double deck structures, are 1,900 ft and 1,700 ft long, respectively. The superstructures are comprised of two parallel steel plate girders supporting transverse floor beams and two-way noncomposite concrete deck slabs. Typical span lengths are 100 ft cantilevered plate girders with a drop-in hinged girder segment between them. The cantilevered girders overhang adjacent piers in an arrangement known as Gerber Framing. The east

approach, which spans over both land and water, has 14×89 steel H-pile foundations supporting reinforced concrete pile caps, shafts, diaphragms, bent caps, and rectangular columns. The foundation was constructed using sheet pile cofferdams. The substructures of the west approach are similar to the dual-shaft concrete piers supporting the truss spans described below.

The main span structure, with a combined length of 14,875 ft, includes two identical double-deck cantilever trusses of 1070 ft spanning the primary and secondary shipping channels, the side channel anchor spans equal to one-half the length of their main spans and constant depth truss spans. Constant depth, double-deck trusses with spans of 289 ft connect the cantilever trusses and the plate girder approach structures. Ten panel warren trusses, with portals of 36 1-3/4" height by 42'-0" width, include 24WF stringers, 14WF chevron bracings, and WF truss members fabricated using a combination of riveted, built-up sections and standard rolled shapes. The truss floor beam-stringer system supports a noncomposite, lightweight concrete deck slab. The truss spans are supported through 9" diameter pins in steel shoes as part of chevron braced flexible steel towers, which are in turn connected to individual pier shafts. The base of each shaft is belled to accommodate 14×89 steel H-piles. These battered piles range in length from 13 ft to over 180 ft. At some locations, the concrete substructures extend up to the underside of the trusses, and at these locations, the braced towers are omitted. Nine of the 43 belled piers supporting the truss spans are quadruple-shaft anchor piers providing longitudinal restraint to the truss structures.

20.2.8.8.2 Seismic Retrofit Performance Criteria

Although the bridge is an important structure, as a result of a relatively low traffic volume, it was decided that the Richmond-San Rafael Bridge only needed to meet no-collapse criteria for the SEE, which has a mean return period in the range of 500 to 2,000 years (GSD-JV, 1999a). The main design requirement is no collapse of any part of the bridge with the following seismic performance criteria under SEE:

- Damage levels sufficient to cause bridge closure for repairs.

- Limited access for several days following the earthquake.

- Require months for full restoration of service.

The seismic design criteria are summarized as follows:

- Pile Foundations – moderate local buckling of existing steel H-pile at low cycles is allowed. Drifts exceeding the established criteria are justified on a case-by-case basis using a low cycle fatigue damage assessment (GSG-JV, 1997a).

- Concrete Substructures – unconfined concrete compression strain of 0.004 is allowed.

- Truss Chords – buckling of 289-ft span truss chords is acceptable.

- Eccentrically Braced Frame (EBF) and Special Moment Resisting Frame (SMRF) towers – a low cycle fatigue evaluation was used to show that the tower frames

could survive the damage imposed by one or two half-cycle drifts exceeding the code-based nominal capacities (GSD-JV, 1997b).

- Truss Shoe Pins – designed by Drucker's formula as defined in Reference (GSD-JV, 1999a)

20.2.8.8.3   Seismic Retrofit Analysis

The design earthquakes for the bridge are the M_w = 8 earthquake on the San Andreas Fault and the M_w = 7.25 earthquake on the Hayward fault. The corresponding target rock response spectra for acceleration time history development were at the 84th percentile level. Figure 20.2.8-48 shows a typical target pile cap response spectrum used for the final analysis.

Spectrum-compatible, multi-support, free-field mudline time history motions (Figure 20.2.8-49) were developed based on the target response spectra. Soil-Foundation-Structure-Interaction (SFSI) considering as-built soil profiles were performed to obtain the final input motions.
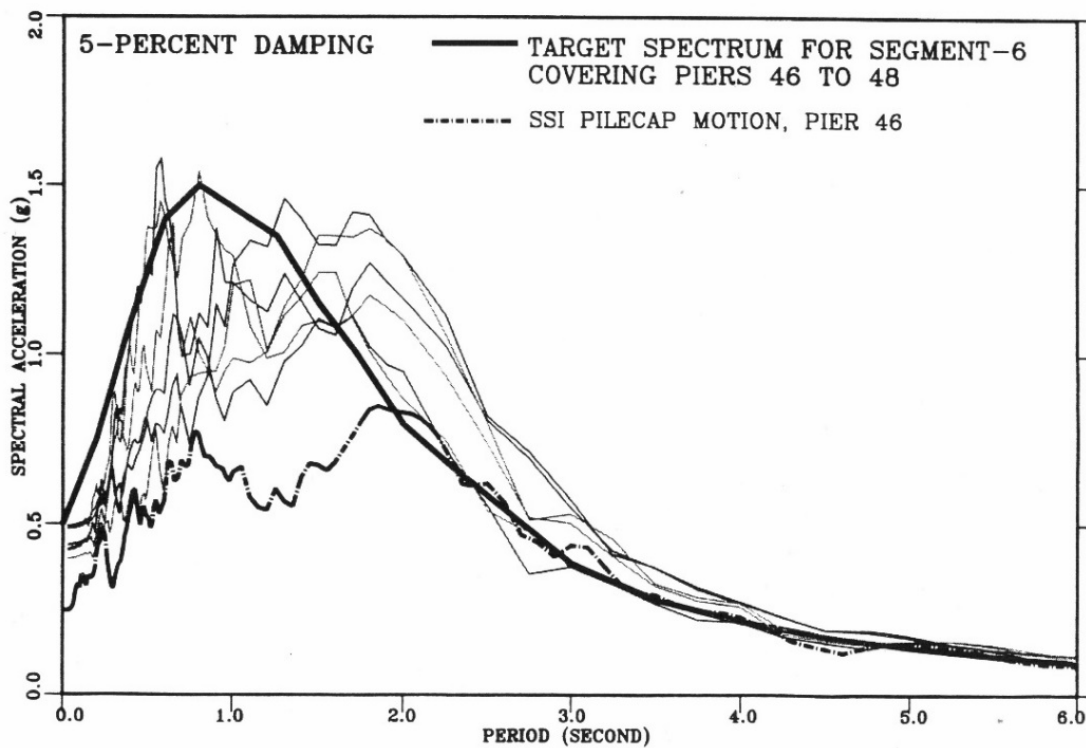
Figure 20.2.8-48 Target Response Spectrum for Pile Caps

from Piers 46 to 48 (GSD-JV, 1999b)
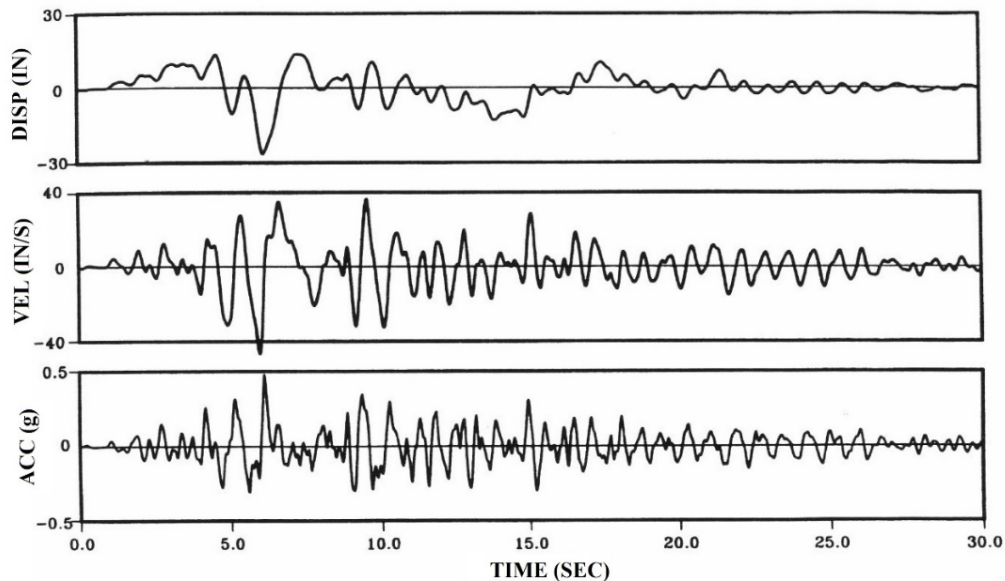
Figure 20.2.8-49 Time History of Transverse Component

at Pier 47 Mudline (GSD-JV, 1999b)

Many different models, "component", "local", "global", and "substructure" models, were developed using SAP90, SADSAP, and ADINA programs.

Component models were used to estimate the nonlinear behavior and capacities of structural members such as H-piles, pile-groups, laced steel towers, Eccentrically Braced Frame (EBF) shear links, and truss members. Local models were used to investigate the regional behavior, especially the structural behavior of the towers, Soil-Foundation-Structure-Interaction (SFSI) of the H-piles and CISS/CIDH piles, and the superstructure trusses. Figure 20.2.8-50 shows a local model for a typical pier with EBF in the final design in which a 6x6 stiffness matrix was used to represent the pile resistance and beam elements, and springs were used for each H-pile.

The global model was used for a nonlinear, ductility-based multi-support time-history analysis to determine the displacement demands of the main truss span (Figure 20.2.8-51). The nonlinearities considered in the global analysis/design model consisted of inelastic features such as (1) eccentrically braced frames and special moment resisting frame towers; (2) lead-core rubber isolation bearings; (3) controlled rocking at the cantilever structure A-Frame towers; (4) hydraulic viscous dampers and gap elements at the intermediate expansion joints; and (5) nonlinear truss chords behavior. Other nonlinear behaviors were simulated using adjusted "secant" stiffness, including (1) plastic hinges at the base of existing tower legs, (2) plastic hinges in the truss posts as a result of truss racking, (3) longitudinal racking of the truss floor beams; (4) nonlinear soil-pile interaction; and (5) plastic deformation of concrete substructure shafts and columns. Geometric nonlinearities and P-Δ effects were also considered.
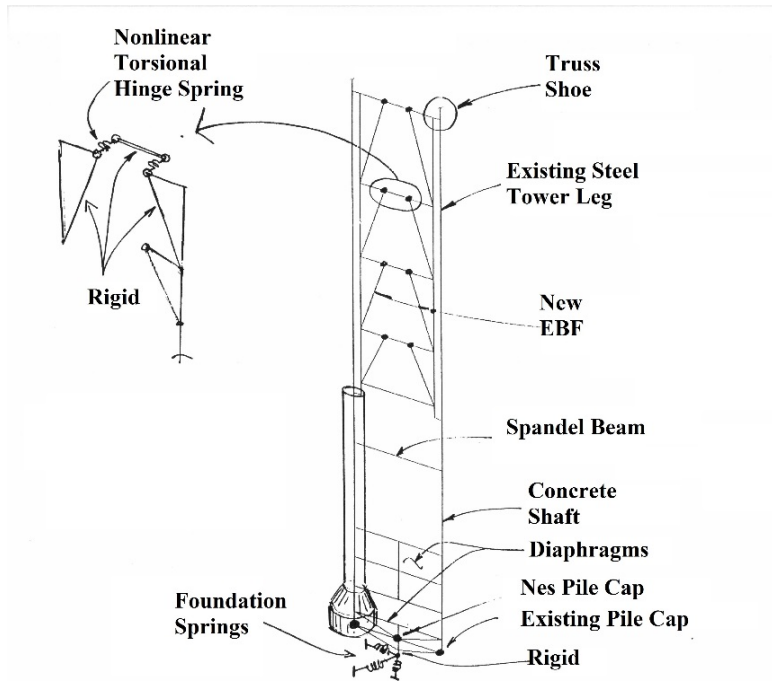
Figure 20.2.8-50 Typical Pier and EBF Model (GSD-JV, 1999b)
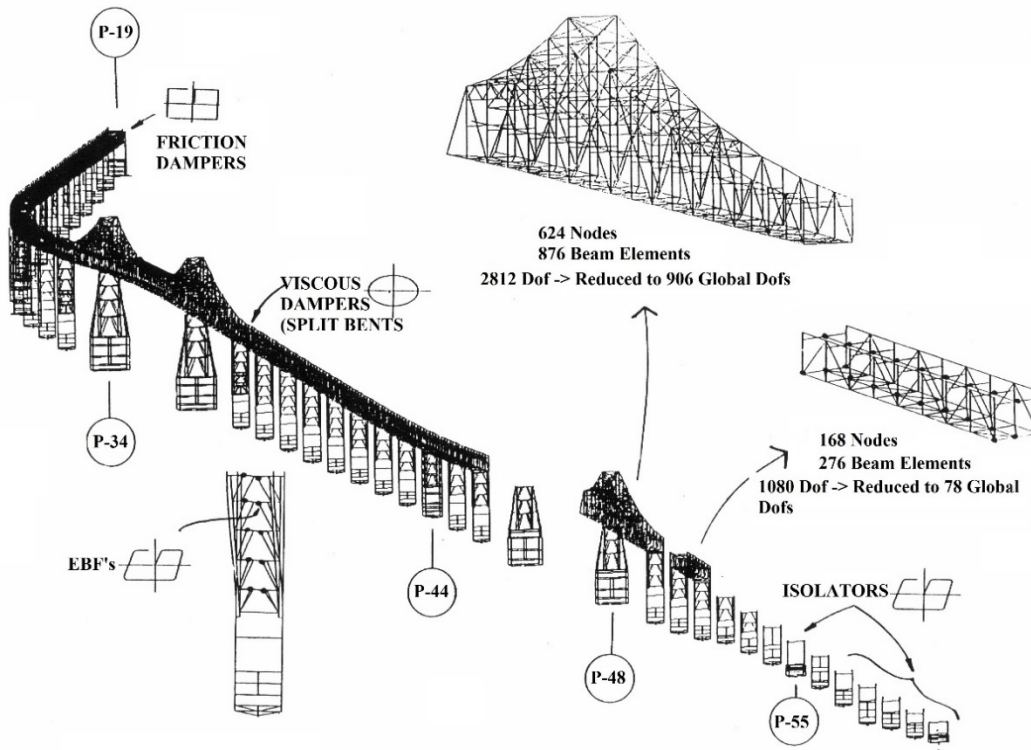
Figure 20.2.8-51 Richmond-San Rafael Bridge Global Model in

Final Design (GSD-JV, 1999b)

The Rayleigh damping for the regional model of 10% for larger foundations and 5% for the global model were used in the analysis.

For individual steel members in the superstructure, forces such as axial loads and biaxial moment interaction are evaluated by the AISC specifications. For steel towers, reinforced concrete flexural members, and foundations, displacements are evaluated by nonlinear finite element analysis.

20.2.8.8.4   Retrofit Strategies

A comprehensive vulnerability assessment for the existing main span indicated that the bridge, without being retrofitted, would collapse during the SEE. The most vulnerable deficiencies include the bucking of concentric inverted V-bracing in the steel towers; the buckling and fracture of battered H-piles supporting the foundations; shear failure of the spandrel beams in the substructure; and failure of the upper or lower chords in the truss superstructure.

The bridge was seismically retrofitted in 2005, as shown in Figure 20.2.8-52.

Figure 20.2.8-52 Retrofitted Richmond-Sam Rafael Bridge Main Span

The truss superstructure retrofit included:

- Installing new sway bracing above the upper deck of the cantilever truss spans at locations where they were originally omitted while strengthening the existing portal and sway frames.

- Adding new longitudinal mid-height bracing members at cantilever truss spans.

- Adding high strength bolted web cover plates on end lower chord members of all 289-ft trusses.

- Replacing truss shoe pins with new high strength steel pins at many 289-ft trusses.

- Strengthening connections of all floor beams to the vertical truss posts using high strength rods and bolted brackets.

- Reframing the truss to create seismic isolation joints at Piers 19 and 61 to prevent pounding and separate the truss spans from the plate girder approach structures (Figure 20.2.8-53).

- Installing seismic isolation lead-rubber bearings at piers without steel towers.

- Installing viscous dampers and large supporting brackets at the superstructure expansion joints (Figure 20.2.8-53).

- Replacing existing expansion joints at the split tower bent with steel finger joints and replacing bearings at Pier 58 with seismic isolation bearings.

- Installing new steel support frames and transverse lockup beams under the decks between the two bottom chords at the expansion towers.

- Adding longitudinal restrainers at each exterior stringer along both the upper and the lower decks of the bridge at deck expansion joints.

Figure 20.2.8-53 Seismic Isolation Bearings and Viscous Dampers

The steel tower and concrete substructure retrofit included:

- Replacing the existing two-leg laced steel towers with ductile EBFs for the taller towers (Figure 20.2.8-54) and SMRFs for the shorter towers.

- Adding both longitudinal and transverse EBFs on all four faces of the four-leg anchor towers (Figure 20.2.8-55).

- Adding transverse EBFs and longitudinal SMRFs on four-legged towers supporting the main cantilever spans (Figure 20.2.8-55).

- Adding slot-bolted friction dampers at the base of each leg of existing cantilever towers to control the uplift.

- Adding precast jackets around all two-bell piers to strengthen the shear capacities of the concrete substructures (Figure 20.2.8-56)

- Strengthening diaphragm walls at the four-bell piers, except Piers 19, 55, and 61, using new thicker walls (Figure 20.2.8-57).
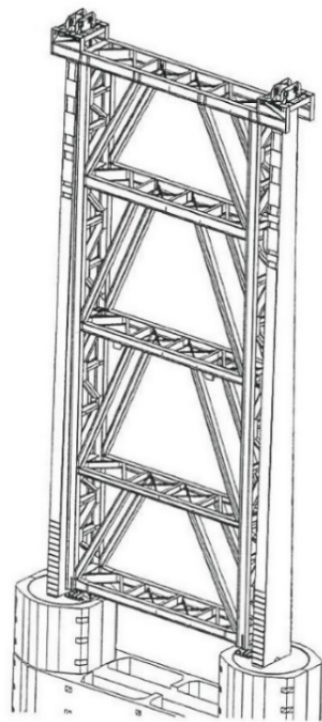
(a)*   (b)

Figure 20.2.8-54 EBFs for Two-Leg Tower (*Vincent and Abrahamsen, 1998)
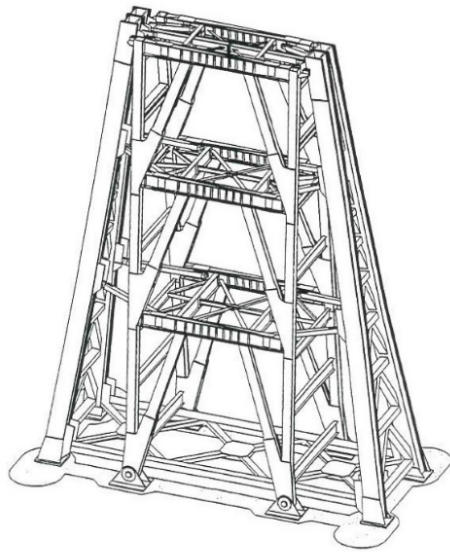
(a)*   (b)

Figure 20.2.8-55 EBFs for Four-Leg Tower (*Vincent and Abrahamsen, 1998)

(a)*   (b)

Figure 20.2.8-56 Precast Jacket for Two-Bell Piers   (*Dahlgren and Vincent, 1998)

Figure 20.2.8-57 Diaphragm Strengthening for Four-Bell Piers Under Construction

The foundation retrofit included:

- Installing two larger diameter (126 in. and 150 in) cast-in-steel-shell (CISS) or cast-in-drilled-hole (CIDH) concrete piles with permanent steel casings for Piers 22, 33, 36-38, 41, 42, 46, and 39 through a new precast pile cap placed between the existing bells (Figure 20.2.8-58).

- Installing four larger diameter (126 in. to 150 in.) CISS or CIDH concrete piles with permanent steel casings for Piers 47 and 48 through a new precast pile cap placed between the existing bells.

- Installing 12 to 32 micro piles of 8.625 in. through cored holes in the existing foundation bells for Piers 39, 40, 50-54, and 50-56.

Figure 20.2.8-58 Cast-in-Steel-Shell (CISS) Piles under Construction

20.2.8.9 San Francisco-Oakland Bay Bridge West Span

20.2.8.9.1 Bridge Description

The San Francisco-Oakland Bay Bridge (SFOBB), the main connection of San Francisco Bay, is one of the most important bridges in the United States. The bridge has an upper and lower concrete deck that carries five lanes in each direction and provides service to over 280,000 vehicles daily. The West Span (Figures 20.2.8-59 and 20.2.8-60) of 10,292 ft includes three continuous truss approach spans of 389 ft + 95 ft + 377 ft and the twin suspension bridges arranged end-to-end around a center anchorage. The twin bridges have main spans of 2310 ft, back spans of 1160 ft, and 1171 ft, and are virtually identical. The double deck stiffening truss is made up of built-up members, laced members, and some rolled sections (Figure 20.2.8-61). The bridge was open to traffic on November 12, 1936.
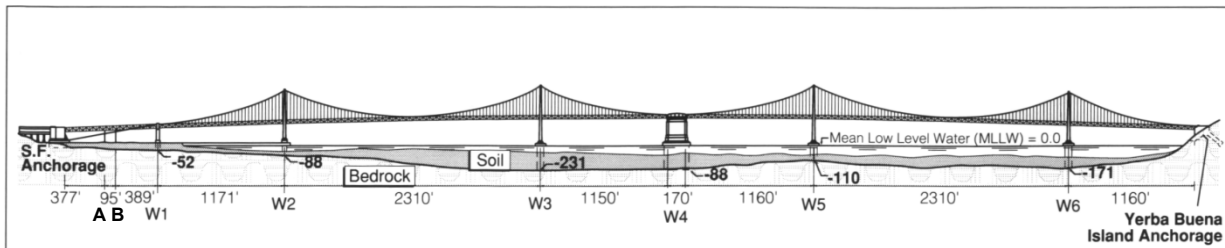
Figure 20.2.8-59 Overview of San Francisco-Oakland Bay Bridge West Span

Figure 20.2.8-60 Sunset at SFOBB West Span
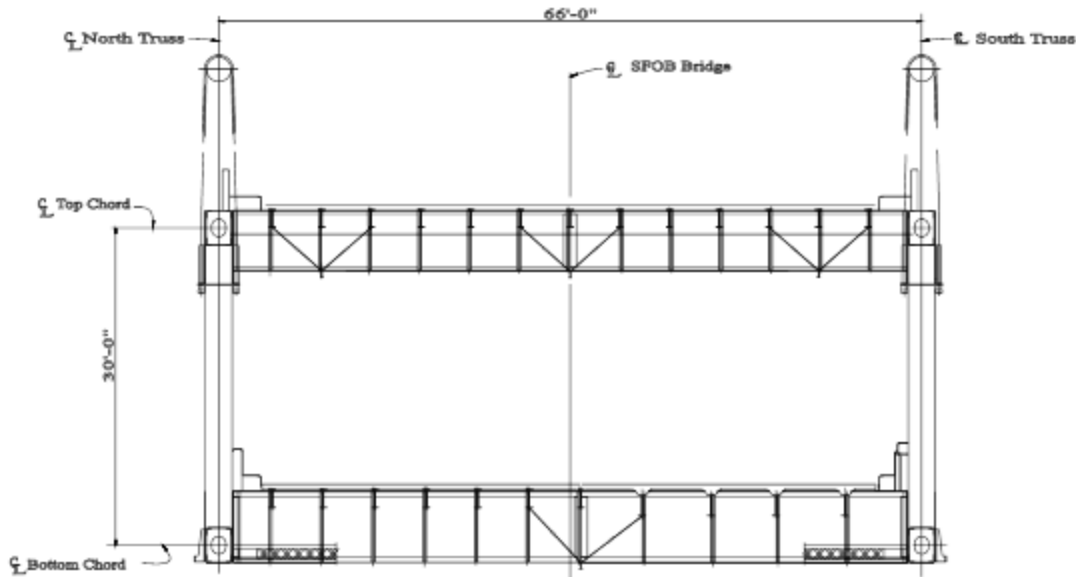
Figure 20.2.8-61 Cross Section of Stiffening Truss Spans

All the towers are similar, except that Towers W2 and W6 are about 420 ft tall, while Towers W3 and W5 are about 470 ft. The tower legs are cellular in cross-section, made up of 1 in. thick vertical web plates connected along their edges with angles. Tower W2 is supported by a gravity concrete pier which was constructed in a sheet-pile cofferdam 90 ft below water. Towers W3, W5, and W6 are supported by cellular, hollow, reinforced concrete caissons which extend from 110 ft to 230 ft below water level. Pier W4 is a central anchorage for the twin, end-to-end suspension bridges and is supported by a hollow cross section caisson of 92 ft x 197 ft which is formed using fifty-five 15 ft diameter by 5/16 in. thick steel cylinders. It extends 220 ft below the water and 280 ft above the water. It was the largest pier in the world at the time of its construction. All the caissons were socketed into the underlying bedrock.

20.2.8.9.2 Seismic Retrofit Performance Criteria

The SFOBB was designated as an *Important* Bridge. The seismic retrofit of SFOBB West Span was the top priority of the California Department of Transportation. The seismic retrofit design criteria of SFOBB west spans were developed (Caltrans, 1997) by considering both the SEE, which has a mean return period in the range of 1,000 to 2,000 years and the FEE, which has a mean return period of 300 years with a 40 percent probability of exceedance during the expected life of the bridge.

The bridge is expected to remain serviceable after a SEE. Serviceable is defined as sustaining repairable damage with minimum impact on the functionality of the bridge structure. Also, the bridge is expected to be open to emergency vehicles immediately following the event, provided Caltrans personnel can provide access. The bridge is also expected to remain fully operational after a FEE. Fully operational is defined as full

accessibility to both decks by current normal daily traffic. The structure may suffer repairable damage, but repair operations may not impede traffic in excess of what is currently required for normal daily maintenance.

The objectives of the seismic retrofit for SFOBB West Spans (Caltrans, 1997) are:

- To keep the critical bridge structural members in an essentially elastic range during the SEE.

- To devise expansion joint assemblies between bridge frames that either retain traffic support or, with the installation of deck plates, can carry the designated traffic after being subjected to SEE displacements.

- To provide ductile load paths and detailing to ensure bridge safety if future demands might exceed those demands resulting from current SEE ground motions.

- To meet the acceptance force D/C and corresponding damage index developed for the project.

20.2.8.9.3   Seismic Retrofit Analysis

Three sets of dynamic time histories with three component accelerations and displacements for each support location were developed. These 80-s motions corresponded to a magnitude Mw = 8 event on the San Andreas fault approximately 9.3 miles from the west end of the SFOBB West Spans. Figure 20.2.8-62 shows the longitudinal displacement time history for Pier W5.
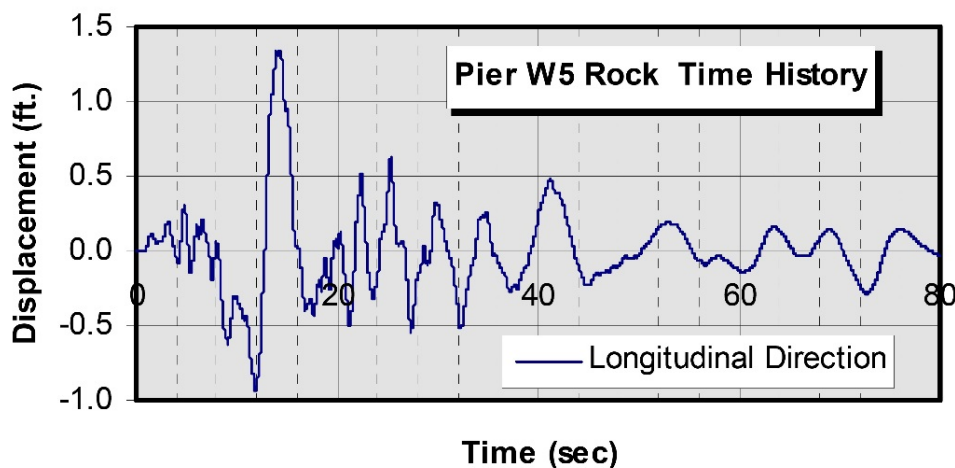
Figure 20.2.8-62 Longitudinal Displacement Time History at Pier W5

The ground motion time histories were generated for each soil layer at each support. Appropriate nonlinear foundation springs (both *p-y* and *t-z*) were developed for these soil layers, through which the motion was directed.

Three different models, "local", "regional", and "global" models, were developed using ADINA (Automatic Dynamic Incremental Nonlinear Analysis) (ADINA, 1997).

Local models emphasize the localized behavior, especially complex inelastic and nonlinear behavior of each tower base, caisson base, tower leg, lattice member, bent and pier footings, etc. Modeling the boundary conditions at the bottom of the caisson was a challenging task. To evaluate the displacement capacity of the existing caisson foundations and to provide rocking moment-rotational springs for demand models, the local models for the caisson foundations were developed using 3D solid finite elements including contact surface elements, continuum elements, and nonlinear springs to simulate rock material, as well as geometric and material nonlinearities. From these large detailed local models, appropriate boundary conditions were obtained and placed on the simpler demand regional models. The stresses in both the rock and caisson material were monitored and checked against capacities, which came from as-built data, tests, and theoretical and analytical solutions. Figure 20.2.8-63 shows the Pier W1 rocking model. To evaluate the behavior and capacities of tower bases, the local model, with shell elements as shown in Figure 20.2.8-64a, was developed. The tower base model was analyzed for material and geometric nonlinearities as well as member and plate buckling.
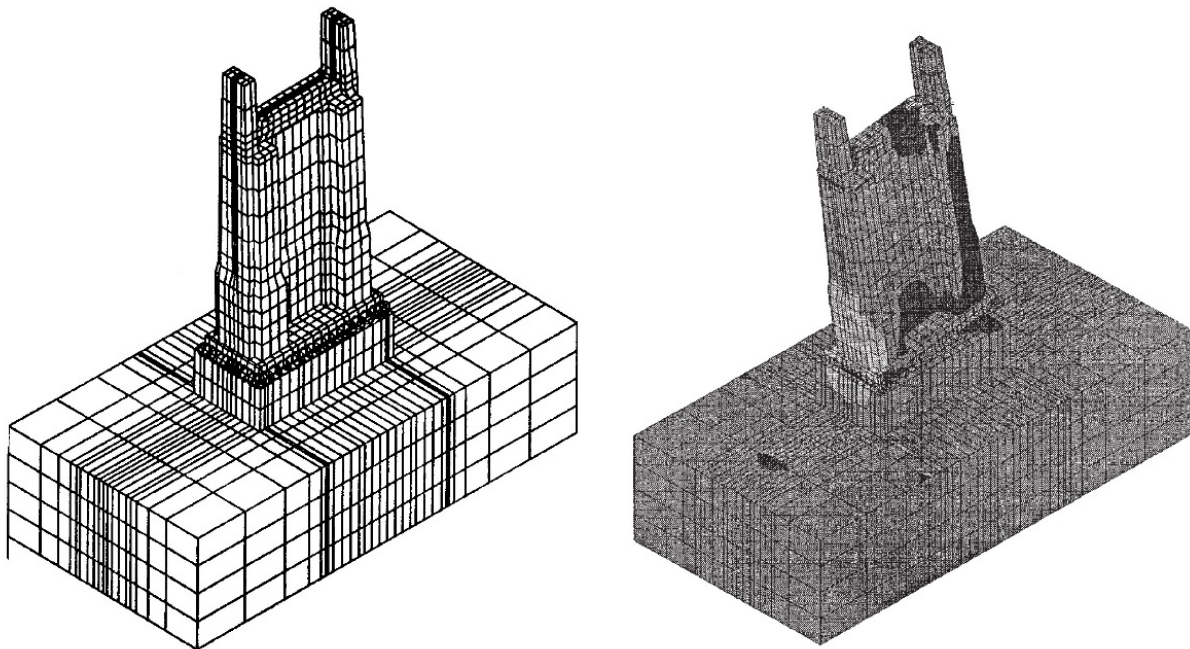
Figure 20.2.8-63 Pier W1 Rocking Model
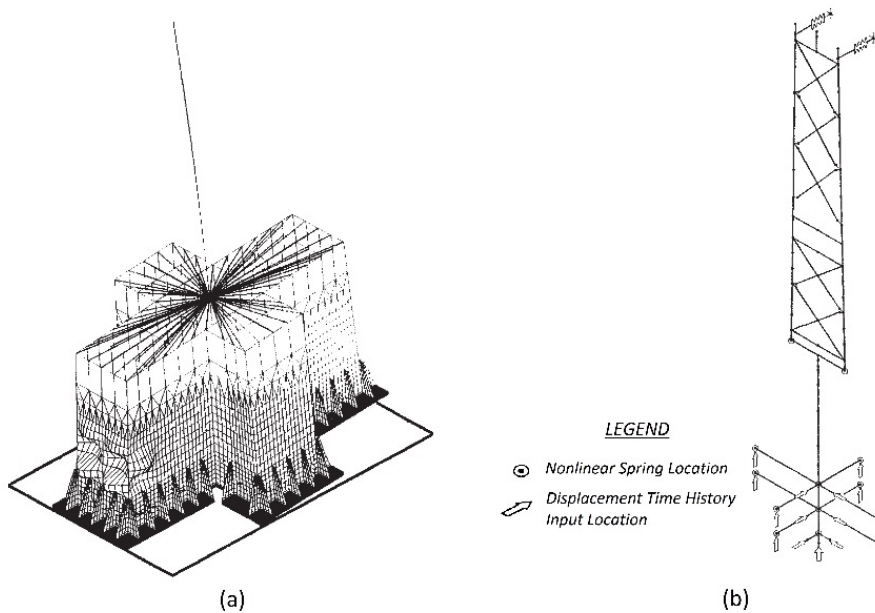
Figure 20.2.8-64 Pier-Tower W5 (a) Local Model and (b) Regional Model

Regional models concentrate on regional behavior, especially the structural behavior of towers, caissons, anchorage housings, connections, stiffening trusses, continuous trusses, etc. To determine caisson demands, as well as to provide input motions to the uncoupled global model, the regional models were developed. These tower/caisson regional models consist of elastic beam elements and include nonlinear rocking rotational springs, nonlinear soil springs, hydrodynamic mass, buoyancy, nonlinear tower rocking springs, elastic cable springs, and added mass from the superstructure interaction. Figure 20.2.8-64b shows Pier-Tower W5 regional model.

The global models focus on the overall behavior, especially the superstructure behavior of the SFOBB West Spans, and include simplifications of complex structural elements. Two global models were developed to have one final model that would inherit qualities from both. They were assembled from the regional models and preassembled groups of members to facilitate the development of such large models. The detailed global model has 32,000 degrees of freedom and some 10,000 elements (Figure 20.2.8-65).

The Soil-Foundation-Structure-Interactions were considered using non-linear springs in the global and regional models. Effective section properties for lattice members (Duan et al., 2000) were developed and used in the global models.

The Rayleigh damping for regional models of 10%, except 15% for Tower 3 and 5% for the global model, was used in the analysis of existing structures. The Rayleigh damping for regional models of 8%, except 12% for Tower 3 and 3% for the global model, was considered in the analysis of retrofitted structures.
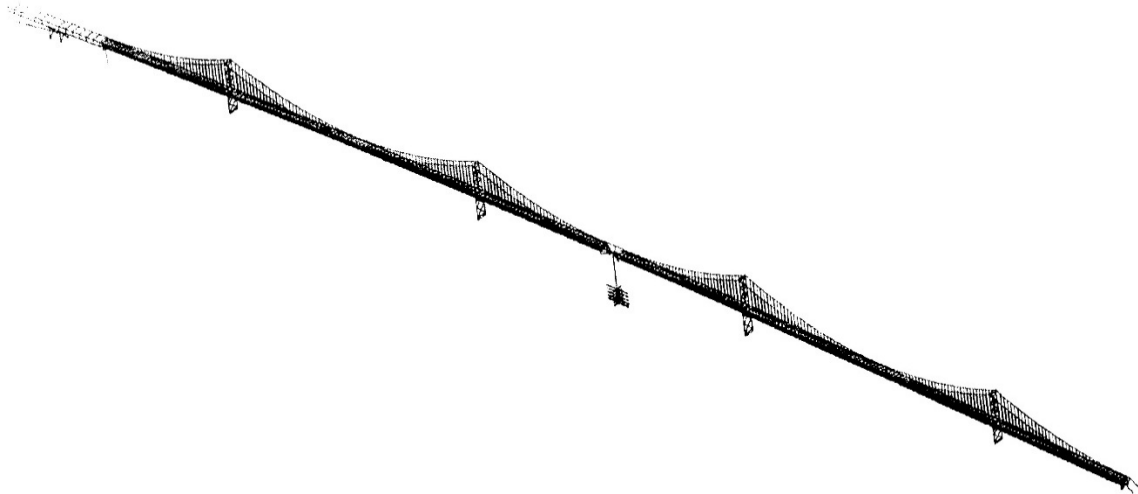
Figure 20.2.8-65 SFOBB West Span Global Model

20.2.8.9.4 Retrofit Strategies

The West Span was seismically retrofitted in 2004 to improve operational and safety standards to the greatest extent possible and to achieve the project-specific performance-based seismic design criteria (Caltrans 1997; Reno and Pohll 1998). The retrofit project not only opened under the original engineer's estimate but was also constructed and closed out for less than the engineer's estimate plus contingencies. This project was a remarkable feat for complicated steel retrofit work such as was encountered on the SFOBB West Span Retrofit (Figure 20.2.8-66).
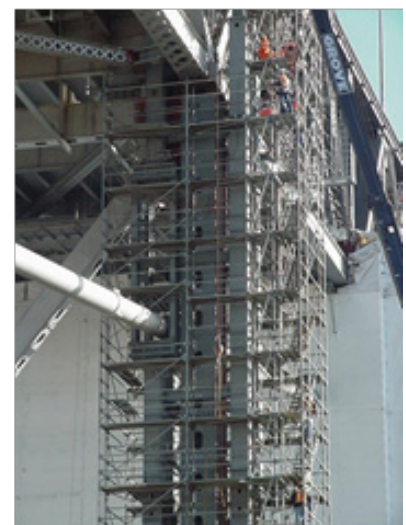
Figure 20.2.8-66 SFOBB West Span under Retrofit Construction

The superstructure retrofit included:

- Adding cable ties at midspan of both suspension bridge main spans to help control longitudinal movement.

- Strengthening of the floorbeam to vertical connection with tie-rods and additional plates.

- Strengthening of the stiffening truss chords and diagonals by the addition of plates and the replacement of lacings with perforated plates and/or additional plates (Figure 20.2.8-67).

- Adding a new upper deck lateral bracing system using a tube section in a chevron configuration.

- Replacing the complete lower deck lateral bracing system with ductile members.

- Strengthening gusset connections by replacing rivets with high-strength bolts and by adding edge stiffeners.

- Modifying the truss to tower connection to allow greater relative longitudinal movement and installing a total of 96 viscous dampers between each chord and the tower or the anchorage (Figure 20.2.8-68).

- Installing the friction pendulum isolation bearings for the Continuous Trusses to reduce substructure loading.
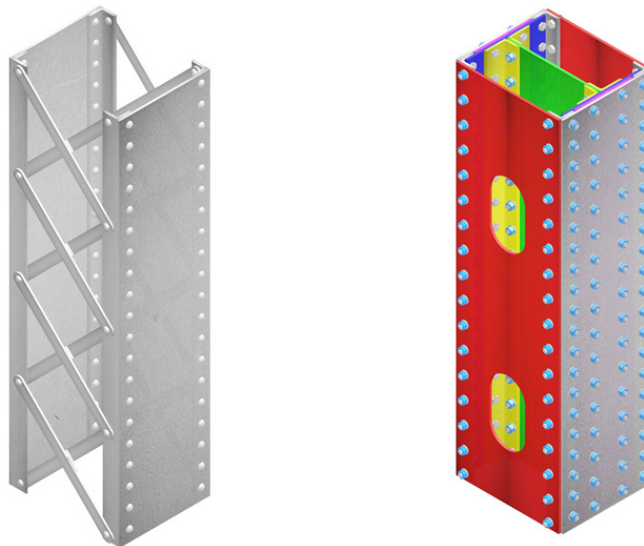
Figure 20.2.8-67 Stiffening Truss Member Retrofit

Figure 20.2.8-68 Suspension Span Dampers

The tower retrofit (Figure 20.2.8-69) included:

- Installing new anchor bolts to resist uplift forces and installing internal pipe shear keys at the base.

- Strengthening the cable saddle connection to the top of the tower.

- Strengthening gusset connections by replacing rivets with high-strength bolts and by adding additional plates.

- Adding new longitudinal and transverse stiffeners to strut and diagonal plates.

- Installing new plates for tower legs.

The pier and foundations retrofit included:

- Strengthening Pier W1, Bents A and B foundations, and Pier W4 (Figure 20.2.8-70) by providing either concrete or steel jackets around the foundation.

- Drilling and grouting vertical high-strength rods to the full height of the foundation for Pier W2.

- Adding concrete jackets, drilling, and grouting high-strength rods vertically, and prestressing horizontally through the pedestals for Piers W2, W3, W5, and W6.
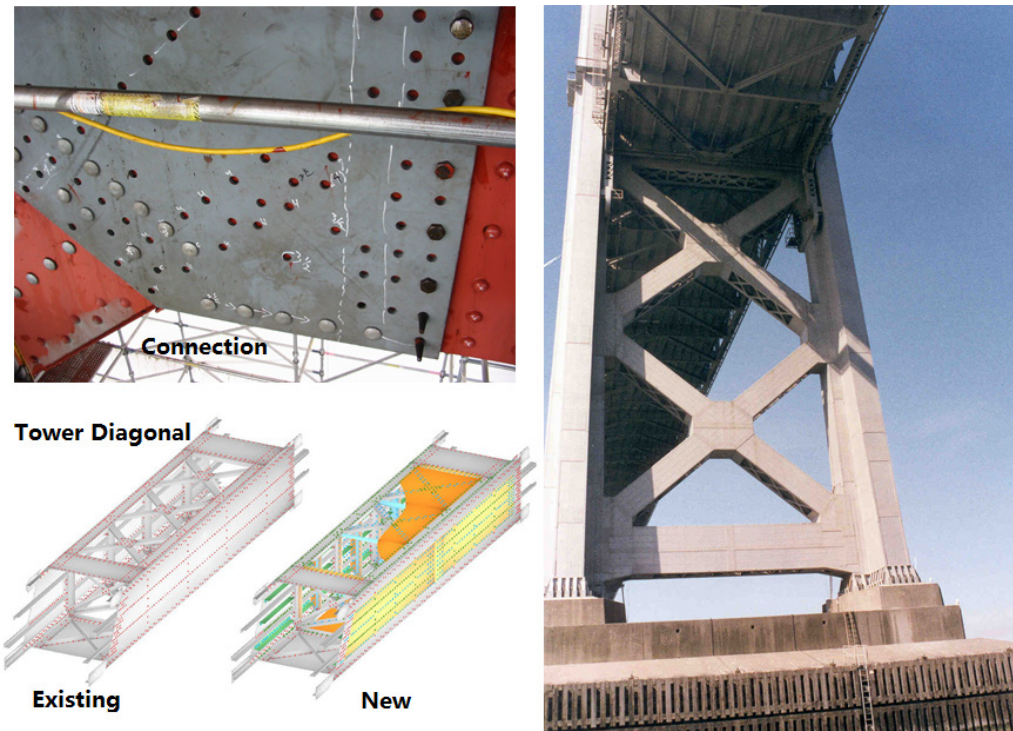
Figure 20.2.8-69 Tower Retrofit

Figure 20.2.8-70 Pier W4 – Central Anchorage Retrofit

20.2.9 SEISMIC DESIGN EXAMPLE 1 – DUCTILE CONCRETE SUBSTRUCTURE STRATEGY

20.2.9.1 Steel Girder Bridge Data

A three-span continuous composite plate girder bridge superstructure with spans of 110 ft – 165 ft – 125 ft has been designed for Strength, Service, and Fatigue limit states as illustrated in Chapter 6.2. The superstructure is 58 ft wide. The elevation and plan are shown in Figure 20.2.9-1. The typical section is shown in Figure 20.2.9-2. The framing plan and the elevation of the girder are shown in Figures 20.2.9-3 and 20.2.9-4.

Structural steel:	A 709 Grade 50 for web, flanges, and splice plates
	F_y = 50 ksi; E_s = 29,000 ksi
	A 709 Grades 50/36 for cross frames and stiffeners, etc.
	F_y = 50/36 ksi
Deck Concrete:	f_c' = 3600 psi E_c = 3,640 ksi; Modular Ratio n = 8
Column Concrete:	f_c' = 4000 psi E_c = 3,834 ksi;
Deck Slab:	Concrete deck slab thickness = 9.125 in.
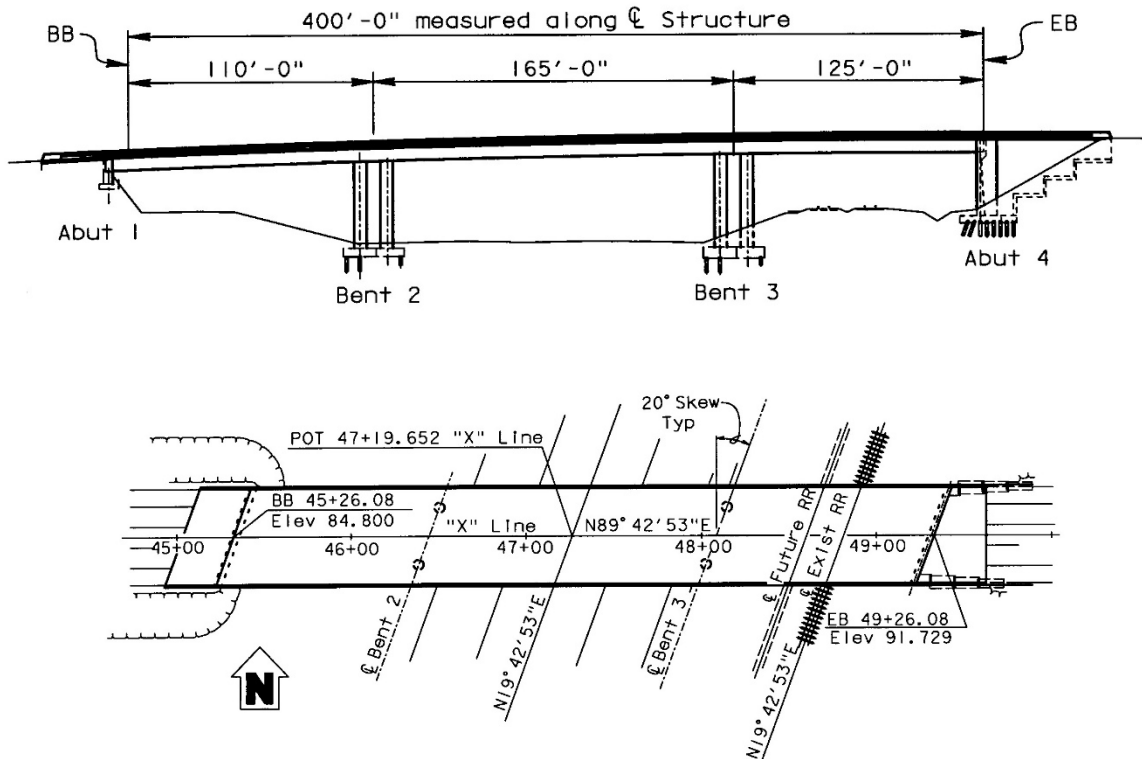
Figure 20.2.9-1   Three-span Continuous Steel Plate Girder Bridge
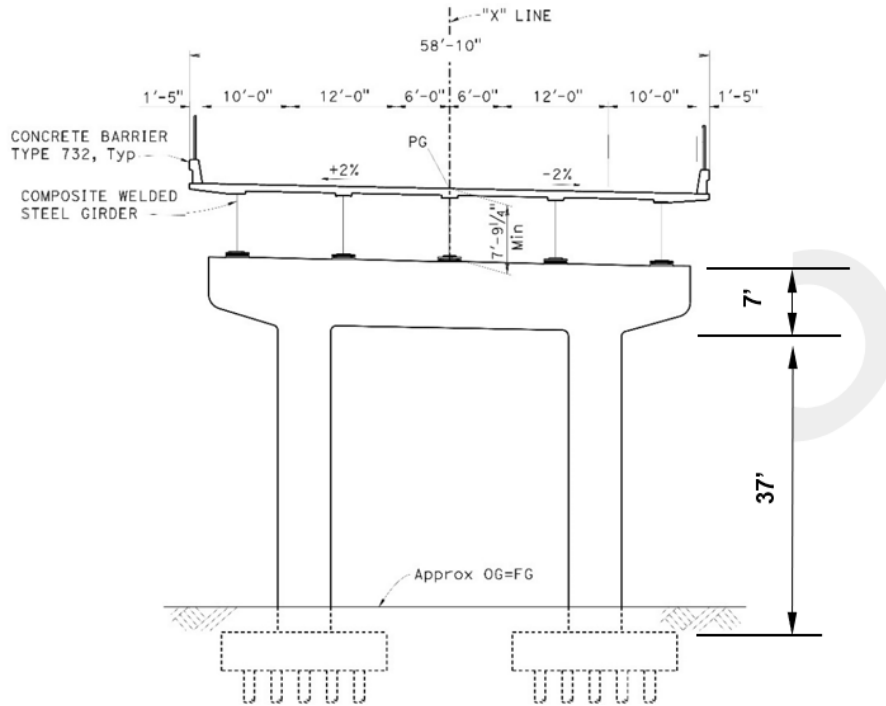
Figure 20.2.9-2   Typical Section
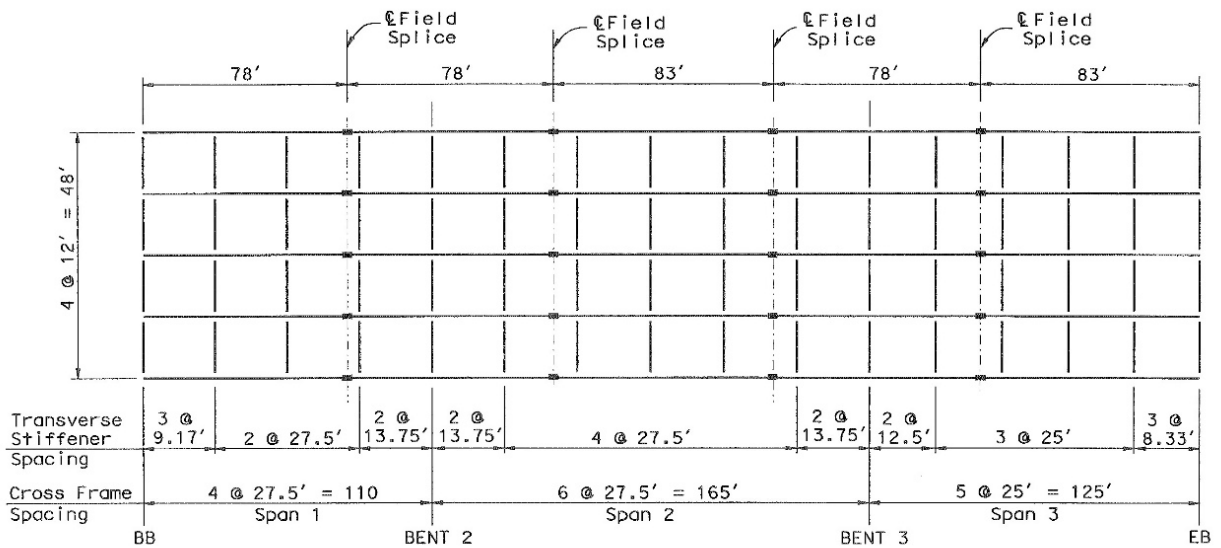
Figure 20.2.9-3 Framing Plan (Skew not Shown)
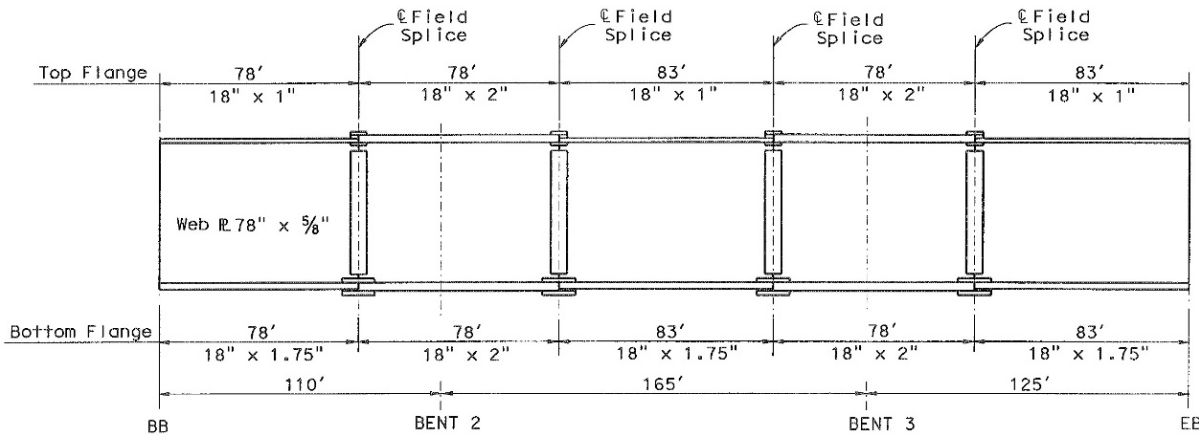
Figure 20.2.9-4 Elevation of Interior Girder

For convenience in this example, the ends of the girder have been assumed to match the BB and EB locations.

The bridge crosses a roadway and railroad tracks. The foundations are supported on piles due to poor soil conditions. The ground motion at the bridge site is assumed to be:

Soil Profile: $V_{s30} = 700$ ft/sec

Magnitude: 8.0 ± 0.25

Peak Ground Acceleration: 0.5g

The design (input) acceleration response spectrum is shown in Figure 20.2.9-5.
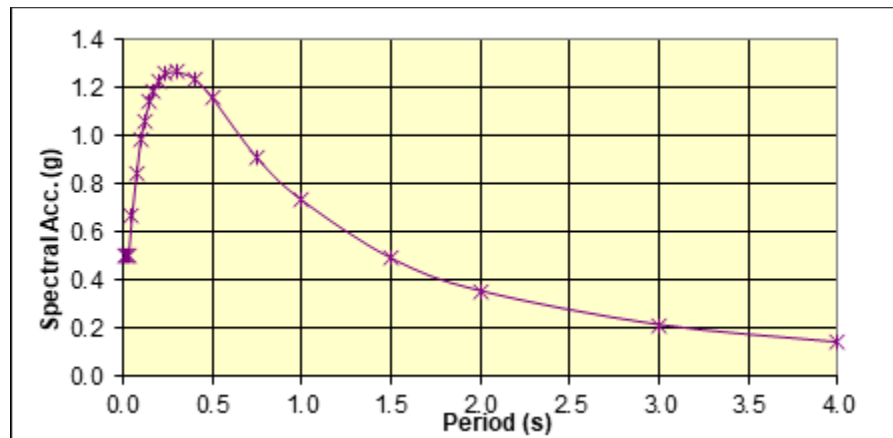
Figure 20.2.9-5 Design (Input) Acceleration Response Spectrum

20.2.9.2 Design Requirements

Perform the following seismic design in accordance with the *SDSSB* (Caltrans, 2016), the *SDC* (Caltrans, 2019a), *AASHTO-CA BDS-08* (AASHTO, 2017; Caltrans, 2019b).

- Select column size and reinforcement
- Determine displacement demands
- Determine displacement capacities
- Design end cross frame

20.2.9.3 Select Column Size and Reinforcement

20.2.9.3.1 Column Size

Based on the strength limit state design, the dead load acting on the top of the column is about 1,150 kips at Bent 3. In general, the concrete column diameter can be estimated by

$$0.1A_g f_c' = P_{DL}$$

$$D_c = \sqrt{40P_{DL}/(\pi f_c')} = \sqrt{40 \times 1150/(3.1416 \times 4.0)} = 60.5 \text{ in.}$$

The column diameter is taken as 5.0 ft.

20.2.9.3.2 Bent Cap Width

$$B_{cap} = D_c + 2.0 = 5.0 + 2.0 = 7.0 \text{ ft} \qquad\qquad (SDC \ 4.7.3\text{-}1)$$

20.2.9.3.3 Column Longitudinal and Transverse Reinforcement

Based on Article 5.3.9 of the *SDC*, the steel area of column longitudinal reinforcement should be within 1% to 4% column gross area. Let's take 1.5% area ratio as the initial design (also from DL + LL design):

$$A_s = 0.015A_g = 0.015\left(\frac{\pi}{4}\right)\left[5.0(12)\right]^2 = 0.015(2827) = 42.41 \text{ in.}^2$$

Use #11 rebar, the total rebar numbers are 42.41/1.56 = 27.19, take 28 bars.

For transverse reinforcement, take #7@6 as the initial design.

20.2.9.3.4 Column Cross-Section Analysis

CSIBridge Section Designer is used to calculate column effective properties. Figure 20.2.9-6 shows the column cross section.
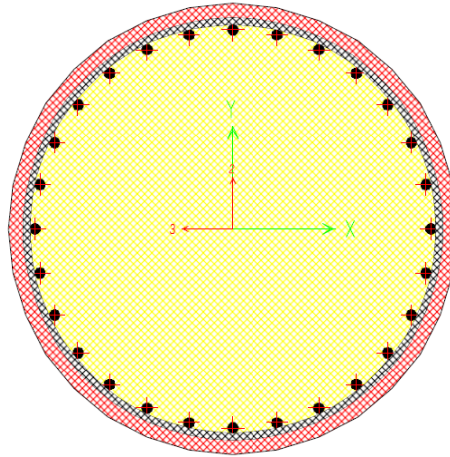
Figure 20.2.9-6 Column Cross Section

Taking the expected material properties as specified in Article 3.3.1 of the *SDC*, Figures 20.2.9.7 and 20.2.9.8 show the Moment Curvature and corresponding section properties for Bent 2 columns and Bent 3 columns, respectively.

Results for Exact-Integration

ϕ_y	= 0.000999 rad/ft
ϕ_u	= 0.0112 rad/ft
M_y	= 5,200 kip-ft
M_p	= 7,177 kip-ft
I_e	= 12.46 ft⁴
P	= 1160 kip
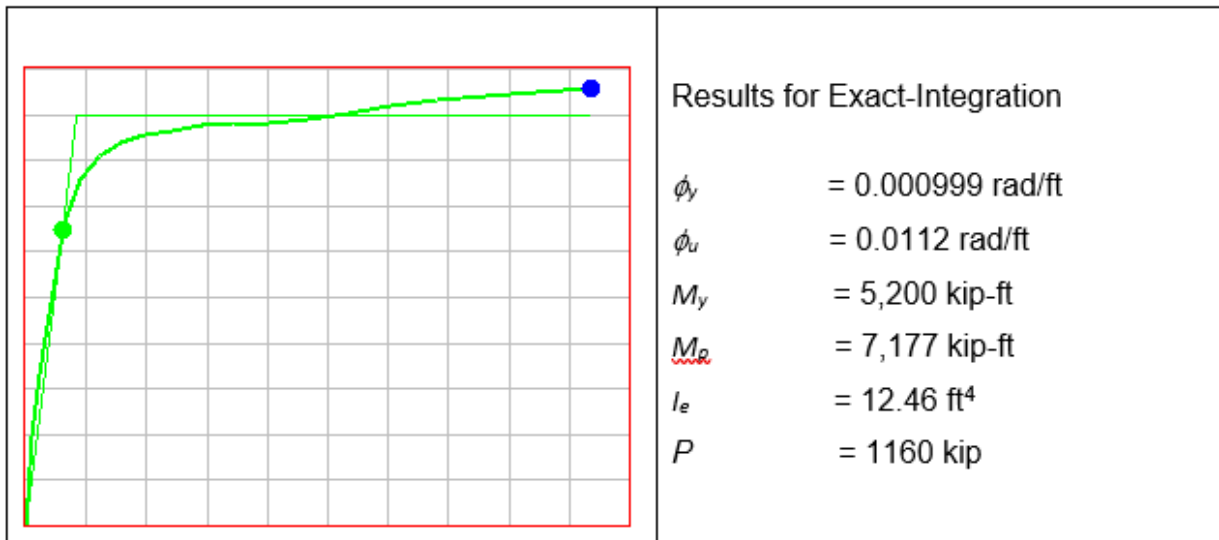
Figure 20.2.9-7 Moment Curvature – Bent 2 Columns

Results For Exact-Integration

ϕ_y	= 0.0009981 rad/ft
ϕ_u	= 0.0111 rad/ft
M_y	= 5,267 kip-ft
M_p	= 7,223 kip-ft
I_e	= 12.57 ft⁴
P	= 1200 kip
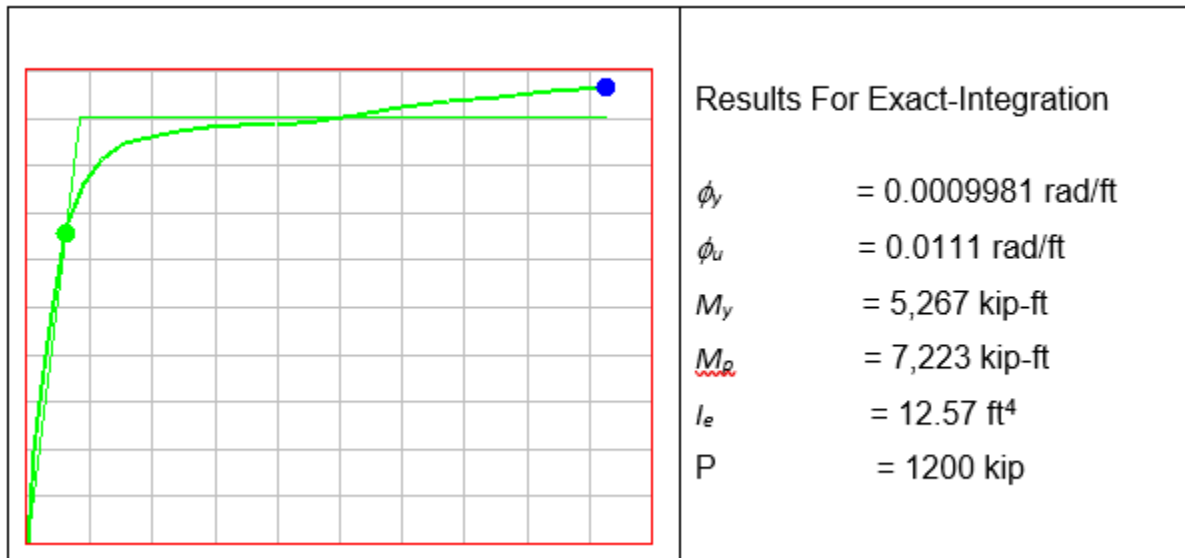
Figure 20.2.9-8 Moment Curvature – Bent 3 Columns

20.2.9.4 Determine Displacement Demands

20.2.9.4.1 CSIBridge Model

In CSIBridge Program, there is a Steel I-Girder Bridge Template. After defining the superstructure section, bent cap section, column section, end diaphragm, intermediate diaphragm, etc., it's relatively easy to build a steel girder bridge model by assigning various sections to the corresponding members. Figure 20.2.9-9 illustrates the CSIBridge model for the example bridge.
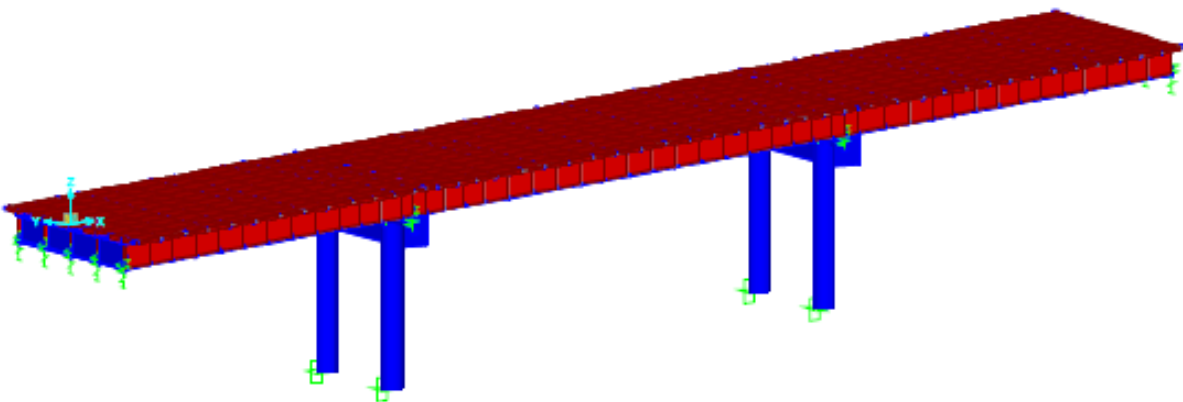
Figure 20.2.9-9 3-D CSIBridge Model for Example Bridge

It is necessary to emphasize that the modeling of a steel girder bridge is different from the modeling of a concrete box girder bridge.

First, for a concrete box girder bridge, the girders are usually integrated with the bent caps, and connections between columns and footings are designed as "Pinned" connections for multi-column bents. However, for a steel girder bridge, the girders generally are not integrated with bent caps, but each girder sets on a bearing pad with several anchor bolts connecting them to the bent cap. There are special shear keys to limit the girder movement transversely in case the anchor bolts fail during the design earthquake. Therefore, for a steel girder bridge, the bottom of the column should be designed as a "Fixed" connection.

Second, if the bearing pad connecting the steel girder and the bent cap is an isolation element, the properties of this isolator should be included in the CSIBridge model.

For the example bridge, the bottom of the column is modeled as "Fixed" in the CSIBridge model. The bearing pad is not included in the model due to it lacking of isolation element properties.

20.2.9.4.2 Abutment Longitudinal and Transverse Stiffness

A standard seat type abutment with a backwall width of 50.83 ft along the skew direction is chosen since the bridge length is 400 ft. To engage the soil resistance behind the abutment back wall as much as possible, it is recommended that a concrete end diaphragm be incorporated at the end span, see Figure 20.2.9-10.
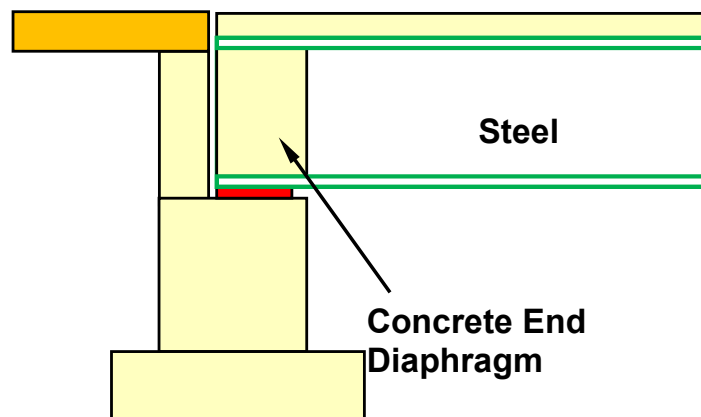
Figure 20.2.9-10 Steel Girder with Concrete End Diaphragm

Based on *SDC*, the initial abutment longitudinal stiffness can be estimated by

$$K_{abut} = w_{abut}(5.5h_{abut} + 20)e^{-\theta/45}$$
(*SDC* 6.3.1.2-5)

in which w_{abut} is abutment backwall width along the skew direction; h_{abut} is abutment backwall height and θ is abutment skew. In this example, w_{abut} = 50.83 ft, h_{abut} = 8.0 ft and θ = 20 deg., the calculated abutment longitudinal stiffness is K_{abut} = 2,086 k/in.

From the *SDC*, the ultimate soil resistance is calculated by

$$F_{abut} = W_{abut} \left(\frac{5.5h_{abut}^{2.5}}{1+2.37h_{abut}} \right) e^{-\theta/45} = 1{,}626 \text{ kip} \qquad (SDC\ 6.3.1.2\text{-}4)$$

Assuming a gap of 2.0 in., (based on temperature movement) abutment effective displacement is as

$$\Delta_{eff} = \Delta_{gap} + \Delta_{abut} = \Delta_{gap} + F_{abut}\ /\ K_{abut} = 2.0 + 1626\ /\ 2086 = 2.78 \text{ in.} \quad (SDC\ 6.3.1.2\text{-}2)$$

Abutment effective longitudinal stiffness is

$$K_{eff} = F_{abut}\ /\ \Delta_{eff} = 1626\ /\ 2.78 = 585 \text{ kip/in.} \qquad (SDC\ 6.3.1.2\text{-}1)$$

The effective abutment transverse stiffness is assumed as half of the adjacent bent transverse stiffness in accordance with Article 6.3.2 of the *SDC*.

20.2.9.4.3 Seismic Displacement Demands

The calculation steps include: 1) run CSIBridge (CSI, 2021) with column effective stiffness and abutment effective stiffness; 2) check abutment displacement responses in the longitudinal direction and force responses in the transverse direction; 3) determine if the stiffness iterations are needed; 4) final run and find the bridge displacement demands in both directions.

For the longitudinal direction, the displacement response at Abutment 1 is 5.41 in. from the initial run. Per *SDC* Eq. (6.3.1.3-1), the displacement coefficient R_A = 5.41/2.78 = 1.95. Since R_A < 2.0, the initial analysis displacement of 5.41 in. can be taken as the final bridge longitudinal displacement demand.

For the transverse direction, the force reactions are 640 kips and 660 kips at Abutment 1 and Abutment 4 respectively. Assuming 16 piles are used to support Abutment 1 and Abutment 4, and the shear capacity for each pile is 40 kips. Based on Caltrans successful practice, the allowed maximum transverse force demand is usually limited to 75% of total pile shear capacity: 0.75 x 40 x 16 = 480 kip. It is seen that the transverse force responses from the initial run are well over the maximum limit. The next step is to reduce the abutment transverse stiffness and run CSIBridge again, then check force responses against the allowed limit. This iterative process goes on until the force responses are slightly less than the allowed limit. The final run yields the transverse displacement demands.

The final displacement responses are summarized in Table 20.2.9-1. Fundamental period *T* = 1.26 second.

Table 20.2.9-1 Displacement Demands (Δ_D)

Bent	Longitudinal Displacement (in.)	Transverse Displacement (in.)
Bent 2	5.38	9.59
Bent 3	5.39	9.98

20.2.9.5 Determine Displacement Capacity

20.2.9.5.1 Longitudinal Displacement Capacity

The displacement capacity of a bridge can be estimated by a push-over analysis. In general, an individual bent is separated from the 3-D bridge model, and the push-over analyses are performed in the bridge longitudinal direction as well as in the bridge transverse direction for each bent.

For the example bridge, as discussed before, the steel girders are sitting on the bent caps. It is difficult to restrain the bent cap rotation longitudinally by those steel girders. Therefore, it is reasonably assumed that the longitudinal push of each bent can be modeled with the bottom column "fixed" and the top free (cantilever). For this kind of simplified bent model, the displacement capacity can be easily computed by equations given in the *SDC*. The detailed calculations are listed in Table 20.2.9-2.

Chapter 20.2 – Seismic Design of Steel Bridges

Table 20.2.9-2 Longitudinal Displacement Capacity

Parameters	Calculations	Bent 2	Bent 3
Column Height H (in.)	-	528.0	528.0
Rebar Diameter d_{bl} (in.)	-	1.41	1.41
Rebar f_{ye} (ksi)	-	68.0	68.0
Plastic Hinge Length L_p (in,)	$0.08H + 0.15f_{ye}d_{bl} \geq 0.3f_{ye}d_{bl}$ (*SDC* 5.3.4-1)	56.62	56.62
Yield Curvature ϕ_y (rad/in.)	CSIBridge Results	0.0000833	0.0000832
Yield Displacement Δ_y (in.)	$\phi_y H^2 / 3$ (*SDC* C5.2.2-2)	7.74	7.74
Ultimate Curvature ϕ_u (rad/in.)	CSIBridge Results	0.000933	0.000925
Ultimate Displacement Δ_C (in.)	$\Delta_y + L_p(\phi_u - \phi_y)(H - L_p / 2)$ (*SDC* C5.2.2-1)	31.79	31.55
Displacement D/C Ratio	$\Delta_C \geq \Delta_D$ (*SDC* 3.5.1-1)	31.79 > 5.38	31.55 > 5.39
Displacement Ductility Demand μ_d	Δ_D / Δ_y (*SDC* Table 4.4.1-1)	0.70 < 5.0	0.70 <5.0

The table shows that the longitudinal displacement D/C ratio, displacement ductility capacity, and displacement ductility demand are all satisfied for both Bent 2 and Bent 3.

20.2.9.5.2 Transverse Displacement Capacity

Figure 20.2.9-11 illustrates individual Bent 2 and Bent 3 frames in CSIBridge. For any multi-column bents, there is always an overturning effect when the bent moves transversely. Therefore, when calculating the transverse displacement capacity of a bent, one must consider this overturning effect. In the CSIBridge Program, there is a subroutine, especially for push-over analysis, which is used to evaluate the transverse displacement capacity for this steel bridge example. Figure 20.2.9-12 shows the force-displacement curve with the maximum lateral force of 420 kips at Bent 2 by CSIBridge push-over analysis. A similar curve can be drawn for Bent 3. Table 20.2.9-3 summarizes the yield displacements and ultimate displacements in the transverse direction for Bent 2 and Bent 3. It is seen that the transverse displacement D/C ratio, displacement ductility capacity, and displacement ductility demand are all satisfied for both Bents 2 and 3.
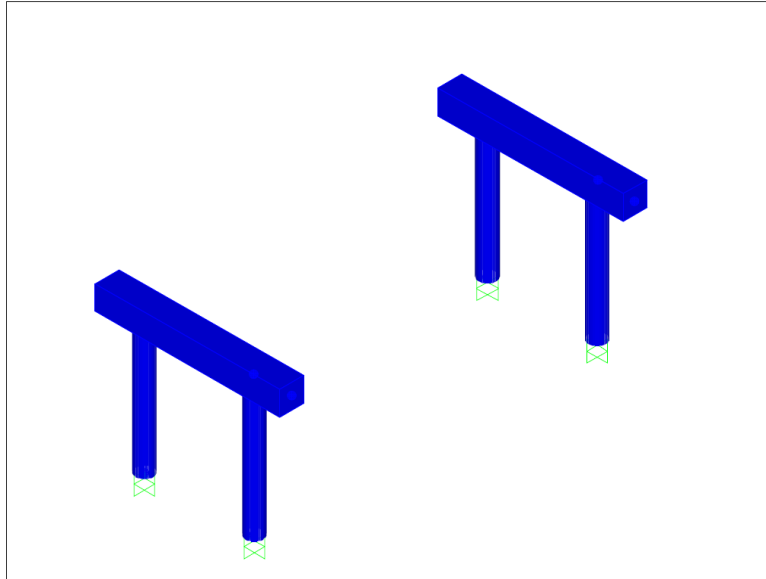
Figure 20.2.9-11 Individual Bent for Transverse Push-over Analysis

Figure 20.2.9-12 Force-Displacement Curve at Bent 2

Table 20.2.9-3 Transverse Displacement Capacity

Parameters	Calculations	Bent 2	Bent 3
Column Height H (in.)	-	528.0	528.0
Rebar Diameter d_{bl} (in.)	-	1.41	1.41
Rebar f_{ye} (ksi)	-	68.0	68.0
Plastic Hinge Length L_p (in.)	$0.08H + 0.15f_{ye}d_{bl} \geq 0.3f_{ye}d_{bl}$ (SDC 5.3.4.1)	56.62	56.62
Yield Displacement Δ_y (in.)	CSIBridge Results	5.92	6.02
Ultimate Displacement Δ_C (in.)	CSIBridge Results	19.80	20.02
Displacement D/C Ratio	$\Delta_C \geq \Delta_D$ (SDC 3.5.1-1)	19.8 > 9.59	20.02 > 9.98
Displacement Ductility Demand μ_d	Δ_D / Δ_y	1.62 <5.0	1.66<5.0

20.2.9.6 Design End Cross Frames

20.2.9.6.1 Select End Cross Frame Type

An inverted V-type end cross frame is selected and is shown in Figure 20.2.9-13. For a skew angle of 20-degree, girder spacing along the skew direction is 12′/cos(20º) = 12.77 ft.
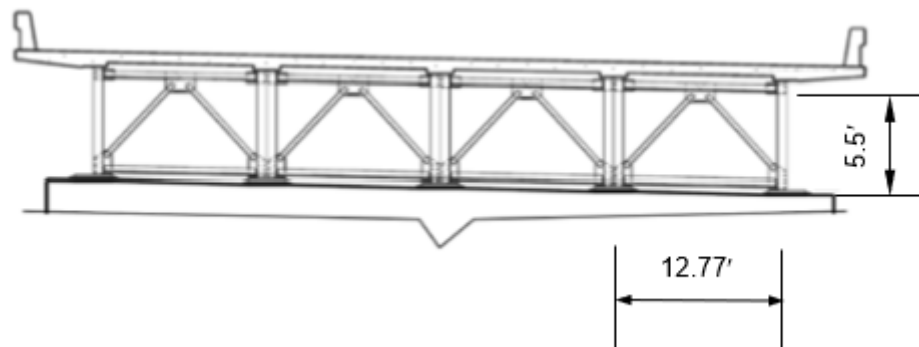
Figure 20.2.9-13 End Cross Frame

Use A709 Grade 36 steel, F_y =36 ksi ; F_u = 58 ksi. From *SDSSB* Table 2.4-1, the ratio of the expected yield strength to the specified minimum yield strength, R_y = 1.5 for rolled shapes, and 1.3 for plates, respectively; the ratio of the expected tensile strength to the specified minimum tensile strength, R_t = 1.2 for the both rolled shapes and plates.

For rolled shapes: $F_{ye} = R_y F_y = (1.5)(36) = 54$ ksi   (*SDSSB* 2.4-1)

For plates: $F_{ye} = R_y F_y = (1.3)(36) = 46.8$ ksi   (*SDSSB* 2.4-1)

$F_{ue} = R_t F_u = (1.2)(58) = 69.6$ ksi   (*SDSSB* 2.4-2)

Distances between working points for braces are as follows:

Diagonal: $L_{dg} = \sqrt{5.5^2 + 6.385^2} = 8.43$ ft $= 101.2$ in.

Top strut: $L_{ts} = 6.385$ ft $= 76.6$ in.

Bottom strut: $L_{bs} = 12.77$ ft $= 153.2$ in.

20.2.9.6.2 Determine Force Demands

The force demand for an end cross frame is the overstrength lateral force of the substructure. For Bent 2, the lateral load capacity of 420 kips of the substructure in the transverse direction is obtained by a pushover analysis, as discussed in Section 20.2.9.5.2.

Using an overstrength factor of 1.2 for the expected plastic shear for a ductile concrete substructure as specified in (*SDC* 4.4.2.1), the total overstrength horizontal force transferred to the entire four-bay end cross frame system is:

$$V_{04} = (1.2)(420) = 504 \text{ kip}$$

Equal distribution of lateral load is assumed for each bay of inverted v-bracings as follows:

$$V_{01} = \frac{504}{4} = 126 \text{ kip}$$

Tension and compression force demands for each diagonal are obtained by the joint equilibrium of the free body diagram. For brevity, the cross slope of the bridge is not considered in this example, and we will assume identical angles for the bracing system as shown in Figure 20.2.9-14:
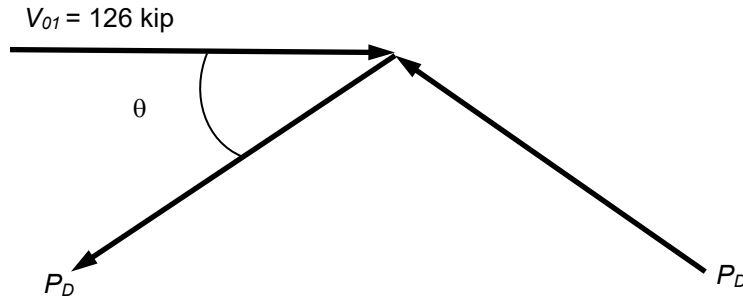
Figure 20.2.9-14   Joint Equilibrium

$$\cos\theta = \frac{76.6}{101.2} = 0.757; \quad \theta \approx 40.81°$$

$$P_D = \frac{V_{01}}{2\cos\theta} = \frac{126}{2(0.757)} = 83.2 \text{ kip}$$

20.2.9.6.3   Design Diagonals

Select Section

Try L 5×5×1/2 as shown in Figure 20.2.9-15

Check width-to-thickness ratio

$$\lambda = b/t = 5/(1/2) = 10 < \lambda_r = 0.45\sqrt{\frac{E_s}{F_y}} = 12.8 \quad \text{but } \lambda = 10 > \lambda_{ps} = 0.30\sqrt{\frac{E_s}{F_y}} = 8.5$$

Section meets capacity-protected member ratios for unstiffened compression elements per Article 6.9.4.2.1 and can develop full nominal yield stress under uniform axial compression before the onset of local buckling, but the section is not ductile (λ_{ps}) per *SDSSB* Table 4.2-1.

A_g = 4.79 in.^{2}; $r_x = r_y$ = 1.53 in.; r_z = 0.980 in.; $\bar{x} = \bar{y} = 1.42$ in.; b = 5 in.
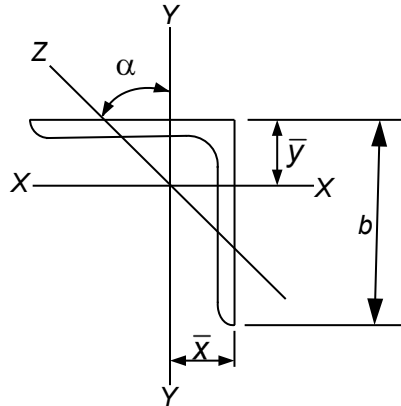
Figure 20.2.9-15 Single Angle

Check Limiting Effective Slenderness Ratio

Caltrans *SDSSB* Table 4.3-1 requires that the effective slenderness ratio for capacity protected brace members KL_b/r shall not exceed 200. For single angles, buckling occurs about the minor principal axis (*Z-Z*). Using an unbraced length of the brace member $L_z = L_{dg}$ = 101.2 in. and effective length factor K = 1.0 (Article 4.6.2.5), the minimum effective slenderness ratio is:

$$\frac{KL_z}{r_z} = \frac{(1.0)(101.2)}{0.98} = 103.3 < 200 \qquad \text{O.K.}$$

Calculate Design Compression Strength

A single angle member is typically connected through one leg only and is subjected to combined axial compression and flexural moments about principal axes. Article 6.9.4.4 provides simplified equations for effective slenderness ratios to be used in Articles 6.9.2.1 and 6.9.4.1.

For equal-leg angles that are individual members, $\dfrac{L_{dg}}{r_x} = \dfrac{101.2}{1.53} = 66.14 < 80$

$$\left(\frac{KL}{r}\right)_{eff} = 72 + 0.75\frac{L_{dg}}{r_x} = 72 + 0.75(66.14) = 122 \qquad \text{(AASHTO 6.9.4.4-1)}$$

Expected nominal axial compression resistance, $P_{nc,}$ is calculated as follows:

$$P_e = \frac{\pi^2 E}{\left(\dfrac{KL}{r}\right)^2_{eff}} A_g = \frac{\pi^2 (29,000)}{(122)^2}(4.79) = 92.1 \text{ kip} \qquad \text{(AASHTO 6.9.4.1.2-1)}$$

$$P_o = F_{ye} A_g = (54)(4.79) = 258.7 \text{ kip}$$

$$\frac{P_e}{P_o} = \frac{92.1}{258.7} = 0.356 < 0.44$$

$$P_{nc} = 0.877 P_e = 0.877(92.1) = 80.8 \text{ kip} \qquad \text{(AASHTO 6.9.4.1.1-2)}$$

Using a resistance factor $\phi = 1.0$ as specified by *SDSSB* Article 2.6.4, design compression strength is:

$$P_{CC} = \phi P_{nc} = (1.0)(80.8) = 80.8 \text{ kip} \approx P_D = 83.2 \text{kip} \quad \text{It is within 3\%, say OK}$$

Calculate Design Tension Strength

Expected nominal axial tension resistance, $P_{nt,}$ is calculated in accordance with Article 6.8.2.

$$P_{nt} = F_{ye} A_g = (54)(4.79) = 258.7 \text{ kip}$$

Using $\phi = 0.9$ as specified by *SDSSB* Article 2.6.4, design tension strength is:

$$P_{CT} = \phi P_{nt} = (0.9)(258.7) = 232.8 \text{ kip} > P_D = 83.2 \text{ kip (AASHTO 6.8.2.1-1)}$$

20.2.9.6.4 Design Top Strut

The design of the top strut itself for seismic forces in the cross frame is usually not critical. It is compositely connected to the concrete deck end diaphragm with shear connector studs. However, during the construction of the deck, the top strut is to provide lateral stability to the top flange and is usually designed for 2 percent of the flange yield strength.

The top flange area: $\qquad\qquad\qquad\qquad\qquad A_f = (18)(2) = 36 \text{ in.}^2$

Two percent of the expected flange yield strength:

$$P_D = 0.02 F_y A_f = (0.02)(36)(36) = 25.9 \text{ kip}$$

Select Section

Try L 4×4×7/16, A_g = 3.3 in.^{2}; $r_x = r_y$ = 1.22 in.; r_z = 0.777 in.

$\bar{x} = \bar{y} = 1.15$ in.

$$\lambda = \frac{b}{t} = \frac{4}{7/16} = 9.14 < \lambda_r = 0.45\sqrt{\frac{E_s}{F_y}} = 12.8 \qquad .$$

Section meets nonslender element requirement as specified in Article 6.9.4.2.1

Check Limiting Effective Slenderness Ratio

$$\frac{KL_{ts}}{r_z} = \frac{(1.0)(76.6)}{0.777} = 98.6 < 200 \qquad\qquad (SDSSB \text{ Table 4.3-1})$$

Calculate Design Compression Strength

For equal-leg angles that are individual members, $\dfrac{L_{ts}}{r_x} = \dfrac{76.6}{1.22} = 62.8 < 80$

$$\left(\frac{KL}{r}\right)_{eff} = 72 + 0.75\frac{L_{ts}}{r_x} = 72 + 0.75(62.8) = 119.0 \qquad\qquad (AASHTO\ 6.9.4.4\text{-}1)$$

$$P_e = \frac{\pi^2 E}{\left(\dfrac{KL}{r}\right)_{eff}^2} A_g = \frac{\pi^2(29000)}{(119.0)^2}(3.3) = 66.7 \text{ kip} \qquad\qquad (AASHTO\ 6.9.4.1.2\text{-}1)$$

$$P_o = F_{ye}A_g = (54)(3.3) = 178.2 \text{ kip}$$

$$\frac{P_e}{P_o} = \frac{66.7}{178.2} = 0.374 < 0.44$$

$$P_{nc} = 0.877P_e = 0.877(66.7) = 58.5 \text{ kip} \qquad\qquad AASHTO\ 6.9.4.1.1\text{-}2)$$

Using a resistance factor ϕ = 1.0 as specified by *SDSSB* Article 2.6.4, design compression strength is as:

$$P_{CC} = \phi P_{nc} = (1.0)(58.5) = 58.5 \text{ kip } > P_D = 35.9 \text{ kip} \qquad\qquad \text{OK}$$

20.2.9.6.5   Design Bottom Strut

The force in the bottom strut may be assumed zero. It is usually designed for 2 percent of the flange yield strength to provide lateral stability to the bottom flange during construction.

The maximum bottom flange area: A_f = (18)(2) = 36 in.

Two percent of the flange yield strength is

$$P_D = 0.02 F_y A_f = (0.02)(36)(36) = 25.9 \text{ kip}$$

Select Section

Try L 5×5×1/2, A_g = 4.79 in.^{2} ; $r_x = r_y$ = 1.53 in.; r_z = 0.980 in.

$$\lambda = \frac{b}{t} = \frac{5}{0.5} = 10 < \lambda_r = 0.45 \sqrt{\frac{E_s}{F_y}} = 12.8$$

Section meets nonslender element requirement as specified in Article 6.9.4.2.1.

Check Limiting Effective Slenderness Ratio

$$\frac{KL_{bs}}{r_z} = \frac{(1.0)(153.2)}{0.98} = 156 < 200 \qquad\qquad (SDSSB \text{ Table 4.3-1})$$

Calculate Design Compression Strength

For equal-leg angles that are individual members, $\dfrac{L_{bs}}{r_x} = \dfrac{153.2}{1.53} = 100.1 > 80$

$$\left(\frac{KL}{r}\right)_{eff} = 32 + 1.25 \frac{L_{bs}}{r_x} = 32 + 1.25(100.1) = 157.1 \qquad (\text{AASHTO } 6.9.4.4\text{-}2)$$

Axial resistance is calculated in accordance with Article 6.9.4.1 as follows:

$$P_e = \frac{\pi^2 E}{\left(\dfrac{KL}{r}\right)_{eff}^2} A_g = \frac{\pi^2 (29000)}{(157.1)^2}(4.79) = 55.5 \text{ kip} \qquad (\text{AASHTO } 6.9.4.1.2\text{-}1)$$

$$P_o = F_{ye} A_g = (54)(4.79) = 258.7 \text{ kip}$$

$$\frac{P_e}{P_o} = \frac{55.5}{258.7} = 0.215 < 0.44$$

$$P_{nc} = 0.877P_e = 0.877(55.5) = 48.7 \text{ kip} \qquad \text{(AASHTO 6.9.4.1.1-2)}$$

For ϕ = 1.0 as specified by *SDSSB* Article 2.6.4, design compression strength is:

$$P_{CC} = \phi P_{nc} = (1.0)(48.7) = 48.7 \text{ kip} > P_D = 25.9 \text{kip} \qquad \text{OK}$$

20.2.9.6.6   Design Diagonal Connection at Lower Left

The lower diagonal connection of the inverted v-brace is shown in Figure 20.2.9-16.
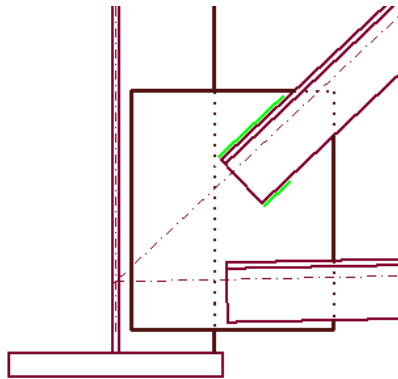
Figure 20.2.9-16 Gusset Plate Connection at Lower Left

Design Fillet Welds

Using F_{exx} = 70 ksi and ϕ = 0.9 (*SDSSB* 2.6.4), the design shear resistance of the weld metal is:

$$R_r = 0.6\phi F_{exx} = (0.6)(0.9)(70) = 37.8 \text{ ksi} \qquad \text{(AASHTO 6.13.3.2.4-1)}$$

For L5×5×1/2 as shown in Figure 20.2.9.6-3, $\bar{y}$ = 1.42 in.; b = 5 in.; we select weld size of 0.3125 in., the effective size of a fillet weld, t_e = (0.707)0.3125 = 0.221 in. and the design strength of 0.3125 in. fillet weld per inch of length is as follows:

$$R_{rw} = R_r t_e = (37.8)(0.221) = 8.35 \text{ kip/in.}$$

Since this is an elastic design, and diagonal tension and compression forces are identical, the welds may be designed for the compression strength capacity of the diagonal. But, for this example, the welds are designed for the overstrength force demand P_D = 83.4 kips as shown in Figure 20.2.9-17.
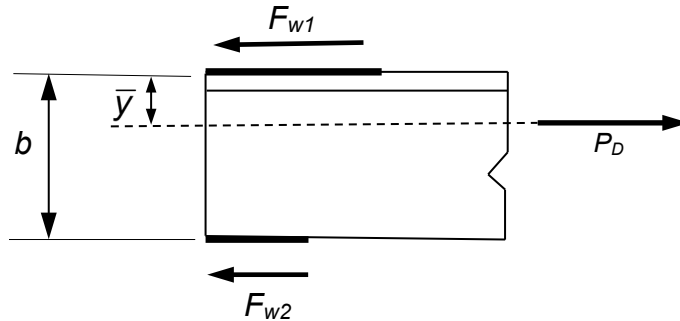
Figure 20.2.9-17   Angle to Gusset Welds

The required force for the longer weld length L_{w1} is obtained by

$$F_{w1} = P_D\left(1 - \frac{\bar{y}}{b}\right) = (83.4)\left(1 - \frac{1.42}{5}\right) = 59.7 \text{ kip}$$

Required force for shorter weld length L_{w2} is obtained by

$$F_{w2} = P_D\left(\frac{\bar{y}}{b}\right) = (83.4)\left(\frac{1.42}{5}\right) = 23.7 \text{ kip}$$

Required longer weld length L_{w1} is obtained by

$$L_{w1} = \frac{F_{w1}}{R_{rw}} = \frac{59.7}{8.35} = 7.15 \text{ in.} \qquad \text{Use 7 ½ in. for 5/16 in. weld}$$

Required shorter weld length L_{w2} is obtained by

$$L_{w2} = \frac{F_{w2}}{R_{rw}} = \frac{23.7}{8.35} = 2.83 \text{ in.} \qquad \text{Use 3 in. for 5/16 in. weld}$$

Check Compression Strength of Gusset Plate

Try ASTM A709 Grade 36, plate thickness t_g = 0.375 in.

$$r = \frac{t_g}{\sqrt{12}} = (0.289)(0.375) = 0.108 \text{ in.} \; ; \; F_y = 36 \text{ ksi}; \quad F_u = 58 \text{ ksi}$$

$$F_{ye} = R_y F_y = (1.3)(36) = 46.8 \text{ ksi} \qquad\qquad (SDSSB\ 2.4\text{-}1)$$

$$F_{ue} = R_t F_u = (1.2)(58) = 69.6 \text{ ksi} \qquad\qquad (SDSSB\ 2.4\text{-}2)$$

Effective Whitmore section width as shown in Figure 20.2.9-18 is as follows:

$$w_g = 5 + (7.5 + 3)\ tan\ 30^o = 11.06 \text{ in.}$$

Effective Whitmore Section Area is:

$$A_g = w_g t_g = (11.06)(0.375) = 4.15 \text{ in.}^2$$

From *SDSSB* C7.5.4, K = 1.2, and the unbraced length is calculated by *SDSSB* C7.5.4-1. From Figure 20.2.9-18, L_1 = 5.1 in.; L_2 = 3.0 in., and L_3 = 10.1 in. The average length of the unbraced length for the Whitmore section is obtained as follows:

$$L = \frac{L_1 + L_2 + L_3}{3} = \frac{5.1 + 3.0 + 10.1}{3} = 6.1 \text{ in.} \qquad (SDSSB\ C7.5.4\text{-}1)$$
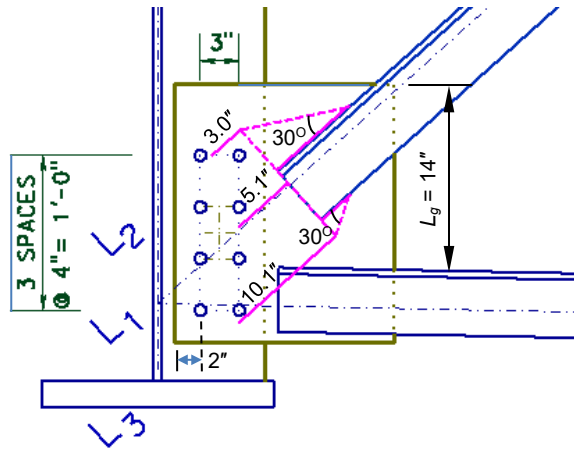
Figure 20.2.9-18 Whitmore Section of Gusset Plate

$$\frac{KL}{r} = \frac{(1.2)(6.1)}{0.108} = 67.8$$

$$P_e = \frac{\pi^2 E}{\left(\frac{KL}{r}\right)^2} A_g = \frac{\pi^2 (29{,}000)}{(67.8)^2}(4.15) = 258 \text{ kip} \qquad (AASHTO\ 6.9.4.1.2\text{-}1)$$

$$P_o = F_{ye} A_g = (46.8)(4.15) = 194 \text{ kip}$$

$$\frac{P_e}{P_o} = \frac{258}{194} = 1.33 > 0.44$$

$$P_{nc} = \left[0.658^{(P_o/P_e)}\right] P_o = \left[0.658^{194/258}\right](194) = 142 \text{ kip} \qquad (AASHTO\ 6.9.4.1\text{-}1)$$

Using a resistance factor ϕ = 1.0 as specified by *SDSSB* Article 2.6.4, the design compression strength of the gusset plate is as

$$P_{CC} = \phi P_{nc} = (1.0)(142) = 142 \text{ kip} > P_D = 83.2 \text{ kip} \qquad \text{OK}$$

Check Tension Strength of Gusset Plate

Nominal yield strength on the gross section is:

$$P_{nt} = F_{ye}A_g = (46.8)(4.15) = 194 \text{ kip}$$
(AASHTO 6.8.2.1-1)

Nominal fracture strength on the net section with one bolt diameter d = 0.875 in.; U = 1.0; and R_p = 1.0, is:

$$\begin{aligned}
P_{nf} &= F_{ue}A_nR_pU = F_{ue}(w_g - d)t_gU \\
&= (69.6)\left[(11.06 - 0.875)(0.375)\right](1.0)(1.0) = 266 \text{ kip}
\end{aligned}$$
(AASHTO 6.8.2.1-2)

Using a resistance factor ϕ = 0.9 as specified by *SDSSB* Article 2.6.4, the design tension strength is controlled by yielding on the gross section as:

$$P_{CT} = \phi P_{nt} = (0.9)(194) = 174 \text{ kip} > P_D = 83.2 \text{ kip}$$
O.K.

Check Unsupported Edge Length

From Figure 20.2.9-18, the unsupported edge length of the gusset plate is L_g = 14 in.

$$\frac{L_g}{t_g} = \frac{14}{0.375} = 37.3 < 2.06\sqrt{\frac{E_s}{F_y}} = 2.06\sqrt{\frac{29000}{36}} = 58.5 \qquad \text{O.K.} \qquad (SDSSB\ 7.5.2\text{-}1)$$

Design Bolts

Try high strength bolts - ASTM F3125 Grade A325-X high strength bolts, F_{ub} = 120 ksi; diameter d = 7/8 in.; bolt area A_b = 0.601 in.[2]; threads are excluded from the shear plane. Try four rows at a spacing of 4 in. as shown in Figure 20.2.9-18.

Determine Nominal Resistance per Bolt

For a single shear plane, N_s = 1

$$R_n = 0.56A_bF_{ub}N_s = (0.56)(0.6)(120)(1) = 40.3 \text{ kip} \qquad (AASHTO\ 6.13.2.7\text{-}1)$$

Check the clear end distance L_c = 2.0 – (0.875+0.0625)/2 =1.53 in. < 2d = 1.75 in.

The expected nominal bearing resistance for each bolt hole on gusset plate material is:

$$R_{ne} = 1.2L_ctF_{ue} = (1.2)(1.53)(0.375)(69.6) = 47.9 \text{ kip} \qquad (AASHTO\ 6.13.2.9\text{-}2)$$

It is obvious that bolt shear resistance controls and the nominal shear resistance per bolt are 40.3 kips. Using a resistance factor ϕ = 0.9 as specified by *SDSSB* Article 2.6.4, design shear strength per bolt is as:

$$R_{bs} = \phi R_n = (0.9)(40.3) = 36.3 \text{ kip}$$

Try four rows at a spacing of 4 in. as shown in Figure 20.2.9-19.
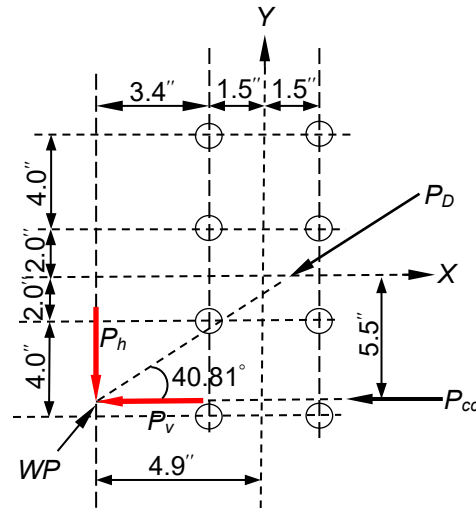
Figure 20.2.9-19 Bolt Pattern of Diagonal Connection at Lower Left

Force acting on the working point (WP) is assumed as the overstrength compression force demand P_D = 83.2 kip and bottom strut design compression strength P_{CC} = 48.7 kips.

Resultant horizontal force:
$$P_h = P_D \cos(40.81°) + P_{CC}$$
$$= (83.2)\cos(40.81°) + 48.7 = 111.7 \text{ kip } (\leftarrow)$$

Resultant vertical force:
$$P_v = P_D \cos(90° - 40.81°) =$$
$$= (83.2)\cos(49.19°) = 54.4 \text{ kip } (\downarrow)$$

The upper and lower right corner bolts are usually the most highly stressed and will be investigated. The "Vector" method is used to calculate shear force R on the top right bolt.

The polar moment of inertia, I_p, of the bolt group as shown in Figure 20.2.9-19 with respect to the center of gravity of the bolt group is calculated as follows:

$$I_p = \sum x^2 + \sum y^2 = 8(1.5)^2 + 4(6)^2 + 4(2)^2 = 178 \text{ in.}^2$$

Factored shear forces applied on the lower right corner bolt are as:

$$R_x = \frac{M_x y}{I_p} = \frac{(111.7)(5.5)(6)}{178} = 20.71 \text{ kip } (\leftarrow)$$

$$R_y = \frac{M_x x}{I_p} = \frac{(54.4)(4.9)(1.5)}{178} = 2.25 \text{ kip } (\downarrow)$$

$$R_v = \frac{P_v}{8} = \frac{54.4}{8} = 6.80 \text{ kip } (\downarrow)$$

$$R_h = \frac{P_h}{8} = \frac{111.7}{8} = 13.96 \text{ kip } (\leftarrow)$$

$$R_{bolt} = \sqrt{(R_x + R_h)^2 + (R_y + R_v)^2}$$

$$= \sqrt{(20.71 + 13.96)^2 + (2.25 + 6.80)^2} = 35.80 \text{ kip}$$

$$R_{bolt} = 35.8 \text{ kip} < R_{bs} = 36.3 \text{kip} \qquad \text{OK}$$

20.2.9.6.7 Design Diagonal Connection at Top Strut

For the diagonal connection at the top strut, the loads are transferred through WP without bending. Use high strength bolts - ASTM F3125 Grade A325 high strength bolts, diameter $d = 7/8$ in.; threads are excluded from the shear plane.

Required bolt number $= V_{o1}/R_{bs} = 126/36.3 = 3.5$. Use four bolts, as shown in Figure 20.2.9-20.
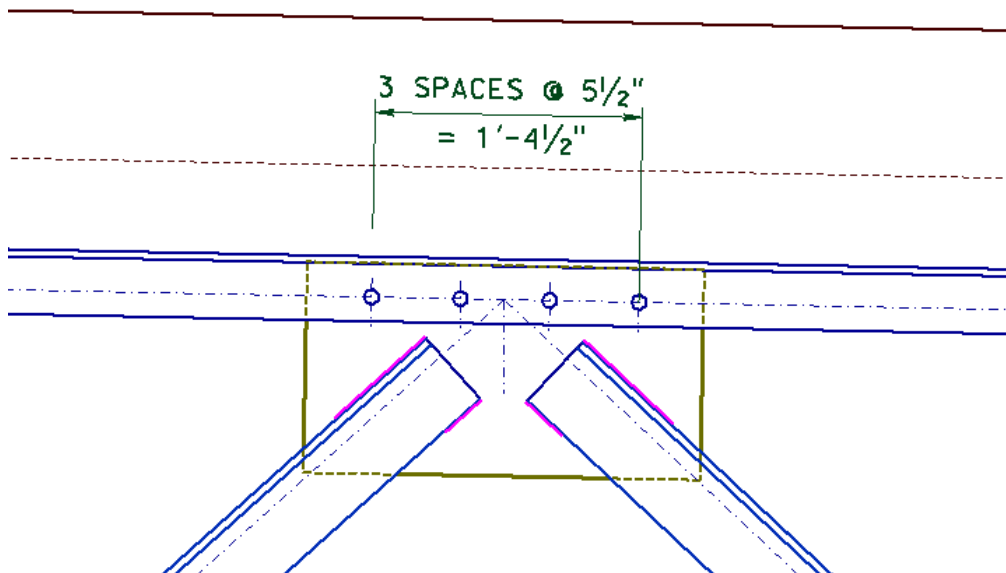
Figure 20.2.9-20 Diagonal Connection at Top Strut

The design of welds and gusset plates is similar to the diagonal connection at the lower left and is not illustrated. Note, since this is a single angle brace, the working point for fabrication may run through either the member gage, the mid-point or the center of gravity of the member, whichever is the most convenient for both design and fabrication.

20.2.9.6.8   Design Shear Connectors

The force demand for shear connectors in each bay is obtained in Section 20.2.9.6.2, V_{01} = 126 kips.

Shear connectors will be located along the central two-thirds of the top chord of the end cross frames to minimize the axial forces on the shear connectors, thus improving their cyclic responses in accordance with *SDSSB* 6.7.

Concrete deck slab, $f_c' = $ 3600 psi

$$f_{ce}' = 1.3 f_c' = (1.3)(3.6) = 4.68 \text{ ksi} < 5.0 \text{ ksi,   Use } f_{ce}' = 5.0 \text{ ksi} \qquad (SDC\ 3.3.6\text{-}4)$$

$$E_c = 33 w_c^{3/2}\sqrt{f_{ce}'} = (33)(150)^{1.5}\sqrt{5{,}000} = 4{,}286{,}826 \text{ psi} = 4{,}287 \text{ ksi} \quad (SDC\ 3.3.6\text{-}1)$$

 Try 7/8" diameter welded shear studs with $F_u = 60$ ksi (AASHTO 6.4.4)

$$A_{sc} = \frac{0.875^2 \pi}{4} =\; 0.6 \text{ in.}^2$$

The expected nominal strength of one shear connector is obtained as

$$Q_{ne} = 0.5 A_{sc}\sqrt{f_{ce}' E_c} = (0.5)(0.6)\sqrt{(5.0)(4{,}287)} = 43.9 \text{ kip}$$
$$> A_{sc} F_u = (0.6)(60) =\; 36.0 \text{ kip}$$

(AASHTO 6.10.10.4.3-1)

Use $Q_{ne} =$ 36.0 kip and $\phi = 0.95$ from *SDSSB* Article 2.6.4

The design strength of one shear stud is as follows:

$$Q_r = \phi Q_{ne} =\; (0.95)(36) =\; 34.2 \text{ kip}$$

The required number of shear studs is: $n = \dfrac{V_{0I}}{Q_r} = \dfrac{126}{34.2} = 3.68$

Use 6 studs per bay.

20.2.9.6.9 Design Shear Keys

Rebars in the concrete shear key are shown in Figure 20.2.9-21. The calculations of the rebar development lengths shall be in accordance with Article 5.10.8.2 and are not illustrated here.

Chapter 20.2 – Seismic Design of Steel Bridges
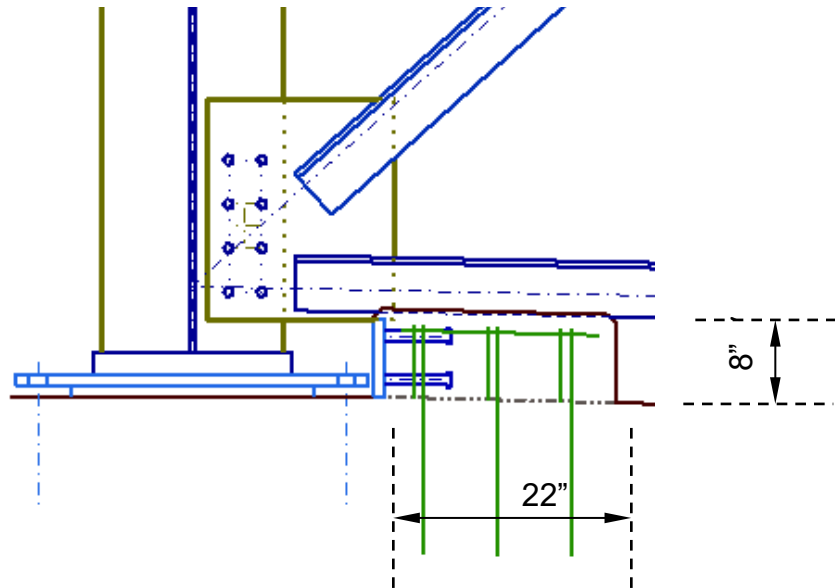
Figure 20.2.9-21 Concrete Shear Key

The interface width considered to be engaged in the shear transfer is $b_{vi} = 22$ in.

The interface length considered to be engaged in the shear transfer is $L_{vi} = 12$ in.

The depth of the shear key $d = 8$ in.

$$A_{cv} = b_{vi}L_{vi} = (12)(22) = 264 \text{ in.}^2$$

Try 6 # 5 bar, $A_{vf} = 6(0.31) = 1.86$ in.^{2}; $f_y = 60$ ksi

$$A_{vf} = 1.86 \text{ in.}^2 > \frac{0.05A_{cv}}{f_y} = 0.220 \text{ in.}^2 \quad \text{O.K.} \qquad \text{(AASHTO 5.7.4.2-1)}$$

Article 5.7.4.4 specifies that for normal weight concrete placed against a clean concrete surface, free of laitance, with surface intentionally roughened to an amplitude of 0.25 in., cohesion factor, $c = 0.24$ ksi; friction factor, $\mu = 1.0$; the fraction of concrete strength available to resist the interface shear, $K_1 = 0.25$; the limiting interface shear resistance, $K_2 = 1.5$ ksi.

For the shear key, the permanent net compressive force normal to the shear plane $P_c = 0.0$.

For the extreme limit state (seismic), $\phi = 1.0$ \qquad (AASHTO 6.5.5)

The nominal shear resistance is obtained as follows:

$$V_{ni} = cA_{cv} + \mu(A_{vf}f_y + P_c) = (0.24)(264) + (1.0)(1.86)(60) = 175 \text{ kip} \quad \text{(AASHTO 5.7.4.3-3)}$$

$$V_{ni} = 175 \text{ kip} < K_1f'_cA_{cv} = (0.25)(3.6)(264) = 238 \text{ kip} \qquad \text{O.K.} \quad \text{(AASHTO 5.7.4.3-4)}$$

$$V_{ni} = 175 \text{ kip} < K_2 A_{cv} = (1.5)(264) = 396 \text{ kip} \qquad \text{O.K.} \quad \text{(AASHTO 5.7.4.3-5)}$$

$$\phi V_{ni} = (1.0)(175) = 175 \text{ kip} > V_{01} = 126 \text{ kip} \qquad \text{O.K.}$$

20.2.9.6.10 End Cross Frame Sketch

A sketch of the end cross frame for a single bay is shown in Figure 20.2.9-22.
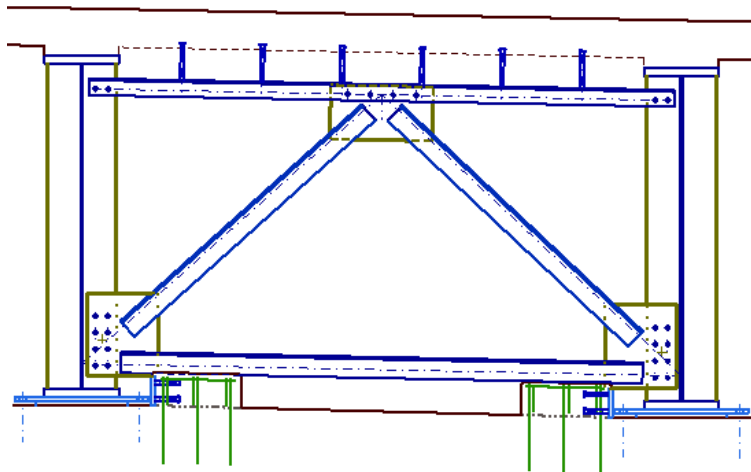
Figure 20.2.9-22 End Cross Frame Sketch -Single Bay

20.2.10   SEISMIC DESIGN EXAMPLE 2 – DUCTILE END CROSS FRAME STRATEGY

For a slab-on-steel girder bridge, when the peak ground acceleration is less than 0.4g, the bridge girders are equally spaced and straight, and the skew angle is less than 10 degrees, the ductile end cross frame design strategy is permitted to be used to prevent damage in other parts of the structure as specified in *SDSSB* Article 6.3. The following example is provided to illustrate the design procedure for a ductile end cross frame.

20.2.10.1 Steel Girder Bridge Data

Example Bridge 2 is the same as Example Bridge 1, as shown in Section 20.2.9, except the skew angle is 5 degrees. The bridge crosses a roadway and railroad tracks. Deep pile foundations are used due to poor soil conditions. The ground motion at the bridge site is assumed to be:

Soil Profile: $\qquad\qquad V_{s30} = 700$ ft/sec

Magnitude: $\qquad\qquad 8.0 \pm 0.25$

Peak Ground Acceleration: 0.4g

The design (input) acceleration response spectrum is shown in Figure 20.2.10-1.
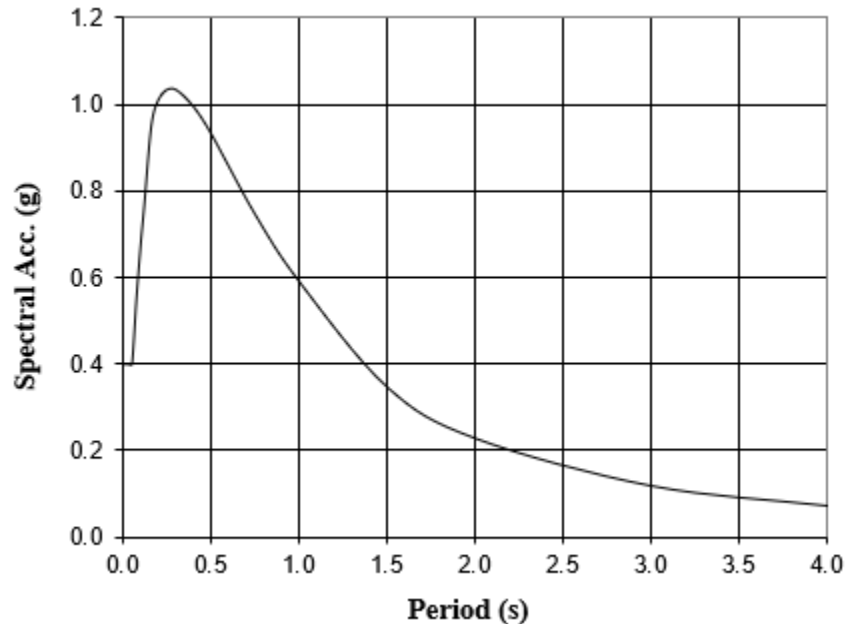
Figure 20.2.10-1   Design (Input) Acceleration Response Spectrum

20.2.10.2 Design Requirements

Perform the following seismic design in accordance with *SDSSB* (Caltrans, 2016), the *SDC* (Caltrans, 2019a), *AASHTO-CA BDS-08* (AASHTO, 2017; Caltrans 2019b).

- Select Column Size and Reinforcement
- Determine displacement demands
- Design ductile end cross frames
- Determine displacement capacities

20.2.10.3 Select Column Size and Reinforcement

20.2.10.3.1 Column Size

Same as Example 1, the column diameter is taken as 5.0 ft.

20.2.10.3.2 Bent Cap Width

$$B_{cap} = D_c + 2.0 = 5.0 + 2.0 = 7.0\,\text{ft} \qquad\qquad (SDC\ 7.4.3\text{-}1)$$

20.2.10.3.3 Column Longitudinal and Transverse Reinforcement

Same as Example 1, take 1.5% of the gross column cross section area for the initial longitudinal main reinforcement design.

$$A_s = 0.015 A_g = 0.015 \left(\frac{\pi}{4} \right) \left[5.0(12) \right]^2 = 42.41 \text{ in.}^2$$

Use #11 rebar, the total number of rebars= 42.41/1.56 = 27.19; use 28 bars.

For transverse reinforcement, take #7@6 as the initial design.

20.2.10.3.4 Column Cross-Section Analysis

See Section 20.2.9.3.4.

20.2.10.4   Determine Displacement Demands

20.2.10.4.1 CSIBridge Model

See Section 20.2.9.4.1.

20.2.10.4.2 Abutment Longitudinal and Transverse Stiffness

Same as Example 1, a concrete end diaphragm, as shown in Figure 20.2.9.4-2, is used. Based on the *SDC,* the initial abutment longitudinal stiffness can be estimated by

$$K_L = w_{abut}(5.5 h_{abut} + 20)e^{-\theta/45} \qquad\qquad (SDC\ 6.3.1.2\text{-}5)$$

in which w_{abut} is abutment backwall width, h_{abut} is abutment backwall height, and θ is abutment skew. In this example, w_{abut} = 50.83 ft, h_{abut}= 8.0 ft and θ = 5 deg., the calculated abutment longitudinal stiffness is K_{abut} = 2,911 k/in.

From the *SDC*, the maximum soil resistance is calculated by

$$F_{abut} = w_{abut} \left(\frac{5.5 h_{abut}^{2.5}}{1 + 2.37 h_{abut}} \right) e^{-\theta/45} = 2,269 \text{ kip} \qquad\qquad (SDC\ 6.3.1.2\text{-}4)$$

Assuming a gap of 2.0 in., (based on temperature movement) abutment effective displacement is as

$$\Delta_{eff} = \Delta_{gap} + \Delta_{abut} = \Delta_{gap} + F_{abut} / (K_{abut}) = 2.0 + 2269 / 2911 = 2.78 \text{ in.} \ (SDC\ 6.3.1.2\text{-}2)$$

The abutment effective longitudinal stiffness is:

$$K_{eff} = \frac{F_{abut}}{\Delta_{eff}} = \frac{2269}{2.78} = 816 \ \text{kip/in.}$$
(*SDC* 6.3.1.2-1)

The effective abutment transverse stiffness is assumed as 50% of the adjacent bent transverse stiffness per *SDC* 6.3.2.

20.2.10.4.3   Seismic Displacement Demands

The same procedure as Example 1 is used to calculate seismic displacement demands. After several iterations, the final displacement demands at the top of the deck are summarized in Table 20.2.10-1. Fundamental period $T = 0.97$ sec.

Table 20.2.10-1 Displacement Demands (Δ_D)

Bent	Longitudinal Displacement (in.)	Transverse Displacement (in.)
Bent 2	2.97	6.47
Bent 3	2.99	6.65

20.2.10.5 Design Ductile End Cross Frames

20.2.10.5.1   Select End Cross Frame Type

An inverted V-type end cross frame is selected and is shown in Figure 20.2.10-2. For a skew angle of 5 degrees, girder spacing along the skew direction is 12 ft/cos(5º) = 12.05 ft.
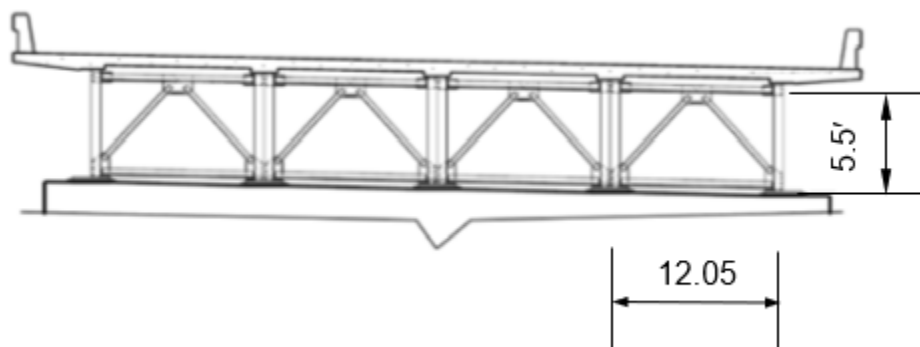
Figure 20.2.10-2 End Cross Frame

Use A709 Grade 36 steel, F_y =36 ksi ; F_u = 58 ksi. From *SDSSB* Table 2.4-1, the ratio of the expected yield strength to the specified minimum yield strength, R_y = 1.5 for rolled shapes, and 1.3 for plates, respectively; the ratio of the expected tensile strength to the specified minimum tensile strength, R_t = 1.2 for the both rolled shapes and plates.

For rolled shapes: $F_{ye} = R_y F_y = (1.5)(36) = 54$ ksi   (*SDSSB* 2.4-1)

For plates: $F_{ye} = R_y F_y = (1.3)(36) = 46.8$ ksi   (*SDSSB* 2.4-1)

$F_{ue} = R_t F_u = (1.2)(58) = 69.6$ ksi   (*SDSSB* 2.4-2)

Distances between working points for braces are as follows:

Diagonal: $L_{dg} = \sqrt{5.5^2 + 6.025^2} = 8.16$ ft $= 97.9$ in.

Top strut: $L_{ts} = 6.025$ ft $= 72.3$ in.

Bottom strut: $L_{bs} = 12.05$ ft $= 144.6$ in.

20.2.10.5.2   Design Diagonals

Select Section

Try L 2$_{1/2}$×2$_{1/2}$×5/16 as shown in Figure 20.2.10-2
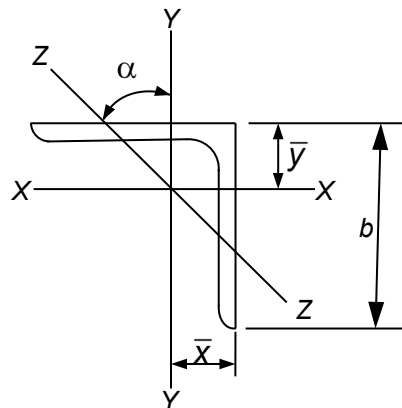
A_g =1.46 in.^{2} ; $r_x = r_y = 0.756$ in.; $r_z = 0.481$ in.

$\bar{x} = \bar{y} = 0.735$ in; $b = 2.5$ in.

Figure 20.2.10-2 Single Angle

Check Width-to-Thickness Ratio

$$\lambda = b \, / \, t = 2.5 \, / \, (0.3125) = 8.0 < \lambda_{ps} = 0.3\sqrt{\frac{E_s}{F_y}} = \sqrt{\frac{29000}{36}} = 8.5$$

Section meets ductile component requirement specified in *SDSSB* Table 4.2-1.

$$\lambda = b \, / \, t = 8.0 < \lambda_r = 0.45\sqrt{\frac{E_s}{F_y}} = 12.8 \qquad\qquad \text{(AASHTO 6.9.4.2.1)}$$

Section meets the nonslender element requirement specified in Article 6.9.4.2.1:

Check Limiting Effective Slenderness Ratio

Caltrans *SDSSB* Table 4.3-1 requires that the effective slenderness ratio for ductile compression bracing members, KL_b/r shall not exceed 200. For buckling about the minor principal axis (*Z-Z*), using the unbraced length $L_z = L_{dg}$ = 97.9 in. and the effective length factor *K* = 1.0 for single angles regardless of end conditions (Article 4.6.2.5), the effective slenderness ratio is:

$$\frac{KL_z}{r_z} = \frac{(1.0)(97.9)}{0.481} = 203.5 > 200 \qquad \text{within 2\% error, Say OK.}$$

Calculate Expected Nominal Axial Compression Strength

Compression strength is calculated in accordance with Articles 6.9.2.1 and 6.9.4.1 with simplified equations for effective slenderness ratios specified by Article 6.9.4.4.

For equal-leg angles that are individual members $\dfrac{L_{dg}}{r_x} = \dfrac{97.9}{0.756} = 129.5 > 80$

$$\left(\frac{KL}{r}\right)_{eff} = 32 + 1.25\frac{L_{dg}}{r_x} = 32 + 1.25(129.5) = 193.9 \qquad\qquad \text{(AASHTO 6.9.4.4-2)}$$

The axial resistance is calculated in accordance with Article 6.9.4.1 as follows:

$$P_e = \frac{\pi^2 E}{\left(\dfrac{KL}{r}\right)^2_{eff}} A_g = \frac{\pi^2 (29{,}000)}{(193.9)^2}(1.46) = 11.12 \text{ kip} \qquad \text{(AASHTO 6.9.4.1.2-1)}$$

$$P_o = F_{ye} A_g = (54)(1.46) = 78.84 \text{ kip}$$

$$\frac{P_e}{P_o} = \frac{11.12}{78.84} = 0.141 < 0.44$$

$$P_{nc} = 0.877 P_e = 0.877(11.12) = 9.75 \text{ kip} \qquad \text{(AASHTO 6.9.4.1.1-2)}$$

The expected nominal post-buckling strength is:

$$P_{npb} = 0.3 P_{nc} = (0.3)(9.75) = 2.93 \text{ kip} \qquad \text{(\emph{SDSSB} 5.2.5.4)}$$

The expected nominal axial tension strength is calculated as follows:

The gross section yielding:

$$P_n = F_{ye} A_g = (54)(1.46) = 78.84 \text{ kip} \qquad \text{(AASHTO 6.8.2.1-1)}$$

The net section fracture:

$$P_{nf} = F_{ue} A_n R_p U = (69.6)(1.46)(1.0)(1.0) = 101.6 \text{ kip} \qquad \text{(AASHTO 6.8.2.1-2)}$$

The expected nominal axial tension strength is controlled by the gross section yield and is equal to 78.84 kips.

The idealized plastic strength for the diagonal brace is:

$$\text{Tension:} \quad P_t = 1.17 P_n = (1.17)(78.84) = 92.2 \text{ kip} \qquad \text{(\emph{SDSSB} 2.6.6)}$$

$$\text{Compression:} \quad P_c = 1.17 P_{npb} = (1.17)(2.92) = 3.4 \text{ kip} \qquad \text{(\emph{SDSSB} 2.6.6)}$$

Using an overstrength factor Ω of 1.2, the overstrength force for diagonal braces is:

$$\text{Tension:} \quad P_{to} = \Omega P_t = (1.2)(92.2) = 110.6 \text{ kip} \qquad \text{(\emph{SDSSB} 2.6.3)}$$

$$\text{Compression:} \quad P_{co} = \Omega P_{npb} = (1.2)(3.4) = 4.1 \text{ kip} \qquad \text{(\emph{SDSSB} 2.6.3)}$$

20.2.10.5.3 Calculate Horizontal Overstrength Force

Using an overstrength factor Ω of 1.2 for the ductile end cross frame as discussed in Section 20.2.5.3, the overstrength horizontal force transferred to the substructure due to

one ductile end cross frame is obtained by the joint equilibrium as shown in Figure 20.2.10-3 as follows:
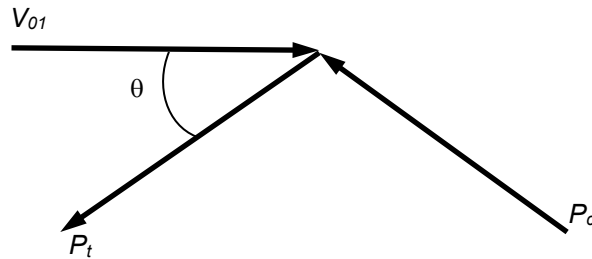
Figure 20.2.10-3   Joint Equilibrium

$$\cos\theta = \frac{72.3}{97.9} = 0.739; \quad \theta \approx 42.40°$$

$$V_{o1} = \Omega(P_t + P_c)\cos\theta = (1.2)(92.2 + 3.4)(0.739) = 84.8 \text{ kip}$$

The total overstrength horizontal force transferred to the substructure due to four ductile end cross frames is as follows:

$$V_{o4} = 4V_{o1} = (4)(84.8) = 339.2 \text{ kip}$$

20.2.10.5.4   Design Top Strut

Since the top strut of the end cross frame is connected to the concrete deck slab by shear studs, there is no need to design the top strut for transferring seismic force. Therefore, the top strut is designed for 2 percent of the flange yield strength to provide lateral stability to the top flange during construction.

The top flange area: $\quad A_f = (18)(2) = 36 \text{ in.}^2$

Two percent of the flange yield strength:

$$P_D = 0.02F_y A_f = (0.02)(36)(36) = 25.9 \text{ kip}$$

Select Section

Try L 4×4×7/16, $\quad A_g = 3.3 \text{ in.}^2$; $\quad r_x = r_y = 1.22 \text{ in.}$; $\quad r_z = 0.777 \text{ in.}$

$$\lambda = b/t = 4/(7/16) = 9.14 < \lambda_r = 0.45\sqrt{\frac{E}{F_y}} = 0.45\sqrt{\frac{29,000}{36}} = 12.8$$

Chapter 20.2 – Seismic Design of Steel Bridges

Section meets nonslender element requirement as specified in Article 6.9.4.2.1

Check Limiting Effective Slenderness Ratio

$$\frac{KL_{ts}}{r_z} = \frac{(1.0)(72.3)}{0.777} = 93.05 \; < 200 \qquad\qquad \text{O.K. (}SDSSB \text{ Table 4.3-1)}$$

Calculate Design Compression Strength

For equal-leg angles that are individual members, $\dfrac{L_{ts}}{r_x} = \dfrac{72.3}{1.22} = 59.26 \; < 80$

$$\left(\frac{KL}{r}\right)_{eff} = 72 + 0.75 \frac{L_{ts}}{r_x} = 72 + 0.75(59.26) = 116.5 \qquad\qquad \text{(AASHTO 6.9.4.4-1)}$$

Axial resistance is calculated in accordance with Article 6.9.4.1 as follows:

$$P_e = \frac{\pi^2 E}{\left(\dfrac{KL}{r}\right)_{eff}^2} A_g = \frac{\pi^2 (29{,}000)}{(116.5)^2}(3.3) = 69.6 \; \text{kip} \qquad\qquad \text{(AASHTO 6.9.4.1.2-1)}$$

$$P_o = F_{ye} A_g = (54)(3.3) = 178.2 \; \text{kip}$$

$$\frac{P_e}{P_o} = \frac{69.6}{178.2} = 0.391 < 0.44$$

$$P_{nc} = 0.877 P_e = 0.877(69.6) = 61.0 \; \text{kip} \qquad\qquad \text{(AASHTO 6.9.4.1.1-2)}$$

Using a resistance factor $\phi = 1.0$ as specified by *SDSSB* Article 2.6.4, design compression strength is as follows:

$$P_{CC} = \phi P_{nc} = (1.0)(61.0) = 61.0 \; \text{kip} \; > P_D = 25.9 \; \text{kip} \qquad\qquad \text{O.K.}$$

20.2.10.5.5 Design Bottom Strut

For an inverted V-type cross frame, the lateral force is mainly resisted by diagonal members, and the force in the bottom strut is usually assumed as zero. We select an angle L 6×6×1/2 to provide lateral stability to the bottom flange during construction and to design for 2 percent of the flange yield strength. The design calculations are similar to the above for the top strut and are not illustrated here.

20.2.10.5.6 Design Diagonal Connection at Lower Left

The lower diagonal connection of the inverted v-brace is shown in Figure 20.2.10-4.
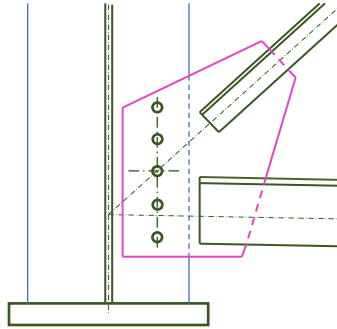
Figure 20.2.10-4 Gusset Plate Connection at Lower Left

Design Fillet Welds

Using F_{exx} = 70 ksi and ϕ = 0.9 (*SDSSB* 2.6.4) and selecting weld size t_w = 5/16″ = 0.3125 in., as calculated in Example 1 in Section 20.2.9.6.6, the design strength of 5/16″ fillet weld per inch of length is as follows:

$$R_{rw} = R_r t_e = (37.8)(0.221) = 8.35 \text{ kip/in.}$$

For L 21/2×21/2×5/16 as shown in Figure 20.2.10.2, $\bar{y} = 0.735$ in. ; b = 2.5 in.

SDSSB 7.1 requires that the design strength of a connection for ductile members shall not be less than the effect of the overstrength force of a ductile member. Therefore, the welds are required to design for an overstrength tension force of the diagonal brace, P_D = P_{to} = 110.6 kips as shown in 20.2.10-5.
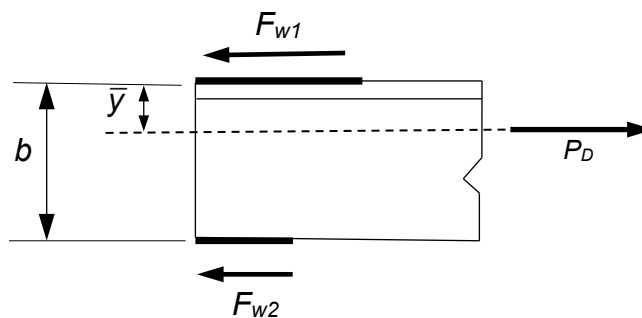
Figure 20.2.10.5-5 Angle to Gusset Welds

The required force for the longer weld length l_{w1} is obtained by

$$F_{w1} = P_D\left(1 - \frac{\bar{y}}{b}\right) = (110.6)\left(1 - \frac{0.735}{2.5}\right) = 78.1 \text{ kip}$$

The required force for shorter weld length l_{w2} is obtained by

$$F_{w2} = P_D\left(\frac{\bar{y}}{b}\right) = (110.6)\left(\frac{0.735}{2.5}\right) = 32.5 \text{ kip}$$

The required longer weld length l_{w1} is obtained by

$$L_{w1} = \frac{F_{w1}}{R_{rw}} = \frac{78.1}{8.35} = 9.35 \text{ in.} \qquad \text{use } 9\ \tfrac{1}{2} \text{ in. for 5/16″ weld}$$

The required shorter weld length l_{w2} is obtained by

$$L_{w2} = \frac{F_{w2}}{R_{rw}} = \frac{32.5}{8.35} = 3.89 \text{ in.} \qquad \text{use 4 in. for 5/16″ weld}$$

Check Compression Strength of Gusset Plate

Try ASTM A709 Grade 36, plate thickness $t_g = 0.375$ in.

$$r = \frac{t_g}{\sqrt{12}} = (0.289)(0.375) = 0.108 \text{ in.} \ ; \quad F_y = 36 \text{ ksi}; \quad F_u = 58 \text{ ksi}$$

$$F_{ye} = R_y F_y = (1.3)(36) = 46.8 \text{ ksi} \qquad\qquad\qquad \text{(SDSSB 2.4-1)}$$

$$F_{ue} = R_t F_u = (1.2)(58) = 69.6 \text{ ksi}$$

The effective Whitmore section width as shown in Figure 20.2.10-6 is as follows:

$$w_g = 2.5 + (9.5 + 4)\ tan\ 30^\circ = 10.29 \text{ in.}$$

The effective Whitmore Section Area is:

$$A_g = w_g\, t_g = (10.29)(0.375) = 3.86 \text{ in.}^2$$

From SDSSB C7.5.4, $K = 1.2$, and the unbraced length is calculated by SDSSB C7.5.4-1. From Figure 20.2.10-6, $L_1 = 7.1$ in.; $L_2 = 2.8$ in., and $L_3 = 11.5$ in. The average length of the unbraced length for the Whitmore section is obtained as follows:

$$L = \frac{L_1 + L_2 + L_3}{3} = \frac{7.1 + 2.8 + 11.5}{3} = 7.1 \text{ in.} \qquad \text{(SDSSB C7.5.4-1)}$$
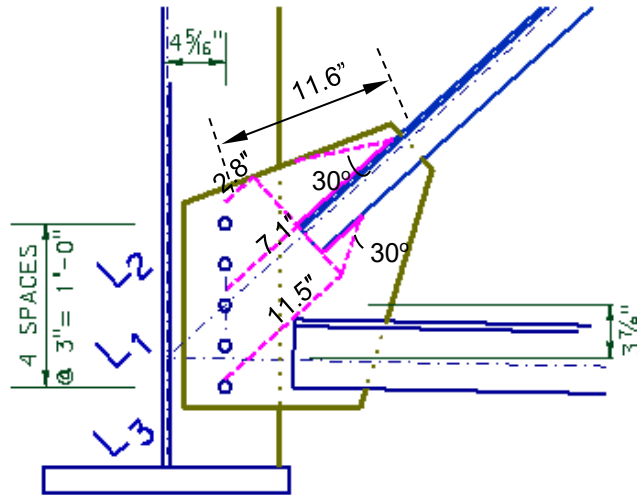
Figure 20.2.10-6 Whitmore Section of Gusset Plate

$$\frac{KL}{r} = \frac{(1.2)(7.1)}{0.108} = 78.9$$

$$P_e = \frac{\pi^2 E}{\left(\frac{KL}{r}\right)^2} A_g = \frac{\pi^2 (29,000)}{(78.9)^2}(3.86) = 177.5 \text{ kip}$$ (AASHTO 6.9.4.1.2-1)

$$P_o = F_{ye} A_g = (46.8)(3.86) = 180.6 \text{ kip}$$

$$\frac{P_e}{P_o} = \frac{177.5}{180.6} = 0.983 > 0.44$$

$$P_{nc} = \left[0.658^{(P_o/P_e)}\right] P_o = \left[0.658^{(180.6/177.5)}\right](180.6) = 118 \text{ kip}$$ (AASHTO 6.9.4.1-1)

Using a resistance factor ϕ = 1.0 as specified by *SDSSB* Article 2.6.4, the design compression strength of the gusset plate is as:

$$P_{CC} = \phi P_{nc} = (1.0)(118) = 118 \text{ kip} > P_{co} = 4.1 \text{ kip}$$ O.K.

Check Tension Strength of Gusset Plate

The nominal yield strength on the gross section is:

$$P_{nt} = F_{ye} A_g = (46.8)(3.86) = 181 \text{ kip}$$ (AASHTO 6.8.2.1-1)

The nominal fracture strength on the net section is:

$$P_{nf} = F_{ue} A_n R_p U = (69.6)[(10.29 - 0.875)(0.375)](1.0)(1.0) = 246 \text{ kip} \quad \text{(AASHTO 6.8.2.1-2)}$$

Using a resistance factor $\phi = 0.9$ as specified by *SDSSB* Article 2.6.4, the design tension strength is controlled by yielding on the gross section as:

$$P_{CT} = \phi P_{nt} = (0.9)(181) = 162 \text{ kip} > P_{to} = 110.6 \text{ kip} \quad\quad\quad \text{O.K.}$$

Check Unsupported Edge Length

From Figure 20.2.10-6, the unsupported edge length, the interior of the gusset, L_g = 11.6 in.

$$\frac{L_g}{t_g} = \frac{11.6}{0.375} = 30.9 < 2.06\sqrt{\frac{E}{F_y}} = 2.06\sqrt{\frac{29,000}{36}} = 58.5 \quad\quad \text{O.K.} \quad (SDSSB \text{ 7.5.2-1})$$

Design Bolts

Try high strength bolts - ASTM F3125 Grade A325-X high strength bolts, F_{ub} = 120 ksi; diameter d = 7/8 in.; bolt area A_g = 0.601 in.^{2}; threads are excluded from the shear plane. As calculated in Section 20.2.9.6.6, the design shear strength per bolt is as:

$$R_{bs} = \phi R_n = (0.9)(40.3) = 36.3 \text{ kip}$$

Try five rows of bolts at a spacing of 3 in. in the vertical direction as shown in Figure 20.2.10-7.
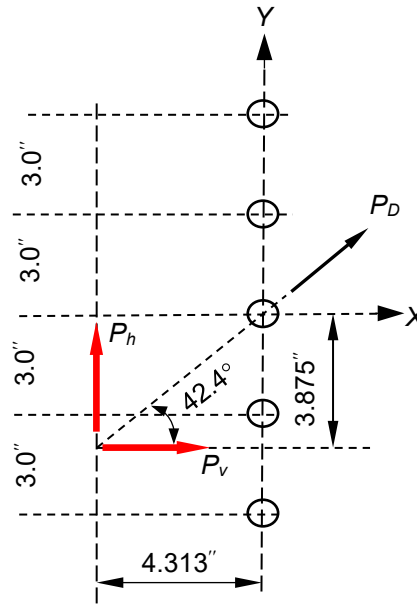
Figure 20.2.10-7 Bolt Pattern of Diagonal Connection at Lower Left

The force acting on the working point is assumed as the overstrength force demand (tension) P_D = 110.6 kips and the bottom strut compression force is not considered conservatively.

The resultant horizontal force: $P_h = P_D \cos(42.4°) = (110.6)\cos(42.4°) = 81.7$ kip ($\rightarrow$)

The resultant vertical force: $P_v = P_D \cos(90° - 42.4°) = 74.6$ kip ($\uparrow$)

The upper and lower bolts are usually the most highly stressed and will be investigated. The "Vector" method is used to calculate the shear force R on the top bolt.

The polar moment of inertia I_p of the bolt group as shown in Figure 20.2.10-7, with respect to the center of gravity of the bolt group, is calculated as follows:

$$I_p = \sum x^2 + \sum y^2 = 2(3)^2 + 2(6)^2 = 90 \text{ in.}^2$$

As shown in Figure 20.2.10.7, horizontal and vertical distances between the working point and the center of gravity of the bolt group are equal to 4.313 in. and 3.875 in., respectively.

The factored shear forces applied on the top bolt are as:

$$R_x = \frac{M_x y}{I_p} = \frac{(81.7)(3.875)(6)}{90} = 21.11 \text{ kip } (\rightarrow)$$

$$R_y = \frac{M_y x}{I_p} = \frac{(74.6)(4.313)(6)}{90} = 21.45 \text{ kip } (\leftarrow)$$

$$R_v = \frac{P_v}{5} = \frac{74.6}{5} = 14.92 \text{ kip } (\uparrow)$$

$$R_h = \frac{P_h}{5} = \frac{81.7}{5} = 16.34 \text{ kip } (\rightarrow)$$

$$R_{bolt} = \sqrt{(R_x + R_y + R_h)^2 + (R_v)^2}$$

$$= \sqrt{(21.11 - 21.45 + 16.34)^2 + (14.92)^2} = 21.9 \text{ kip}$$

$$R_{bolt} = 21.9 \text{ kip } < R_{bs} = 36.3 \text{ kip} \qquad\qquad \text{O.K.}$$

Note: Placing the centroid of a symmetric bolt group near the working line, minimizes eccentricity to that connection; approximately from above:

R_{bolt} = 110.6/ 5 = 22.1 kip.   OK

For practical purposes, holes in connector stiffeners shall be identically placed on both sides of the bay at a fixed elevation from the ends of the web plate. The lower gusset plate areas should be fabricated identically, and also placed at identical fixed heights from the bottom of the web plate. When the slope of cross brace struts is parallel to the cross slope of the deck, the loading to each of the gussets must be examined independently, and the more severe chosen for the design.

20.2.10.5.7 Design Diagonal Connection at Top Strut

For the upper gusset connection at the top strut, the loads are transferred through WP without bending.

It is practical to use the standard gage as the working line for this strut. Use ASTM F3125 Grade A325-X high strength bolts, diameter d = 7/8 in.; threads are excluded from the shear plane.

Select the center of gravity of the bolt group through WP as shown in 20.2.10-8.

The horizontal force demand for the connection is obtained in Section 20.2.10.5.3, V_{01} = 84.8 kips. The vertical tension force demand is induced by the unbalanced overstrength diagonal tension and the compression forces as follows:

$$T_{01} = \Omega(P_t + P_c)\sin\theta = (1.2)(92.2 - 3.4)\sin(42.4°) = 71.9 \text{ kip}$$

The required bolt number = $\dfrac{\sqrt{V_{01}^2 + T_{01}^2}}{R_{bs}} = \dfrac{\sqrt{84.7^2 + 71.8^2}}{36.3} = 3.1$

Use four bolts as shown in Figure 20.2.10-8.
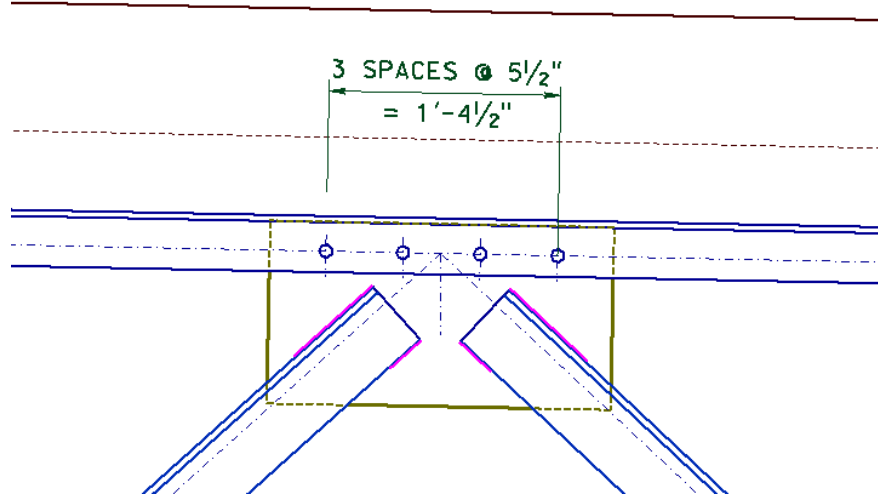
Figure 20.2.10-8 Diagonal Connection at Top Strut

The design of welds and gusset plates is similar to the diagonal connection at the lower left and is not illustrated.

20.2.10.5.8 Design Shear Connectors

The horizontal force demand for shear connectors in each bay is obtained in section 20.2.10.5.3, V_{01} = 84.8 kip. The vertical tension force demand is induced by unbalanced overstrength diagonal tension and compression forces and is obtained in Section 20.2.10.5.7, T_{01} = 71.9 kips.

Try 7/8" diameter welded shear studs with F_u = 60 ksi (Article 6.4.4), and A_{sc} = 0.6 in.^{2}

Use 6 shear stud connectors, 7/8" diameter x 12″ long at a spacing of 18 in. along the central two-thirds of the chord of the end cross frame. The resistance of stud shear connectors subject to the combined shear and axial forces is evaluated in accordance with Article 6.16.4.3.

$$\left(\frac{N_u}{N_r}\right)^{5/3} + \left(\frac{Q_u}{Q_r}\right)^{5/3} \le 1.0 \qquad\qquad \text{(AASHTO 6.16.4.3-1)}$$

The tension force demand for each shear stud is:

$$N_u = \frac{T_{01}}{6} = \frac{71.8}{6} = 12.0 \text{ kip}$$

The shear force demand for each shear stud is:

$$Q_u = \frac{V_{01}}{6} = \frac{84.7}{6} = 14.1 \text{ kip}$$

The depth of the haunch, (soffit to the top of the brace) is $d_h = 5.6$ in.

The width of the haunch parallel to the cross frame is $w_h = 18$ in.

The effective embedment depth of a stud shear connector is $h_{eff} = 11.625$ in.

The effective height of the stud above the top of the soffit to the underside of the head, h_h, is obtained as follows:

$$h_h = h_{eff} - d_h = 11.625 - 5.6 = 6.03 \text{ in.} > \frac{w_h}{3} = \frac{18}{3} = 6 \text{ in.} \quad \text{(AASHTO 6.16.4.3-2)}$$

Use one stud in the transverse direction, group effect modification factor, $\Psi_g = 1.0$.

The longitudinal spacing of studs is 18 in. $< 3 h_{eff} = 34.9$ in., use $\Psi_g = 0.95$.

The width of the end concrete diaphragm shall accommodate flexural bar reinforcement. The 18″ wide end concrete diaphragm is placed at the centerline of the bearing stiffener, but the stud is placed at the centerline of the top strut. Therefore, the smallest edge distance from the center of the stud to the edge of the concrete, $C_a = 9$ in.

$$\Psi_{ed} = 0.7 + 0.3\frac{C_a}{1.5h_h} = 0.7 + 0.3\frac{9}{1.5(6.03)} = 1.0 \quad \text{(AASHTO 6.16.4.3-5)}$$

For shear connectors in this example, the projected area of concrete for a single stud shear connector is approximated from the base of a rectilinear geometric figure that results from projecting the failure surface outward $1.5h_h$ from the centerline of the single connector a single connector, A_{nc} is the same as the projected area of concrete failure for a single stud shear connector based on the concrete breakout resistance in the tension, A_{nco}. Therefore, $A_{nc} / A_{nco} = 1.0$. The tensile capacity is governed by the concrete breakout strength when the shear connector is in tension, and shear connectors are spaced such that their projected cone areas do not overlap.

Use $f'_{ce} = 5.0$ ksi as calculated in Section 20.2.9.6.8, the concrete breakout resistance in the tension of a single stud shear connector in cracked concrete, N_b, is obtained as follows:

$$N_b = 0.76\sqrt{f'_{ce}}h_h^{1.5} = 0.76\sqrt{5.0}\left(6.03\right)^{1.5} = 25.16 \text{ kip} \quad \text{(AASHTO 6.16.4.3-7)}$$

The nominal tensile resistance of a single stud shear connector is obtained as follows:

$$N_n = \psi_g \psi_{ed} \left(\frac{A_{nc}}{A_{nco}} \right) N_b = (0.95)(1.0)(1.0)(25.16) = 23.90 \text{ kip} < A_{sc}F_{ue} = 36.0 \text{ kip}$$

<div align="right">(AASHTO 6.16.4.3-4)</div>

The resistance factor for shear connectors in the tension is specified in Article 6.5.4.2, ϕ_{st} = 0.75.

The factored tensile resistance of a single stud shear connector, N_r is as follows:

$$N_r = \phi_{st} N_n = (0.75)(23.90) = 17.93 \text{ kip}$$ <div align="right">(AASHTO 6.16.4.3-3)</div>

As calculated in Section 20.2.9.6.8, the design strength, i.e., the factored shear resistance of a single shear connector Q_r = 34.2 kip.

Combined shear and tension force interaction is checked as follows:

$$\left(\frac{N_u}{N_r} \right)^{5/3} + \left(\frac{Q_u}{Q_r} \right)^{5/3} = \left(\frac{12.0}{17.93} \right)^{5/3} + \left(\frac{14.1}{34.2} \right)^{5/3} = 0.74 < 1.0 \quad \text{O.K.} \quad \text{(AASHTO 6.16.4.3-1)}$$

Use 6 studs per bay along the central two-thirds of the top chord of the end cross frame.

Use a concrete deck diaphragm of 18 in. wide above the top strut as shown in Figure 20.2.10-9.

20.2.10.5.9 Design Shear Keys

The design calculations are similar to the shear key in Section 20.2.9.6.9 and are not illustrated here.

20.2.10.5.10 Design Deck Diaphragm

Reinforcement in the concrete deck diaphragm needs to be designed to accommodate the vertical force demand induced by unbalanced overstrength diagonal tension and compression forces, as calculated in Section 20.2.10.5.7, T_{01} = 71.9 kips.

Assume simply supported beam with a span length L = 144.6 in., for positive flexure and fixed-fixed beam for negative flexure, conservatively,

The positive moment demand is $M_{up} = T_{01}L/4 = (71.8)(144.6)/4 = 2,596$ kip-in.

The negative moment demand is $M_{un} = T_{01}L/8 = (71.8)(144.6)/8 = 1,298$ kip-in.

For the positive bending:

The effective flange width is determined in accordance with Article 4.6.2.6.5.

$$b_{eff} = \text{smaller} \begin{bmatrix} 18+(2)(6)t_s = 18+(2)(6)(9.125) = 127.5 \text{ in.} \\ 18+(2)(0.1)L = 18+(2)(0.1)(145) = 47 \text{ in.} \end{bmatrix} = 47 \text{ in.}$$

Use b_{eff} = 47 in., d_s = 12 in. as shown in Figure 20.2.10.5-8.

Try 5 # 9 bars, A_s = 5(1.0) = 5.0 in.^{2}

$$c = \frac{A_s f_s}{\alpha_1 f'_c \beta_1 b_{eff}} = \frac{(5.0)(60)}{(0.85)(3.6)(0.85)(47)} = 2.45 \text{ in.} \quad \text{(AASHTO 5.6.3.1.1-4)}$$

$$a = \beta_1 c = (0.85)(2.45) = 2.08 \text{ in.}$$

$$M_n = A_s f_s \left(d_s - \frac{a}{2} \right) = (5.0)(60)\left(12 - \frac{2.08}{2}\right) = 3{,}288 \text{ kip-in.} \quad \text{(AASHTO 5.6.3.2.2-1)}$$

$$M_r = \phi M_n = (0.9)(3{,}288) = 2{,}959 \text{ kip-in.} > M_{up} = 2{,}596 \text{ kip-in.} \quad \text{O.K.}$$

Use 5 #9 bars as shown in Figure 20.2.10-9.

For the negative bending:

Use b = 18 in. and d_s = 12 in. as shown in Figure 20.2.10-9.

Try 3 # 9 Continuous bars, A_s = 3(1.0) = 3.0 in.^{2}

$$c = \frac{A_s f_s}{\alpha_1 f'_c \beta_1 b} = \frac{(3.0)(60)}{(0.85)(3.6)(0.85)(18)} = 3.85 \text{ in.} \quad \text{(AASHTO 5.6.3.1.1-4)}$$

$$a = \beta_1 c = (0.85)(3.85) = 3.27 \text{ in.}$$

$$M_n = A_s f_s \left(d_s - \frac{a}{2} \right) = (3.0)(60)\left(12 - \frac{3.27}{2}\right) = 1{,}866 \text{ kip-in.} \quad \text{(AASHTO 5.6.3.2.2-1)}$$

$$M_r = \phi M_n = (0.9)(1{,}866) = 1{,}679 \text{ kip-in.} > M_{un} = 1{,}298 \text{ kip-in.} \quad \text{O.K.}$$

Use 3 #9 Cont bars as shown in Figure 20.2.10-9.
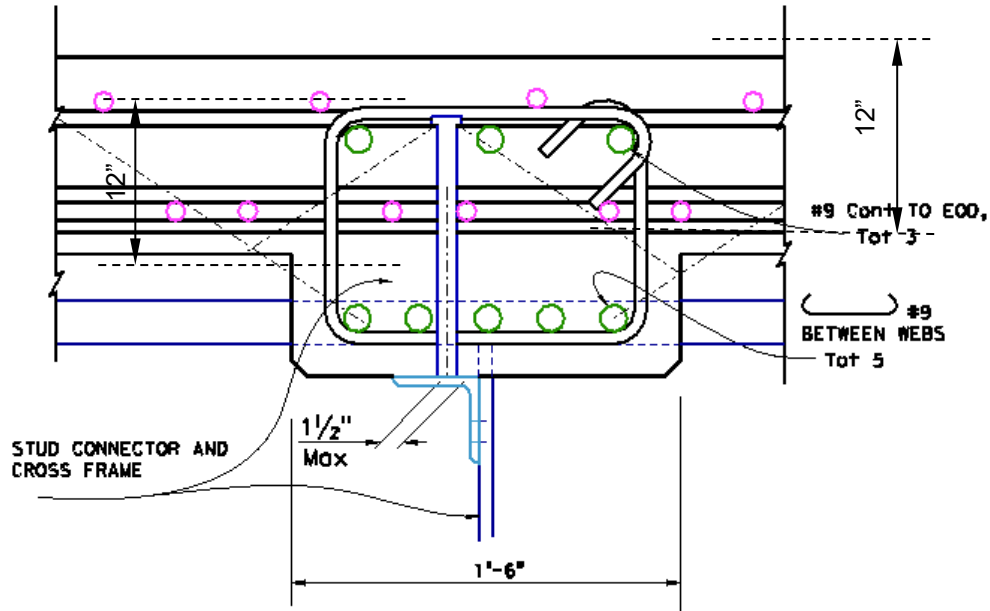
Figure 20.2.10-9 Concrete Diaphragm above Top Strut

20.2.10.5.11 Ductile End Cross Frame Sketch

A sketch of the end cross frame is shown in Figure 20.2.10-10.
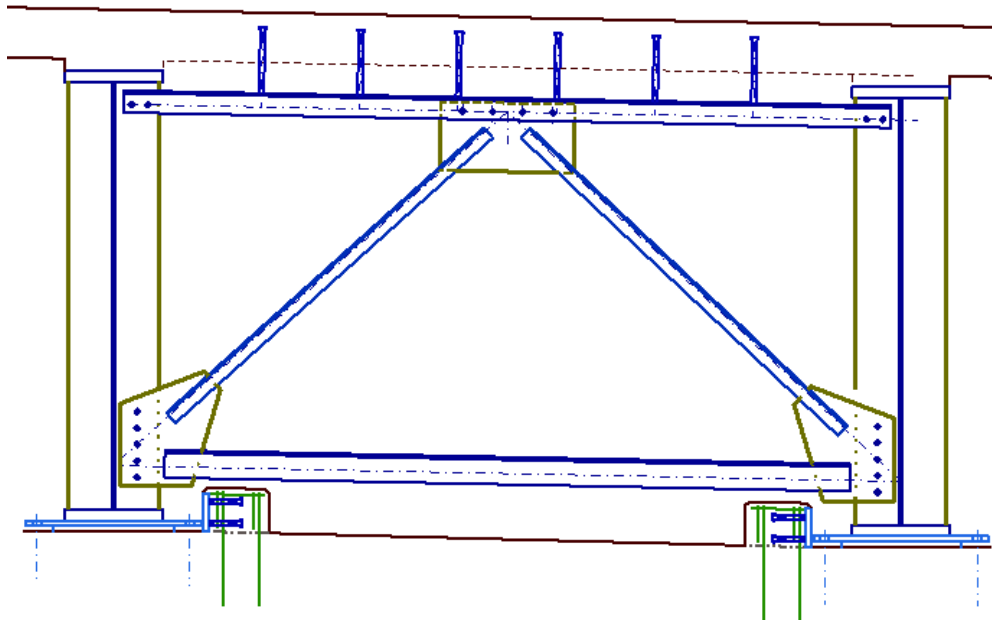
Figure 20.2.10-10 Ductile End Cross Frame Sketch -Single Bay

20.2.10.6 Determine Displacement Capacity

20.2.10.6.1 Longitudinal Displacement Capacity

Same as Example 1, the displacement capacity of a bridge can be estimated by a push-over analysis. The detailed calculations are listed in Table 20.2.10-1. The Table shows that the longitudinal displacement D/C ratio, displacement ductility capacity, and displacement ductility demand are all satisfied for both Bents 2 and 3. It should be pointed out that, the longitudinal displacement demands are much smaller than yield displacements which imply that substructure is expected to perform essentially elastic in the longitudinal direction during the design earthquake.

Table 20.2.10-1 Longitudinal Displacement Capacity

Parameters	Calculations	Bent 2	Bent 3
Column Height H (in.)	-	528.0	528.0
Rebar Diameter d_{bl} (in.)	-	1.41	1.41
Rebar f_{ye} (ksi)	-	68.0	68.0
Plastic Hinge Length L_p (in.)	$0.08H + 0.15f_{ye}d_{bl} \geq 0.3f_{ye}d_{bl}$ (*SDC* 5.3.4-1)	56.62	56.62
Yield Curvature ϕ_y (rad/in.)	CSIBridge Results	0.0000833	0.0000832
Yield Displacement Δ_y (in.)	$\phi_y H^2 / 3$ (*SDC* C5.2.2-2)	7.74	7.74
Ultimate Curvature ϕ_u (rad/in.)	CSIBridge Results	0.000933	0.000925
Ultimate Displacement Δ_C (in.)	$\Delta_y + L_p(\phi_u - \phi_y)(H - L_p/2)$ (*SDC* C5.2.2-1)	31.79	31.55
Displacement D/C Ratio	$\Delta_C \geq \Delta_D$ (SDC 3.5.1-1)	31.79 > 2.97	31.55 > 2.99
Displacement Ductility Demand μ_d	Δ_D / Δ_y (*SDC* Table 4.4.1-1)	0.38 < 5.0	0.38 < 5.0

20.2.10.6.2 Transverse Displacement Capacity

Following the same procedure as in Example 1, Table 20.2.10-2 summarizes the yield displacements of the substructure for Bents 2 and 3.

Table 20.2.10-2 Transverse Yield Displacement of Substructure

Parameters	Calculations	Bent 2	Bent 3
Column Height H (in.)	-	528.0	528.0
Rebar Diameter d_{bl} (in)	-	1.41	1.41
Rebar f_{ye} (ksi)	-	68.0	68.0
Plastic Hinge Length L_p (in)	$0.08H + 0.15f_{ye}d_{bl} \geq 0.3f_{ye}d_{bl}$ (SDC 5.3.4-1)	56.62	56.62
Yield Displacement Δ_{ysub} (in)	CSIBridge Results	5.92	6.02

Displacement capacities of Bents 2 and 3 in the transverse direction include displacement capacity of the ductile end cross frame, Δ_{decf} and the corresponding displacement of the substructure under the overstrength horizontal force, Δ_{sub}. The displacement contributed by bearings can be ignored conservatively.

Braces in a typical concentrically braced frame can be expected to yield and buckle at story drift ratios of about 0.3% to 0.5% and the braces could undergo post-buckling axial deformations 10 to 20 times their yield deformation (AISC, 2016). Experimental testing on ductile end cross frames (Bahrami, et al., 2010) shows that the displacement capacity of a single angle cross frame can undergo story drift ratios of about 6% to 7%. Although the displacement capacity of a steel frame can be evaluated by a refined pushover analysis, it is reasonably and conservatively assumed the displacement capacity of the ductile end cross frame of 4% story height for this example. For the end cross frame as shown in Figure 20.2.10-1, the story height = 5.5 ft, the displacement capacity of the ductile end cross frame, Δ_{decf} is obtained as follows:

$$\Delta_{decf} = 0.04(5.5 \times 12) = 2.64 \text{ in.}$$

From Figure 20.2.9-2, the force-displacement curve for Bent 2, it is seen that the substructure is essentially elastic under an overstrength horizontal force of 338.8 kips of the ductile end cross frame as calculated in Section 20.2.9.5.2 and the corresponding displacement is as follows:

$$\Delta_{sub} = (5.92)\frac{(338.8)}{420} = 4.78 \text{ in.}$$

Therefore, the transverse displacement capacity of Bent 2 is obtained as follows:

$$\Delta_C = \Delta_{decf} + \Delta_{sub} = 2.64 + 4.78 = 7.42 \text{ in.}$$

$$\Delta_C = 7.42 \text{ in.} > \Delta_D = 6.47 \text{ in.} \qquad\qquad \text{O.K.} \qquad (SDSSB \text{ 2.6.1-1})$$

20.2.11 SUMMARY

This chapter presents state-of-the-art and state-of-the-practice on earthquake damage, seismic design concepts and basis, analysis and modeling, general considerations, several actual examples of seismic retrofit, and seismic design of steel bridges. This chapter addresses only some of the many issues incumbent upon bridge designers for desirable seismic performances. Engineers are always encouraged to incorporate, to the best of their ability, the most recent research findings, and the most recent "full-scale evidence" in real earthquakes into their seismic design practice.

NOTATION

A_b = nominal cross-sectional area of the bolt (in.^{2})

A_{cv} = area of concrete considered to be engaged in interface shear transfer (in.^{2})

A_f = flange area (in.^{2})

A_g = gross cross-sectional area of the member; effective Whitmore section area (in.^{2})

A_n = net cross-sectional area of the member (in.^{2})

A_{nc} = projected area of concrete for a single stud shear connector or group of connectors approximated from the base of a rectilinear geometric figure that results from projecting the failure surface outward $1.5h_h$ from the centerline of the single connector or, in the case of a group of connectors, from a line through a row of adjacent connectors (in.^{2})

A_{nco} = projected area of concrete failure for a single stud shear connector based on the concrete breakout resistance in tension (in.^{2})

A_s = area of steel reinforcement (in.^{2})

A_{sc} = cross-sectional area of a stud shear connector (in.^{2})

A_{vf} = area of interface shear reinforcement crossing the shear plane within the area A_{cv} (in.^{2})

a = depth of equivalent rectangular stress block (in.)

B_{cap} = bent cap width (in.)

b = width of an element (in.)

b_{eff} = effective flange width (in.)

b_{vi} = interface width considered to be engaged in shear transfer (in.)

C_a = smallest edge distance from the center of stud to the edge of the concrete (in.)

c = cohesion factor (ksi); distance from the extreme compression fiber to the neutral axis (in.)

D_c = concrete column diameter (in.)

d = nominal diameter of a bolt; depth of the concrete shear key (in.)

d_{bl} = rebar diameter (in.)

d_h = depth of haunch (in.)

d_s = distance from extreme compression fiber to the centroid of the nonprestressed tensile reinforcement measured along the centerline of the web (in.)

E_s = modulus of elasticity of steel (ksi)

F_{abut} = idealized ultimate passive capacity of the backfill behind abutment backwall or diaphragm (kip)

F_C = design strength, or factored resistance (axial/shear force and moment as appropriate) of a capacity-protected component

F_D = force demand (axial/shear force and moment as appropriate) on a capacity-protected component determined by the overstrength forces of adjacent ductile components

F_{eex} = classification strength of weld metal (ksi)

F_u = specified minimum tensile strength of steel (ksi)

F_{ue} = expected tensile strength of steel (ksi)

F_{ub} = specified minimum tensile strength of a bolt (ksi)

F_{w1} = required force for the weld length L_{w1} (kip)

F_{w2} = required force for the weld length L_{w2} (kip)

F_y = specified minimum yield strength of steel (ksi)

F_{ye} = expected yield strength of steel (ksi)

f_s = stress in the nonprestressed tension reinforcement at nominal flexural resistance (ksi);

f_y = specified minimum yield strength of reinforcement (ksi)

f_{ye} = expected yield strength of reinforcement (ksi)

f'_c = specified compressive strength of concrete at 28 days (ksi)

f'_{ce} = expected concrete strength (ksi)

H = column height (in.)

h_{abut} = abutment backwall height (ft)

h_{eff} = effective embedment depth of a stud shear connector (in.)

h_h = effective height of the stud above the top of the soffit to the underside of the head (in.)

K = effective length factor for a compression member in the plane of buckling

K_{abut} = abutment longitudinal stiffness (kip/in.)

K_{eff} = effective abutment longitudinal stiffness (kip/in.)

K_1 = fraction of concrete strength available to resist interface shear

K_2 = limiting interface shear resistance of concrete (ksi)

L = length of a member (in.)

L_b = unbraced length of a compression member (in.)

L_{bs} = bottom strut length (in.)

L_c	=	clear end distance (in.)
L_{dg}	=	diagonal brace length (in.)
L_g	=	unsupported edge length of the gusset plate (in.)
L_p	=	plastic hinge length (in.)
L_{ts}	=	top strut length (in.)
L_{vi}	=	interface length considered to be engaged in shear transfer (in.)
L_{w1}	=	longer weld length (in.)
L_{w2}	=	shorter weld length (in.)
L_z	=	unbraced length of a compression member along the z-axis (in.)
L_1	=	distance from the centerline of the Whitmore section to the interior corner of a gusset (in.)
L_2, L_3	=	distance from the outside corner of the Whitmore section to the edge of a member; negative value shall be used when the part of the Whitmore section enters into the member (in.)
M_n	=	nominal flexural resistance (kip-in.)
M_r	=	factored flexural resistance (kip-in.)
M_u	=	peak moment or ultimate moment (kip-in.)
M_{un}	=	negative moment demand (kip-in.)
M_{up}	=	positive moment demand (kip-in.)
$\boldsymbol{M_w}$	=	moment magnitude scale used to measure the size of earthquakes
M_y	=	yield moment at the onset of yielding of an extreme fiber (kip-in.)
N_b	=	concrete breakout resistance in tension of a single stud shear connector in cracked concrete (kip)
N_n	=	nominal tensile resistance of a single stud connector (kip)
N_r	=	factored tensile resistance of a single stud connector (kip)
N_s	=	number of shear planes
N_u	=	seismic axial force demand per stud at the support cross-frame or diaphragm location under consideration (kip)
P	=	axial force (kip)
P_{CC}	=	design compression strength (kip)
P_c	=	permanent net compressive force normal to the shear plane; idealized plastic strength for compression diagonal brace (kip (kip)
P_{co}	=	overstrength force for a compression diagonal brace (kip)
P_{CT}	=	design tension strength (kip)

P_D	=	force demands for diagonal brace member (kip)
P_{DL}	=	axial dead load (kip)
P_e	=	elastic critical buckling resistance (kip)
P_h	=	resultant horizontal force (kip)
P_{nc}	=	expected nominal axial compression resistance (kip)
P_{nf}	=	expected nominal fracture strength on the net section (kip)
P_{nt}	=	expected nominal axial tension resistance (kip)
P_o	=	nominal yield resistance (kip)
P_t	=	idealized plastic strength for a tension diagonal brace (kip)
P_{to}	=	overstrength force for a tension diagonal brace (kip)
P_v	=	resultant vertical force (kip)
P_y	=	axial yield strength of a steel section (kip)
Q_n	=	nominal shear resistance of a single shear connector (kip)
Q_{ne}	=	expected nominal strength of one shear connector (kip)
Q_r	=	design strength of one shear connector; factored shear resistance of a single shear connector (kip)
Q_u	=	seismic shear demand per stud at the support cross-frame or diaphragm location under consideration due to the governing orthogonal combination of seismic shears (kip)
R_A	=	abutment displacement coefficient
R_{bolt}	=	resultant force in a bolt (kip)
R_{bs}	=	design shear strength of one bolt (kip)
R_n	=	nominal resistance of one bolt (kip)
R_{ne}	=	expected nominal bearing resistance of a bolt hole (kip)
R_p	=	reduction factor for holes taken equal to 0.90 for bolt holes punched full size and 1.0 for bolt holes drilled full size or subpunched and reamed to size
R_r	=	design shear strength of the weld metal (ksi)
R_{rw}	=	design shear strength of a fillet weld per unit length (kip/in.)
R_t	=	ratio of the expected tensile strength to the specified minimum tensile strength
R_y	=	ratio of the expected yield strength to the specified minimum yield strength
r	=	radius of gyration about the axis perpendicular to the plan of the buckling (in.)
r_x	=	radius of gyration about the major axis or x-axis (in.)

r_y	=	radius of gyration about the minor axis or y-axis (in.)
r_z	=	radius of gyration about the principal axis or z-axis (in.)
T_{01}	=	Vertical tension force demand is induced by unbalanced overstrength diagonal tension and compression forces (kip)
t	=	element thickness (in.)
t_e	=	effective size of a fillet weld (in.)
t_g	=	gusset plate thickness (in.)
t_s	=	thickness of a concrete deck (in.)
t_w	=	web thickness (in.)
U	=	reduction factor to account for shear lag
V_{ni}	=	nominal shear resistance of the interface plane (kip)
V_u	=	peak lateral load or ultimate lateral load capacity (kip)
V_y	=	lateral force corresponding to the onset of forming the first plastic hinge (kip)
V_{01}	=	overstrength horizontal force transferred to one cross frame (kip)
V_{04}	=	total overstrength horizontal force transferred to the entire four-bay end cross frame system (kip)
W_{abut}	=	abutment backwall width along the skew direction (ft)
w_c	=	unit weight of concrete (kcf)
w_h	=	width of haunch parallel to the cross frame (in.)
w_g	=	effective Whitmore section width (in.)
$\overline{x}$	=	distance from the centroid of the angle along the x-axis to the outside surface of the angle (in.)
$\overline{y}$	=	distance from the centroid of the angle along the y-axis to the outside surface of the angle (in.)
α	=	angle between the principal axis and the y-axis of an angle section (degree)
β_1	=	stress block factor taken as the ratio of the depth of the equivalent uniformly stressed compression zone assumed in the strength limit state to the depth of the actual compression zone
θ	=	abutment skew (degree)
θ_y	=	yield rotation, rotation corresponding to the onset of yielding in the extreme tension fiber
θ_p	=	plastic rotation angle

θ_u =   ultimate rotation capacity, rotation corresponding to its expected damage level at which the extreme fiber reaches its strain limit as specified in *SDSSB* Table 2.5-1, not to exceed that rotation when the moment resistance degrades towards a minimum of 80 percent of the peak moment resistance

ϕ =   resist factor

ϕ_{st} =   resistance factor for shear connectors in tension specified in Article 6.5.4.2

ϕ_y =   yield curvature (1/rad)

ϕ_u =   ultimate curvature (1/rad)

μ =   friction factor

μ_d =   displacement ductility demand

μ_c =   displacement ductility capacity

λ =   width-to-thickness ratio of elements

λ_{hd} =   limiting width-to-thickness ratio of elements for highly ductile members in the *AISC Seismic Provisions*

λ_{ps} =   limiting width-to-thickness ratio of elements for ductile components

λ_r =   limiting width-to-thickness ratio of elements for capacity-protected components

Ω =   overstrength factor

ω_C =   strain hardening adjustment factor for compression

ω_T =   strain hardening adjustment factor for tension

Ψ_{ed} =   edge distance factor

Ψ_g =   group effect modification factor

Δ_{abut} =   abutment displacement at idealized yield (in.)

Δ_C =   displacement capacity determined by using a static pushover analysis in which both material and geometric nonlinearities are considered (in.)

Δ_D =   displacement demand determined by equivalent static analysis or elastic dynamic analysis with consideration of effective section properties under the design earthquake (in.)

Δ_{eff} =   effective abutment longitudinal displacement when the passive force reaches F_{abut} (in.)

Δ_{decf} =   displacement capacity of ductile end cross frame (in.)

Δ_{gap} =   width of expansion gap at seat abutment (in.)

Δ_{sub} =   displacement capacity of substructure (in.)

Δ_u =   ultimate lateral displacement capacity, the lateral displacement of a component or a system corresponding to its expected damage level limit as specified in *SDSSB* Table 2.5-1, not to exceed that displacement when the lateral resistance degrades towards a minimum of 80 percent of the peak resistance (in.)

Δ_y =   yield displacement, the lateral displacement of a component or a system at the onset of forming the first plastic hinge (in.)

Δ_{ysub} =   yield displacement of substructure (in.)

REFERENCES

1.   AASHTO. (2017). *AASHTO LRFD Bridge Design Specifications*, 8th Edition, American Association of State Highway and Transportation Officials, Washington DC.

2.   AASHTO. (2011). *Guide Specifications for LRFD Seismic Bridge Design*, 2nd ed., American Association of State Highway and Transportation Officials, Washington, DC.

3.   ADINA. (1997).   *ADINA User's and Theory Manual.* ADINA R & D, Watertown, MA.

4.   AISC. (2016). *Seismic Provisions for Structural Steel Buildings,* ANSI/AISC 341-16, American Institute of Steel Construction, Chicago, IL.

5.   AISC. (2010a). *Seismic Provisions for Structural Steel Buildings,* ANSI/AISC 341-10, American Institute of Steel Construction, Chicago, IL.

6.   AISC. (2010b). *Specification for Structural Steel Buildings*, ANSI/AISC 360-10, American Institute of Steel Construction, Chicago, IL.

7.   Akkari, M. and Hoffman, F. (1993). "San Francisco Bayshore Viaduct Seismic Retrofit," *Proceedings of Structural Engineering in Natural Hazards Mitigation*, ASCE, ed. Ang, A.H. and Villaverde, R., April 19-21, Irvine, CA.

8.   Astaneh-Al, A. et al. (1994). "Seismic Performance of Steel Bridges during the 1994 Northridge Earthquake," *Report UCB/CE-STEEL-94/01*, Dept. of Civil Engineering, University of California, Berkeley, CA.

9.   ATC. (1996). *Improved Seismic Design Criteria for California Bridges: Provisional Recommendations*, (ATC-32), Applied Technology Council, Redwood City, CA.

10.   Aviram, A., Mackie, K. R. and Stojadinović, B. (2008). "Guidelines for Nonlinear Analysis of Bridge Structures in California." *Report UCB/PEER 2008/03*, Pacific Earthquake Engineering Research Center, University of California, Berkeley, CA.

11.   AWS. (2020). *Bridge Welding Code*, AASHTO/AWS D1.5:2000, American Welding Society, Miami, FL.

12.   Bahrami, H., Itani, A. M. and Buckle, I. G. (2010). "Guidelines for the Seismic Design of Ductile End Cross Frames in Steel Girder Bridge Superstructures," *Report CCCEE 09-04*, Center for Civil Engineering Earthquake Research, University of Nevada, Reno, NV.

13.   Berman, J. and Bruneau, M. (2008). "Tubular Links for Eccentrically Braced Frames, II: Experimental Verification," *J. Struct. Engrg.*, ASCE, 134(5), 702-712.

14.   Bruneau, M. (2013). "Setting Limits," *Modern Steel Construction*, AISC, February 2013, 52-53.

15. Bruneau, M. (1998). "Performance of Steel Bridges during the 1995 Hyogoken-Nanbu (Kobe Japan) earthquake – a North American Perspective," *Engineering Structures*, 20(12), 1063-1078.

16. Caltrans. (2019a). *Seismic Design Criteria,* Version 2.0, California Department of Transportation, Sacramento, CA.

17. Caltrans. (2019b). *California Amendments to AASHTO LRFD Bridge Design Specifications, 8th Edition*, California Department of Transportation, Sacramento, CA.

18. Caltrans. (2016). *Caltrans Seismic Design Specifications for Steel Bridges,* 2nd Edition*, California Department of Transportation, Sacramento, CA.

19. Caltrans. (2015). *Seismic Retrofit Strategy Report – Sacramento River – Paintersville Bridge*, California Department of Transportation, Sacramento, CA.

20. Caltrans. (2011). *Antioch Toll Bridge Seismic Retrofit Project Final Design Repo*rt, California Department of Transportation, Sacramento, CA.

21. Caltrans. (2001). *Guide Specifications for Seismic Design of Steel Bridges, First Edition,* California Department of Transportation, Sacramento, CA.

22. Caltrans. (1999). *Seismic Design Criteria,* Version 1.1, California Department of Transportation, Sacramento, CA.

23. Caltrans. (1997). *San Francisco - Oakland Bay Bridge West Spans Seismic Retrofit Design Criteria*, Edited by Duan, L., California Department of Transportation, Sacramento, CA.

24. Carden, L. P., Itani, A. M., and Buckle, I. G. (2006a). "Seismic Performance of Steel Girder Bridges with Ductile Cross Frames using Buckling Restrained Braces," *J. Struct. Engrg*., ASCE, 132(3), 338-345.

25. Carden, L. P., Garcia-Alvarez, A. M., Itani, A. M., and Buckle, I. G. (2006b). "Seismic Performance of Steel Girder Bridges with Ductile Cross Frames using Single Angle X Braces," *J. Struct. Engrg*., ASCE, 132(3), 329-337.

26. CSI, (2021). *CSiBridge*, v. 23.3.1, Computers and Structures, Inc., Walnut Creek, CA.

27. CSI, (2019). *CSiBridge*, v. 21.2.0, Computers and Structures, Inc., Walnut Creek, CA.

28. Dahlgren, T. and Vincent, J. (1998). IBC-98-36, "Richmond-San Rafael Bridge Innovative Foundation Retrofit," *Proceeding of International Bridge Conference*, June 15-17. Pittsburgh, PA.

29. Duan, L., Reno, M. and Lynch, J. (2000). "Section Properties for Latticed Members of San Francisco-Oakland Bay Bridge," *J. Bridge Engrg*., ASCE, 5(2), 156-164.

30. Dusicka, P., Itani, A. M. and Buckle, I. G. (2002). "Cyclic Behavior of Shear Links and Tower Assembly of San Francisco-Oakland Bay Bridge Tower," *Report CCCEE 02-06*, Center for Civil Engineering Earthquake Research, University of Nevada, Reno, NV.

31.   Dusicka, P., Itani, A. M. and Buckle, I. G. (2010). "Cyclic Behavior of Shear Links of Various Grades of Plate Steel," *J. Struct. Engrg.*, ASCE, 136(4), 370-378.

32.   Goto, Y., (2014). "Chapter 10: Seismic Design of Thin-Walled Steel and CFT Piers." *Bridge Engineering Handbook, Second Edition: Seismic Design*, Ed. Chen, W. F. and Duan, L., CRC Press, Boca Raton, FL.

33.   GSD-JV, (1997a). *Drift Capacity of Retrofitted Pile Foundations, Richmond-San Rafael Bridge,* November, Prepared by Gerwick/Sverdrup/DMJM Joint Venture, California Department of Transportation, Sacramento, CA.

34.   GSD-JV, (1997b). *Low-Cycle fatigue Evaluation of the Retrofitted Steel Tower on the Richmond-San Rafael Bridge,* November, Prepared by Gerwick/Sverdrup/DMJM Joint Venture, California Department of Transportation, Sacramento, CA.

35.   GSD-JV, (1999a). *Technical Design Criteria, Revision 4,* January 21, Prepared by Gerwick/Sverdrup/DMJM Joint Venture, California Department of Transportation, Sacramento, CA.

36.   GSD-JV, (1999b). *Richmond-San Rafael Bridge Seismic Retrofit Final Peer Review Report,* March, Prepared by Gerwick/Sverdrup/DMJM Joint Venture, California Department of Transportation, Sacramento, CA.

37.   Holombo, J., MacRae, G., Priestley, N. and Seible, F. (1995). "Steel Column Prooftests of the Bayshore and Central Viaducts," *Report No. SSRP-95/05*, University of California, San Diego, La Jolla, CA.

38.   Itani, A. M. and Sedarat, H. (2000). "Seismic Analysis and Design of the AISI LRFD Design Examples of Steel Highway Bridges," *Report No. CEER 00-8*, Center for Civil Engineering Earthquake Research, University of Nevada, Reno, NV.

39.   Kim, Y. P. (2012) "Seismic Retrofit of Antioch Toll Bridge," *Modern Steel Construction,* AISC, February.

40.   Lanning, J., Benzoni, G. and Uang, C. M. (2013) "The Feasibility of Using Buckling-Restrained Braces for Long-Span Bridges: Near-Fault Protocols and Full-Scale Testing," *Report No. SSRP 13/17*. Department of Structural Engineering, University of California, San Diego, La Jolla, CA.

41.   Masroor, T.; Thimmhardy, E.; Mitchell, S.; R., Quiogue, J., Alcantara, O. (2013). "Seismic Retrofit of Dumbarton Toll Bridge," *Proceedings of the Seventh National Seismic Conference on Bridges & Highways: Bridge Resilience for Earthquakes & Other Natural Hazards*, ed. Kapur, J. and Thomas Ostrom, T. May 20-20.2, 2013, Oakland CA.

42.   McDaniel, C. C., Uang, C. M. and Seible, F. (2002). "Cyclic Testing of Suspension Tower Shear Links of the San Francisco-Oakland Bay Bridge," *Report No. SSRP-2001/14*, Department of Structural Engineering, University of California, San Diego, La Jolla, CA.

43.   Monzon, E. V., Itani, A. M. and Grubb, M. A. (2014). "Nonlinear Evaluation of the Proposed Seismic Design Procedure for Steel Bridges with Ductile End Cross Frames," *Report No. CCEER-14-04*, Center for Civil Engineering Earthquake Research, University of Nevada, Reno, NV.

44.   Patty, J., Seible F. and Uang, C. M. (2001). "Seismic Response of Integral Bridge Connections", *Report No. SSRP – 2000/16*, Department of Structural Engineering, University of California, San Diego, La Jolla, CA.

45.   Phillippi, D. J., Benzoni, G. and Hegemier G. (2010). "Experimental Seismic Performance on Dumbarton Bridge Pier 23 and Pier 37," *SSRP 10-08*, Department of Structural Engineering, University of California at San Diego, La Jolla, CA.

46.   Reno, M. and Pohll, M. (1998). "Seismic Retrofit of San Francisco–Oakland Bay Bridge West Span," *Transportation Research Record: Journal of the Transportation Research Board,* 1624:73-81.

47.   Uang, C. M., Tsai, K. C. and Bruneau M. (2014). "Chapter 9: Seismic Design of Steel Bridges," *Bridge Engineering Handbook: Seismic Design*, 2nd Edition, Ed., Chen, W. F. and Duan, L., CRC Press, Boca Raton, FL.

48.   Vincent, J. and Abrahamsen, T. (1998). IBC-98-37, "Eccentrically Braced and Special Moment Resisting Frame Support Bridge Retrofit," *Proceeding of International Bridge Conference*, June 15-17, 1998. Pittsburgh, PA.

49.   Wassef, W. G. et. al. (2004). "Integral Steel Box-Beam Pier Caps," *NCHRP Report 527,* Transportation Research Board, Washington, DC.

50.   Yashinsky, M., Moehle, J. P. and Eberhard, M. O. (2014). "Chapter 32: Earthquake Damage to Bridges," *Bridge Engineering Handbook: Seismic Design*, 2nd Edition, Ed., Chen, W. F. and Duan, L., CRC Press, Boca Raton, FL.

51.   Zahrai, S. M. and Bruneau, M. (1998). "Impact of Diaphragms on Seismic Responses of Straight Slab-on-Girder Steel Bridges," *J. Struct. Engrg.,* ASCE, 124(8), 938-947.

52.   Zahrai, S. M., and Bruneau, M. (1999a). "Ductile End-Diaphragms for the Seismic Retrofit of Slab-on-Girder Steel Bridges," *J. Struct. Engrg.,* ASCE, 125(1), 71-80.

53.   Zahrai, S. M. and Bruneau, M. (1999b). "Cyclic Testing of Ductile End-Diaphragms for Slab-on-Girder Steel Bridges," *J. Struct. Engrg.,* ASCE, 125(9), 987-996.

This page is intentionally left blank.